2010

Historic Bridge Evaluation Using Finite Element Techniques

Helena M. Charron
University of Massachusetts Amherst, hcharron@gmail.com

HISTORIC BRIDGE EVALUATION USING FINITE ELEMENT TECHNIQUES

A Thesis Presented

by

HELENA M. CHARRON

Submitted to the Graduate School of the
University of Massachusetts Amherst in partial fulfillment
of the requirements for the degree of

MASTER OF CIVIL ENGINEERING

May 2010

Civil & Environmental Engineering

HISTORIC BRIDGE EVALUATION USING FINITE ELEMENT TECHNIQUES

A Thesis Presented

by

HELENA M. CHARRON

Approved as to style and content by:

_____

Sergio F. Brena, Chair

_____

Thomas J. Lardner, Member

_____

Sanjay R. Arwade, Member

_____

Richard N. Palmer, Department Head
Civil & Environmental Engineering

ABSTRACT

HISTORIC BRIDGE EVALUATION USING FINITE ELEMENT TECHNIQUES

MAY 2010

HELENA M. CHARRON, B.S., SMITH COLLEGE

M.S., UNIVERSITY OF MASSACHUSETTS AMHERST

Directed by: Professor Sergio F. Brena

The present study examined the application of modern, computer-based analysis methods to two existing historic bridges in Massachusetts. The first bridge featured in this study is the Woronoco Bridge, a reinforced concrete open spandrel arch bridge that was constructed in 1923. It was hoped that a computer-based, parametric study of this bridge would prove it to be deck-stiffened, similar to select bridges of Swiss engineer Robert Maillart. However, the results do not support that there was any intent to reduce bending in the arch as a result of increasing the stiffness of the bridge deck. Instead, the Woronoco Bridge appears to optimize column stiffness in order to reduce bending stresses in the arch. The second bridge featured in this study is the Bardwell's Ferry Bridge, a wrought iron lenticular truss that was constructed in 1882. A finite element model was created to identify the magnitude and location of maximum stresses within a critical lower truss chord (eye bar) connection in order to aid future rehabilitation and monitoring efforts. In addition, this model was used in combination with currently available material data in order to evaluate the fatigue life expectancy of the structure given the current 10 ton posted capacity. It was determined to be below the endurance limit and therefore is safe indefinitely, however, more specific material data is required.

CONTENTS

Page

ABSTRACT iii

LIST OF TABLES..... vi

LIST OF FIGURES..... vii

CHAPTER

1. INTRODUCTION/MOTIVATION 1

PART I: REINFORCED CONCRETE OPEN SPANDREL BRIDGES

2. BACKGROUND..... 7

2.1 Development of the American Open Spandrel Arch Bridge..... 7
2.2 Development of the Deck-Stiffened Arch Bridge 8

2.2.1 Theory behind the Deck-Stiffened Arch Bridge 9
2.2.2 Application of Theory to Select Designs..... 13

2.3 Differences between American and Swiss Designs..... 16

3. PRELIMINARY ANALYSIS..... 19

3.1 Simplified Analysis to the Woronoco Bridge..... 19

4. DEVELOPMENT OF WORONOCO BRIDGE MODEL..... 26

4.1 Identification of Assumptions involved in Simplified Analysis 26
4.2 Evaluation of Modeling Assumptions..... 28

4.2.1 Assumption 1: Pinned Bridge Supports 29
4.2.2 Assumption 2: Pinned Spandrel Columns 33
4.2.3 Assumption 3: Parabolic Shape of Arch 38
4.2.4 Assumption 4: Number of Spandrel Columns 42
4.2.5 Assumption 5: Variation of Arch Stiffness 47

4.3 Assumptions Appropriate for Model of the Woronoco Bridge 50

5. USE OF MODEL TO INVESTIGATE DESIGN CHOICES..... 52

5.1 The Effect of Column Stiffness and Spacing..... 52

5.1.1 Study of Column Stiffness in the Woronoco Bridge..... 53

5.1.1.1 The Effect on Maximum Bending Moment..... 54
5.1.1.2 The Effect on Maximum Axial Forces..... 59
5.1.1.3 The Influence of Aesthetics..... 63
5.1.1.4 Justification for Design Choices..... 65

5.1.2 Study of Column Spacing in the Woronoco Bridge..…… 67

5.1.2.1 The Effect on Maximum Bending Moment.……..67
5.1.2.2 The Influence of Aesthetics……... 70
5.1.2.3 The Effect on Maximum Axial Forces…….. 72

5.2 The Effect of Deck Stiffness……74

5.2.1 Study of Deck Stiffness in the Woronoco Bridge……..74

5.2.1.1 The Effect on Maximum Bending Moment……...75
5.2.1.2 The Effect on Maximum Axial Forces…….. 83
5.2.1.3 The Influence of Aesthetics……... 84
5.2.1.4 Justification for Design Choices…… 87

6. DISCUSSION OF RESULTS…….... 88

PART II: IRON LENTICULAR TRUSS BRIDGES

7. BACKGROUND…….……... 98

7.1 Development of American Lenticular Truss Bridge…….…….. 98

8. FINITE ELEMENT ANALYSIS OF BARDWELL'S FERRY BRIDGE……. 104

8.1 Identification of Critical Connection……... 104
8.2 Maximum Stresses in Critical Connection…….…… 111

8.2.1 Development of ADINA Models…….. 111

8.2.1.1 Concentric Model (Three Bars)……..… 113
8.2.1.2 Eccentric Connection Model (Two Bars)…….. 118

8.2.2 Evaluation of Axial Stress Distribution…… 120
8.2.3 Evaluation of Shear Stress Distribution……124

8.3 Preliminary Fatigue Analysis…….. 130

9. DISCUSSION OF RESULTS……. 132

10. CONCLUSION …….. 136

REFERENCES ……. 139

LIST OF TABLES

Table Page

4.1 Comparison of bending stresses when spandrels are pinned or fixed……35

4.2 Summary of the relationship between aspect ratio and maximum bending in arch…….. 40

4.3 Effect of varying column number on the maximum bending moment…..... 46

5.1 Summary of the thirteen column stiffness models investigated as part of parametric study……..... 54

5.2 The maximum bending moment results from each of the thirteen models in which the column stiffness was incrementally varied….. 56

5.3 The maximum axial forces results from each of the thirteen models in which the column stiffness was incrementally varied……... 61

5.4 The maximum bending moment results from each of the seven models in which the column spacing was incrementally varied…… 69

5.5 The maximum axial forces results from each of the seven models in which the column number was incrementally varied……..... 72

5.6 Summary of the nine deck stiffness models investigated as part of parametric study…… 75

5.7 The maximum bending moment results from each of the nine models in which the deck stiffness was incrementally varied…….. 76

5.8 The maximum axial force results from each of the nine models in which the deck stiffness was incrementally varied……....83

8.1 Material property data used for wrought iron models……..……..... 106

8.2 Maximum axial forces resulting from various truck loads…… 110

8.3 Maximum axial force in connection at different percentages of posted capacity…….. 121

LIST OF FIGURES

Figure Page

2.1a Structural behavior of unstiffened arch……..10

2.1b Structural behavior of stiffened arch……..10

2.2 The influence of deck stiffening on arch bending stress and the existence of a critical point…….. 12

2.3 The influence of deck stiffening on arch bending stress and the location of two different open-spandrel designs……..15

3.1 The Woronoco Bridge showcases American open-spandrel design……..19

3.2 The maximum bending stress in the arch of the Woronoco Bridge using Billington's proposed simplified procedure and actual dimensions of the bridge……22

3.3 The maximum bending stress in the arch of the Woronoco Bridge using Billington's proposed simplified procedure and scaled dimensions of the bridge……23

3.4 The stiffness ratio and arch bending stress of the Woronoco Bridge plotted with reference to two curves…… 24

4.1a Four pinned-supports with spandrel columns pinned at each end……..….. 27

4.1b Moment diagram for the Woronoco Bridge model with maximum moment in the arch, $M_{A,max}$ = 4.64mT, located at quarter-span…...`27

4.2 The bending moment diagram that results from fixing the ends of the arch, but maintaining all other assumptions…… 30

4.3 Part of a construction plan showing the Woronoco Bridge abutment-arch connection……..31

4.4 Elevation of the Schwandbach Bridge……...32

4.5 Photograph of the Woronoco Bridge in which the spandrel columns are visibly enlarged where they are connected to the arch ribs……. 33

4.6a The deformed shape of the Woronoco Bridge model when end moment releases are removed from the spandrel columns..... 34

4.6b The moment diagram of the Woronoco Bridge model when end moment releases are removed from the spandrel columns, $M_{A,max}$ = 1.71 mT..... 34

4.7a Evidence of reinforcement in the spandrel columns that goes into the arch connection..... 36

4.7b Lack of cracking between the spandrel columns and the arch..... 37

4.7c Lack of cracking between the spandrel columns and the deck..... 37

4.8 The parabolic approximation used to represent the existing arch geometry of the Woronoco Bridge..... 39

4.9 Elevation of arch is scaled 75% and the maximum moment in the arch is 4.86 mT, located at quarter-span..... 40

4.10 Elevation of arch is scaled 50% and the maximum moment in the arch is 5.09mT, located at quarter-span..... 41

4.11 Elevation of arch is scaled 25% and the maximum moment in the arch is 5.56mT, located at quarter-span..... 41

4.12 Elevation of arch is scaled 59% and the maximum moment in the arch is 5mT, located at quarter-span..... 42

4.13a Decreased number of spandrel columns with a spandrel located at the anticipated location of maximum bending moment located at quarter-span..... 44

4.13b The moment distribution with decreased number of spandrels, $M_{A,max}$ = 4.89 mT located at quarter-span..... 44

4.14a Decreased number of spandrel columns with a spandrel located at the anticipated location of maximum bending moment..... 45

4.14b The moment distribution with decreased number of spandrels, $M_{A,max}$ = 5.74 mT located at quarter-span, moment in the deck at this location is 13.98 mT..... 45

4.15a Four pinned-supports with spandrel columns pinned at each end……46

4.15b Moment diagram with maximum moment, $M_{A,max}$ = 4.45mT……...46

4.16 Elevation of the Woronoco Bridge model showing three angles and the three corresponding moments of inertia……48

4.17 Moment diagram resulting from changing the approximated stiffness variation to the measured stiffness variation in the arch, $M_{A,max}$ = 8.89 mT……...49

5.1a Bending moment diagram with spandrel columns 8” x 8” square…… 55

5.1b Bending moment diagram with spandrel columns 16” x 16” square…… 55

5.1c Bending moment diagram with spandrel columns 28” x 28” square…… 56

5.2 Plot of the maximum bending moments in the arch, deck and columns as a result of varying the column stiffness…… 57

5.3 Plot of the maximum bending moment in the arch as a result of varying the column stiffness……..58

5.4a Axial diagram with spandrel columns 8” x 8” square……... 60

5.4b Axial diagram with spandrel columns 16” x 16” square……..…..... 60

5.4c Axial diagram with spandrel columns 28” x 28” square……... 60

5.5 Plot of the relationship between column stiffness and maximum axial forces in the three load-carrying members……61

5.6 The axial force distribution that results from a half-span live load is reflected in the sizing of the three load-carrying elements, seen in the elevation of the bridge……. 62

5.7a Elevation with spandrel columns 8” x 8” square……..……64

5.7b Elevation with spandrel columns 16” x 16” square……...64

5.7c Elevation with spandrel columns 28” x 28” square……...65

5.8a Bending moment diagram for nine columns……. 68

5.8b Bending moment diagram for twenty-one columns…….. 68

5.8c Bending moment diagram for forty-one columns……..... 68

5.9 Plot of the maximum bending moments in the arch, deck and columns as a result of varying column number……69

5.10a Elevation with eleven columns…….. 71

5.10b Elevation with twenty-one columns……..…… 71

5.10c Elevation with forty-one columns……..71

5.11 Plot of the relationship between column number and maximum axial forces in the three load-carrying members……73

5.12 Relationship between the maximum bending moment in each element and deck stiffness, based on the all-pinned computer model…….....76

5.13a Bending moment distribution for nine inch deck, all-pinned model……..... 77

5.13b Bending moment distribution for eighteen inch deck, all-pinned model..… 78

5.13c Bending moment distribution for thirty-two inch deck, all-pinned model… 78

5.14 Relationship between the maximum bending moment in the arch and deck stiffness, based on the all-pinned model…… 80

5.15 Relationship between deck stiffness and the maximum bending moment, based on the all-pinned model in which the column ends are unable to transfer moment……81

5.16a Bending moment distribution for nine inch deck, all-fixed model……82

5.16b Bending moment distribution for eighteen inch deck, all-fixed model……. 82

5.16c Bending moment distribution for thirty-two inch deck, all-fixed model…...82

5.17 Relationship between maximum axial force and deck stiffness, based on all-pinned model…… 83

5.18a Axial force distribution for nine inch deck, all-pinned model…….. 85

5.18b Axial force distribution for eighteen inch deck, all-pinned model…… 85

5.18c Axial force distribution for thirty-two inch deck, all-pinned model……. 85

5.19a Elevation of representative Woronoco Bridge model with eighteen inch deck…..... 86

5.19b Elevation of the thirty-two inch deck model.....86

7.1 Bardwell's Ferry Bridge illustrates the two structural forms integrated in lenticular bridges……98

7.2 The truss system is not engaged until there is a non-uniform load acting….99

7.3 One of three deck configurations provided in Douglas's 1878 patent…..….100

7.4 Profile of Douglas's 1885 patent……...…… 101

7.5 The opposition of compression and tension forces result in zero net horizontal force at the abutments, which only need to provide vertical support…….. 102

8.1 Photograph of Bardwell's Ferry Bridge…….105

8.2 Lower chord connection at Bardwell's Ferry Bridge…… 106

8.3 Elevation drawing of the Bardwell's Ferry Bridge with geometries of load-carrying elements……..... 107

8.4 View of 2-dimensional frame built in SAP2000……109

8.5a Axial force envelope that results from a moving truck load……..109

8.5b Axial force envelope that results from a moving truck load……..110

8.6 ADINA model of eccentric eye bar connection……112

8.7 ADINA model of concentric eye bar connection……..... 112

8.8 Concentric eye bar connection uses rectangular solids to create each eye bar and trapezoidal solids to create the pin around which all eye bars are connected…...…… 114

8.9 Each solid was subdivided in order to create meshes of relatively similar size…… 114

8.10 Final mesh of concentric connection model, created from subdivision of solid elements…… 114

8.11 In order to create a pin connection in the connection models, separate surfaces were defined…….. 116

8.12 Axial force distribution in eccentric model prior to definition of separate surfaces…… 117

8.13 Axial force distribution in eccentric model after definition of separate surfaces…… 118

8.14 Axial force distribution in concentric model after definition of separate surfaces…… 118

8.15 Bending occurs in the fixed eye bar of eccentric model when the right end is fixed and tensile force is applied to left end……..…… 119

8.16 Eccentric model in which both ends of pin are fixed and each eye bar is subjected to an equal and opposite tensile force……120

8.17 Axial force distribution of eccentric model in which both ends of pin are fixed and each eye bar is subjected to an equal and opposite tensile force…..……... 120

8.18 ADINA model of critical eye bar connection with axial stress distribution……122

8.19 The axial stress distribution of the front eye bar is similar to the results from the revised two-eye bar model in which the pin is fixed…….....123

8.20 Axial force distribution of three-bar concentric model is similar to previous two models…….. 123

8.21 Concentric connection model in which 1.875kip tensile force is applied to each of the eight nodes at the end of the left eye bar..…. 124

8.22 Cross-section of concentric model showing shear stress distribution resulting from tensile load……. 126

8.23 Cross-section of concentric model showing shear stress distribution resulting from tensile load……..……..…… 126

8.24 Cross-section of connection model showing shear stress distribution resulting from tensile load……. 128

8.25 Three cross-sections of shear distribution throughout eccentric truss connection model……... 129

8.26 S-N curve for notched and unnotched annealed ferritic ductile iron with a tensile strength of 65.8ksi……... 131

CHAPTER 1

INTRODUCTION/MOTIVATION

America's bridge-building history is told in part by photographs, narratives and analyses that have been developed and collected over the years. All documentation of this intriguing history, however, falls short of the surviving historical structures themselves. Unfortunately, the number of historical bridges still standing is ever-decreasing. This is partly due to uncertainty in the merits of the out-dated designs. Organizations such as the Historic American Engineering Record (HAER) suggest that an important step in preserving historic structures is to improve accessibility of data related to specific structures.[1] This paper sheds light on the structural behavior of two historical bridge designs: the iron lenticular truss bridge and the reinforced concrete open spandrel arch bridge. Specifically, an extant example of each bridge design is analyzed using modern, computer-based methods in order to better understand the structural merits of and thereby argue to preserve the two featured historic bridges. Additionally, it is hoped that the analysis methods developed and used for these two bridges can be applied to similar surviving examples of America's historic bridges.

There are two strong motivations behind applying modern analysis methods to evaluate the behavior of historic structures. The first is to better preserve these structures. One of the primary reasons that historic structures are replaced is the uncertainty surrounding the structure's ability to carry modern-day loads. However, this uncertainty can be alleviated through the application of modern analytical tools and should not be an acceptable justification for the destruction of America's historic structures. Many historic structures have withstood the test of time despite the fact that the mechanics

involved are not yet fully understood. Therefore, rather than accept this lack of knowledge, one of the goals of this paper is to increase our understanding of historical bridge behavior by modeling two existing historic bridges, investigating their behavior under specific loading conditions, and validating their structural integrity.

The second reason to investigate historic structures with modern methods is to provide insight for new design. With often scarce documentation of the early American design process, computer models can help to explain why engineers made certain design decisions. It is incredible that in the absence of these computer-based methods, early engineers were able to create a multitude of structures that are still standing and carrying substantial loads today. By understanding the design concerns of early engineers and how these have been incorporated into historic structures, the design and construction of structures that far surpass their life expectancy can be continued.

The lenticular truss bridge and the reinforced concrete open spandrel arch bridge are similar in many ways. Praised for their pleasing aesthetic forms, both designs were prominent in the New England bridge market for a distinct time. Both designs were developed, patented, and constructed before the age of computers and advanced analysis methods. Most fundamentally, however, both the lenticular and open spandrel arch designs utilize the arch in combination with another structural form to accommodate problematic, often non-uniform, live loads. The lenticular design uses the interaction between an arch and a suspension cable while the open spandrel bridge depends on the successful integration of an arch, columns, and a relatively rigid beam to withstand loads. By combining various load-carrying systems, both bridges were able to be lighter in appearance. And while the structural merit of the lenticular bridge was ridiculed by

engineers and the open spandrel arch bridge was praised, these two historical bridge designs represent intriguing attempts to advance bridge design through the innovative integration of two or more structural forms.

This paper is divided into two sections. The first section investigates the structural behavior of the Woronoco Bridge, an existing American reinforced concrete open spandrel arch bridge located in Russell, MA. A significant part of this investigation is the development of a representative American open spandrel bridge computer model. A theoretical model that had been developed to describe the structural behavior of open spandrel bridges designed by Swiss engineer Robert Maillart was used as a starting point. The assumptions inherent in the theoretical model were evaluated one by one in order to determine their applicability in the accurate depiction of American open spandrel arch bridge behavior.

Once the appropriate assumptions had been established and incorporated into the representative computer model, it is used to evaluate the structural behavior and design decisions of the Woronoco Bridge. Specifically, the representative model is subjected to a half span live load in order to compare its behavior with that predicted by the theoretical model describing the response of Maillart's bridges. Maintaining the same half-span live load, several parametric studies are performed to investigate the relationship between stresses in each of the load carrying elements and the stiffness of each of the load carrying elements. The three studies performed in this paper determine the effect of deck stiffness, column stiffness and column spacing on the maximum bending moments and maximum axial forces in each of the three load carrying members. From these relationships, the design decisions relating to each element's stiffness can be

more thoroughly understood. Additionally, the aesthetic implication of different design choices are assessed and determined to play an important part in the design of all three load carrying members.

The second section of this paper investigates the structural behavior of the Bardwell's Ferry Bridge, an iron lenticular truss bridge located in Shelburne, MA. A global, 2D finite element model of the bridge is developed and subjected to various rolling truck loads. These loads are scaled to different percentages of the bridge's current load posting. The forces that result from the loading of this model are then transferred to a local finite element model of a critical connection in the lower truss chord. By applying these forces to a more detailed model that captures the exact geometry and interaction between connection members, the critical locations in the connection can be identified. The magnitude of stresses at these locations can be determined and used to predict the fatigue life of the critical connection. Additionally, the identification of critical stress locations can be used to aid future inspection, monitoring and preservation efforts.

While the procedures used in each of the two sections of this paper are different, the motivation is the same. Each section applies modern, computer-based methods to better describe the structural behavior of a specific historic bridge with the intention of better understanding and preserving the ever decreasing number of historic structures. The two bridge types selected for use in this paper are an interesting pairing and each has its own significant part in America's bridge building history. The lenticular truss bridge dominated the New England bridge market for just under twenty years, despite negative criticism by the engineering community. The reinforced concrete open spandrel arch symbolized a movement away from traditional methods of construction and towards the

innovative use of new materials, the entire time praised by engineers. Despite their differences, however, both combine the arch with other load carrying members in order to make the structure lighter aesthetically. As is the case with many historic structures in America, they are both in need of increased preservation efforts due to the constantly decreasing number of extant examples.

PART I: REINFORCED CONCRETE OPEN SPANDREL BRIDGES

CHAPTER 2

BACKGROUND

2.1 Development of the American Open Spandrel Arch Bridge

The first ten years of the twentieth century were a time of much experimentation with the methods for concrete reinforcement in America. Just after this period, concrete construction became highly standardized and reinforcing bars were favored over steel sections. Well-known engineers such as J.A.L. Waddell acknowledged concrete's prevalence in the bridge building community.[2] In his 1917 treatise, Waddell noted:

> "Although the first patents for reinforced concrete were taken out some sixty years ago…it has been only twenty-five years since it was first applied extensively to bridge construction. Its use has increased so rapidly of late, however, that it is today one of the most important materials which the bridge engineer has at its disposal."[2]

With the relatively quick advancement and standardization of reinforcement came the widespread acceptance of reinforced concrete structures. Embraced for "its great strength, adaptability to a wide variety of circumstances, and its promise of durability"[2], reinforced concrete bridges overwhelmed the New England bridge market during the first half of the twentieth century. The focus soon shifted toward the development of different types of reinforced concrete arches and the receipt of patents. The race to design a more elegant reinforced concrete arch bridge while also minimizing the structure's self weight led to the design of many special versions of concrete arch bridges, including the reinforced concrete open spandrel arch bridge.

In America, several noteworthy engineers contributed to the emergence and embrace of reinforced concrete open spandrel arch bridges. Among these individuals was Edwin Thacher, who published one of the earliest specifications for reinforced concrete and

patented a deformed reinforcing bar that is seen as the predecessor to modern-day re-bar. Additionally, in 1896, Thacher "patented a bridge design incorporating the basic elements of open spandrel construction in vertical posts which carried deck loads to an arch rib."[2] This design not only gave the bridge a lighter appearance but also decreased the dead load of the structure. The latter allowed the arch to be flattened and bridge span to be lengthened. Texts written between 1910 and 1930 promoted the open spandrel design and applauded its aesthetic appearance, claiming it could be fit into any landscape without taking away from its natural beauty.[2]

Another engineer whose patents expressed the aspiration to reduce the bulkiness associated with traditional concrete arches was Daniel B. Luten.[2] In a 1907 patent, Luten designed an arch bridge which featured reinforcement of the arch barrel transversely as well as longitudinally. Stiffening the spandrel in this way permitted thinner arch sections.[3] Recipient of 52 patents, author of 100 technical articles, and designer of approximately 15,000 bridges[2], Luten contributed greatly to the advancement and success of reinforced concrete bridge designs in America.

2.2 Development of the Deck-Stiffened Arch

While engineers in America were working towards softening the appearance and experimenting with stiffening different elements of the reinforced concrete arch, it was abroad in Switzerland that deck-stiffened reinforced concrete arch bridges first flourished. This bridge type utilizes a stiff deck in order to alleviate bending in the arch. As a result, the arch is able to be made noticeably thin and flat. Well documented for his

innovative and graceful designs, Robert Maillart is primarily associated with the successful application of deck-stiffened reinforced concrete arch bridges.

Maillart's deck-stiffened arch bridges are aesthetically similar to American reinforced concrete open spandrel arch bridges. Therefore, it is of interest to investigate the theory behind and structural behavior of deck-stiffened bridges in order to determine whether or not and existing American example is, in fact, deck-stiffened. Not only will this help to better understand the development of American open spandrel bridges, but it will serve as a base upon which to develop an accurate and representative model of and example of the popular American bridge design.

2.2.1 Theory behind the Deck-Stiffened Arch Bridge

When an arch is loaded uniformly, the load is carried solely by axial forces (assuming the arch is not so flat that it behaves as a beam). Therefore, with an open spandrel bridge under uniform load, the deck load goes directly to the arch through vertical spandrels and then to the foundation without any significant bending in the arch. When an arch or open spandrel bridge is loaded over only half of the span, however, bending in the arch will occur unless the deck is sufficiently stiff to resist the deflection of the arch.

To better understand this behavior, author David Billington proposes that we begin by assuming the entire half-span load on the deck goes into the arch, as before[4]. Instead of simply compressing the arch as the full-span uniform load did, the uniform load acting over only half of the span will push the loaded half of the arch downward and the unloaded half of the arch upward. Because the deck is tied to the arch by vertically rigid spandrel columns, the deck will want to deform in a similar pattern (see Figure 2.1a). If

the deck is significantly stiff, however, it may resist the upward deformation of the arch and push the arch back down. If the deck is stiff enough, this resistance to deformation would simulate a uniform downward load on the previously unloaded half of the arch that is equal to half of the load on the loaded half of the span (see Figure 2.1b).

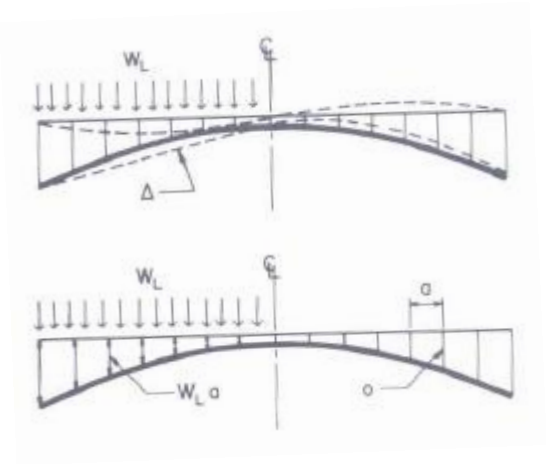

Unstiffened Arches

Figure 2.1a – Structural behavior of unstiffened arch (Figure 9-3a in *Robert Maillart's Bridges*).

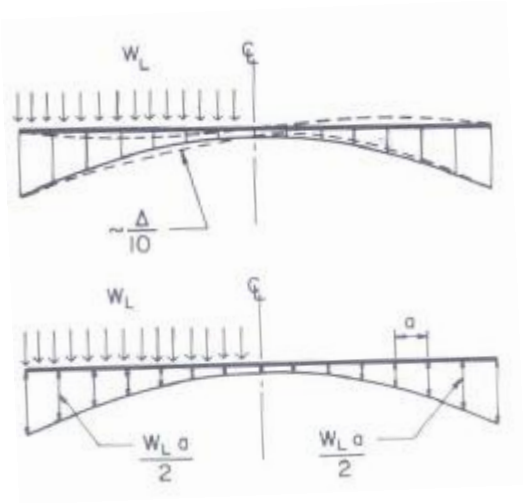

Deck-stiffened Arches

Figure 2.1b – Structural behavior of stiffened arch (Figure 9-3b in *Robert Maillart's Bridges*).

Therefore, when an arch is tied to a stiff deck, "the result is a uniformly loaded arch with axial forces only and a non-uniformly loaded deck with bending forces only."[4] This was Maillart's basis for analysis and it is outlined below in more detail for convenience:

> When one considers a two-hinged arch under a half span load W_L, the moment diagram will be two anti-symmetrical parabolas whose maximum moment values occur at quarter-span. The total half-span load, W_L, will be carried by both the arch and the deck, such that $W_L = W_A + W_G$. Thus, the maximum moment in the arch, M_A, is calculated with the following equation which depends on the part of the total load that is carried by the arch, W_A:

$$M_A = \frac{W_A l^2}{64} \qquad (1)$$

The stiffened deck will follow the same deflection pattern and similarly have maximum bending moment, M_G, at quarter-span as a result of the portion of the total load that is carried by the deck, W_G:

$$M_G = \frac{W_G l^2}{64} \qquad (2)$$

Just as the total load is $W_L = W_A + W_G$, the total moment is $M = M_A + M_G$. The deflection of the deck is straight-forward if we treat the half span as a simply-supported beam. Thus deflection of the beam is calculated as:

$$D_G = \frac{CM_G l^2}{EI_G}, \text{ where } C \text{ is a constant.} \qquad (3)$$

Arch deflections can then be determined by assuming the arch to be parabolic with a variation in moment of inertia such that $I_S \cos\theta_S = I_A$, where I_A is the moment of inertia at the crown of the arch and θ_S = the slope angle of the arch axis at any point.

From this, we get an equation for arch deflection that is similar to that for the deck:

$$D_A = \frac{CM_A l^2}{EI_A}, \text{ where } C \text{ is a constant.} \qquad (4)$$

Because the vertical spandrel columns are assumed to be closely spaced and axially rigid, Billington assumes $D_G = D_A$ and, as a result, the following are true:

$$\frac{M_G}{I_G} = \frac{M_A}{I_A} \qquad (5)$$

$$M_A = \frac{M_G I_A}{I_G} = \frac{M}{(1 + \frac{I_G}{I_A})} \qquad (6)$$

To see how the stiffness of both the arch and deck influence maximum arch bending stress, he looks at the stress in a rectangular arch section of depth h_A:

$$\sigma_A = \frac{M_A \cdot c}{I} = \frac{M_A \cdot h_A}{2 \cdot I_A} \qquad (7)$$

Substituting for M_A in equation (7) with the value from equation (6) gives:

$$\sigma_A = \frac{M}{[2I_G(\frac{I_A}{I_G h_A} + \frac{1}{h_A})]}, \text{ where } I_A = \frac{bh_A^3}{12} \qquad (8)$$

To investigate the effect of h_A on stress, Billington isolates the terms that depend on h_A (the terms in the parenthesis of the denominator). By taking the derivative of these terms with respect to h_A and setting it equal to zero, it is observed that a critical point exists:

$$\frac{bh_A}{6I_G} - \frac{1}{h_A^{\,2}} = 0 \qquad (9)$$

$$\frac{bh_A^{\,3}}{6I_G} = 1 \qquad (10)$$

Therefore, a critical point exists when $\frac{I_G}{I_A} = 2$ or $\frac{I_A}{I_G} = 0.5$.

The existence of a critical point at a stiffness ratio of 0.5 is significant. It is shown visually in David Billington's plot of maximum bending stress in the arch, σ_A, versus the relative stiffness of the arch, I_A/I_G. This plot has been recreated using the procedure outlined above and is shown below in Figure 2.2 for convenience.

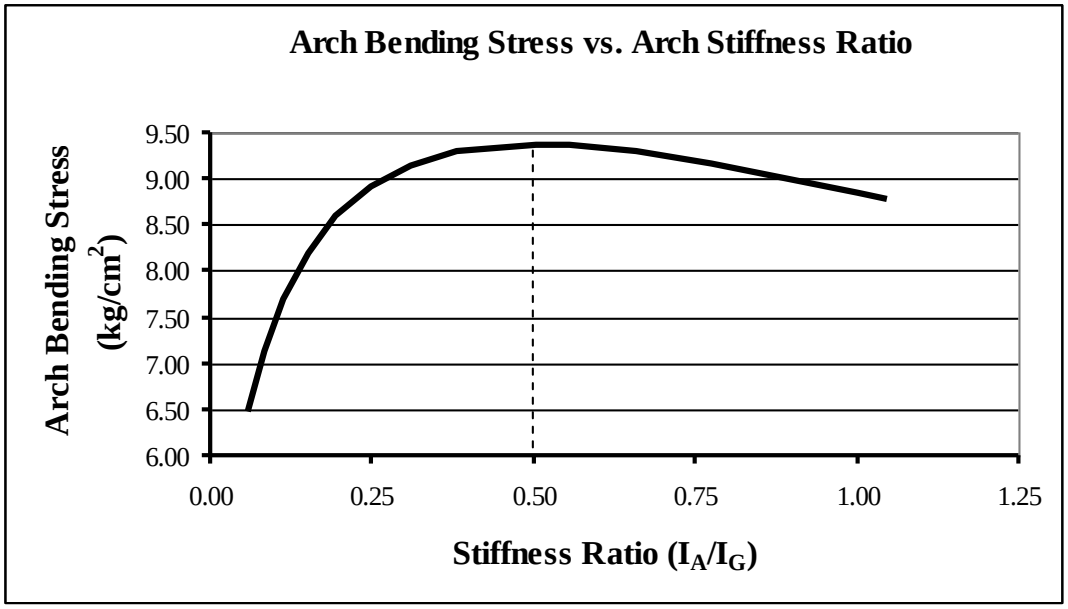

Figure 2.2 – The influence of deck stiffening on arch bending stress and the existence of a critical point (recreated from Figure 9-9 in *Robert Maillart's*

From this curve (Figure 2.2), one can see that if you were to start out with a relatively thin arch ($I_A < I_G/2$), an increase in arch stiffness would not be preferable as it would increase the maximum bending arch stress. On the other hand, if you were to start out with a relatively thick arch, a decrease in arch stiffness would not be preferable as it would increase the maximum bending stress in the arch.

It is important to note that this plot assumes a specific half-span live load, bridge span length and arch geometry; however, similar plots can be generated for different bridge loads, span lengths and arch geometries. Given the simplified procedure outlined above, any alterations to these variables would change the values for maximum bending stress in the arch but would not change the general shape of the curve and the existence of a critical point at the stiffness ratio of 0.5.

2.2.2 Application of Theory to Select Designs

David Billington applies the simplified analysis outlined previously to the Schwandbach Bridge. Using a half-span live load W_L = 1.5 tons/meter, l = 37.4 m, I_A = 0.0028 m^4 and I_G = 0.0485 m^4, he finds that M = 32.8 mT. From equation (6), M_A = 0.0545M = 1.79 mT. This results in a maximum bending stress in the arch (with depth, h_A = 20 cm and width, b = 4.2 m) of 6.4 kg/cm^2 (91 psi tension in bottom and compression in top). Thus, the live-load bending in the arch is reduced from 32.8 mT when it is completely un-stiffened to 1.79 mT with the stiffening deck present at Schwandbach. This reduction is 5.5% of the completely un-stiffened value[4].

As shown in Figure 2.3, the Schwandbach Bridge is located in the first region of the curve where $I_A < I_G/2$ and any increase in the arch thickness will cause the maximum

bending stress in the arch to increase. If instead the arch thickness at the Schwandbach Bridge was 41.2cm instead of 20cm and $I_A = I_G/2$, the maximum arch bending stress on the curve can be determined using equation (6):

$$M_A = \frac{M}{\left(1+\frac{I_G}{I_A}\right)} = \frac{M}{3} = \frac{32.8mT}{3} = 10.92mT$$

The maximum bending stress in the arch that corresponds to this relative arch stiffness ratio of 0.5 is given by substituting values into equation (7):

$$\sigma_A = \frac{10.92mT(0.412m)}{2(0.0245m^4)} = 91\frac{T}{m^2} = 9.19\frac{kg}{cm^2} = 130\,psi\,.$$

Billington observes that the majority of American open spandrel arch bridges of this span length have an arch thickness of at least 41 cm. Assuming that the width of the arch and the deck are the same, this would place most American bridges in the second region of the curve, as shown in Figure 2.3. According to Billington, it was common practice for American bridges to have $I_A = I_G$. From this perspective, decreasing the thickness of the arch would increase the maximum bending stress in the arch and would not be preferable if this was a primary design concern for American engineers as it was for Maillart.

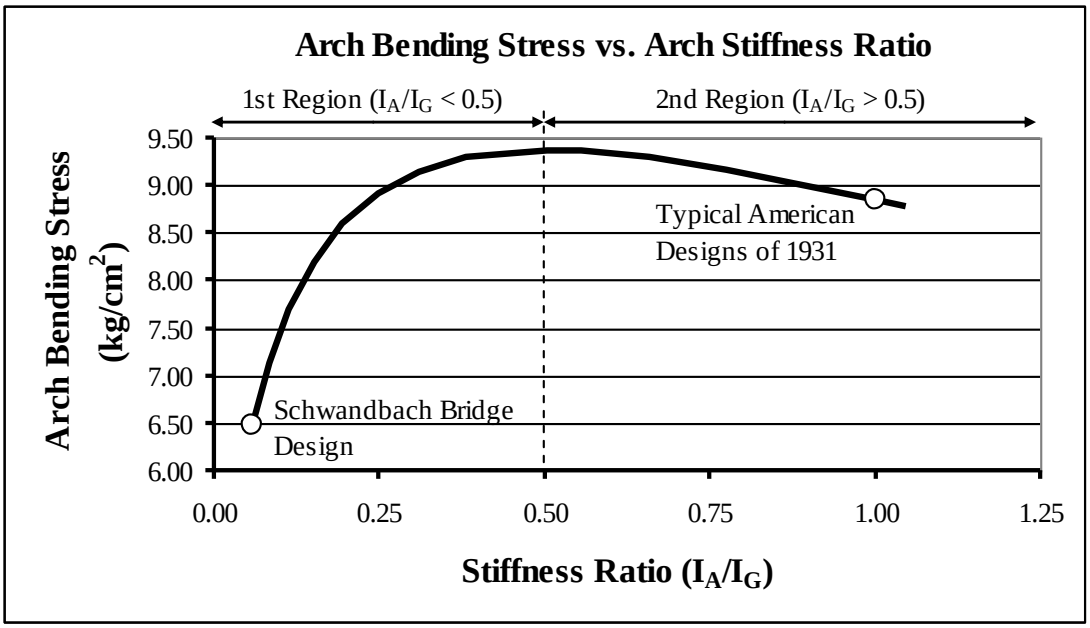

Figure 2.3 – The influence of deck stiffening on arch bending stress and the location of two different open-spandrel designs (recreated from Figure 9-9 in *Robert Maillart's Bridges*).

The fact that the Schwandbach Bridge falls within the first region of the curve shown in Figure 2.3 and that typical American open spandrel bridges fall within the second region demands further investigation and explanation. It is unclear what assumptions are involved in this simplified method and, more importantly, whether or not these assumptions can appropriately be applied to existing examples of American reinforced concrete open spandrel bridges.

Through the use of modern analysis methods and finite element computer models, American open spandrel bridges can be more accurately represented and analyzed. Once the assumptions used in the simplified procedure above are identified and their applicability to American open spandrel bridges evaluated using modern analysis methods, a representative American open spandrel bridge model can be created. This model can then be used to investigate the rationale behind design decisions made for

American open spandrel bridges. Not only will this investigation shed light on the design priorities of early American bridge engineers, but also it will serve as a means to compare the structural behavior of an existing American open spandrel bridge with those of highly acclaimed Swiss engineer Robert Maillart.

2.3 Differences between American and Swiss Designs

Billington proposes that the difference in the location of Swiss and American open spandrel bridges on the curve that plots relative arch thickness and arch bending stress can partly be explained by the different methods used during design development. While Maillart used the simplified theoretically-based analysis outlined in Section 2.2, American engineers seemed to rely heavily on experimental methods to guide their designs. At the same time that Maillart's final deck-stiffened bridge was completed, the American Society of Civil Engineers produced a report regarding the design of reinforced concrete arches. Although American engineers knew of Maillart, the ideas observed in this publication seem to have little in common with those employed by the innovative Swiss engineer[4]. The method proposed in this publication for the analysis of stresses in an open spandrel bridge is cited below:

> "(a) determine the dead-load stresses analytically on the basis that the dead load is carried by the rib [arch] unrestrained by the deck. (b) determine the live-load stresses by an experimental method using elastic models, considering the structure as a whole and not the rib alone. This is important because of the effect of the deck participation upon the stresses in the deck and columns rather than because of its effect upon the stresses in the rib. (c) determine the shrinkage and temperature stresses by an experimental method using elastic models of the structure as a whole." (From Billington's book *Robert Maillart's Bridges*, reference to: C.T. Morris et al., "Final Report of the Special ASCE Committee on Concrete Arches," *Transactions ASCE*, 100 (1935): 1431.)[4]

Unlike Maillart, the American engineers determined the stresses in the deck and the arch that resulted from live loads through experimentation rather than theory. In fact, the publication refers to the theoretical analysis for this type of structure as a complicated undertaking and comments that the time it takes to perform such a task is excessive[4].

Contrary to the theoretical analysis performed by Maillart, the American publication does not indicate that the stiffness of the deck may be increased in order to make the arch thinner. In the American tests that were run, the stiffness of the deck and the arch were often comparable. The result of this oversight was substantial bending in the arch and thus the necessity of a thick arch. While the Americans observed that deck participation could be valuable, much time was spent studying the effect of removing this stiffening effect. Looking again at Figure 2.3, the attempt to reduce deck stiffness is an understandable one if the initial American designs were located within the second region of the curve. In the attempt to understand complex details through the testing of small-scale, partial models, Billington states that American engineers seemed to lack the understanding of overall behavior and interaction of the deck and arch that Maillart relied upon[4].

This provides one explanation for the differences between Swiss and American open spandrel bridges in regards to their location on Billington's curve. Through relying heavily on experimental methods, it is possible that American engineers were not aware of the first region of the curve within which Maillart was focusing his designs. However, there is another possibility that has not yet been discussed in sufficient detail. Perhaps the design concerns for American engineers were such that they were not striving to reduce the maximum bending stress in the arch in the same way as Robert Maillart.

Billington's curve assumes a half-span live load and only investigates the relationship deck stiffness and bending in the arch. It is possible that American engineers were considering different load conditions and other ways of minimizing bending in the arch. This paper focuses on the investigation of the latter possibility.

American reinforced concrete open spandrel arch bridges that are aesthetically similar to those designed by Maillart still stand today. While the evolution of the design is not as thoroughly documented, the end result is comparable: an often elegant combination of an arch and a deck through the employment of vertical elements. Like Maillart, American engineers strove to design thinner structural members that could span greater lengths. Using two different design approaches, however, it is of interest to evaluate a surviving American reinforced concrete open spandrel bridge using modern methods to determine when, if ever, American engineers identified the advantages of deck-stiffening and began to design bridges as Maillart did, with $I_A < I_G/2$. Additionally, it is important to investigate the applicability of Billington's simplified analysis to American open spandrel bridges in order to create a representative model. With this new model, further justification for the differences between American bridges and the bridges of Robert Maillart can be provided.

CHAPTER 3

PRELIMINARY ANALYSIS

3.1 Simplified Analysis to the Woronoco Bridge

In order to perform this study, construction drawings of four existing reinforced concrete open spandrel bridges in Massachusetts were obtained from Mass Highway. The dimensions of each bridge were taken from scaled drawings as well as written descriptions that are available from the Library of Congress (LOC) [2]. Before generating computer models of the bridges using SAP2000 software, each bridge was evaluated using Billington's simplified procedure (outlined in Chapter 2) to determine if any deviated from the expected stiffness ratio for typical American bridges of $I_A/I_G = 1$. Of the four bridges, the Woronoco Bridge (located in Russell, MA) deviated from the expected location on Billington's proposed curve relating the relative stiffness of the arch and maximum bending stress in the arch. The preliminary analysis of the Woronoco Bridge (Figure 3.1) is provided below.

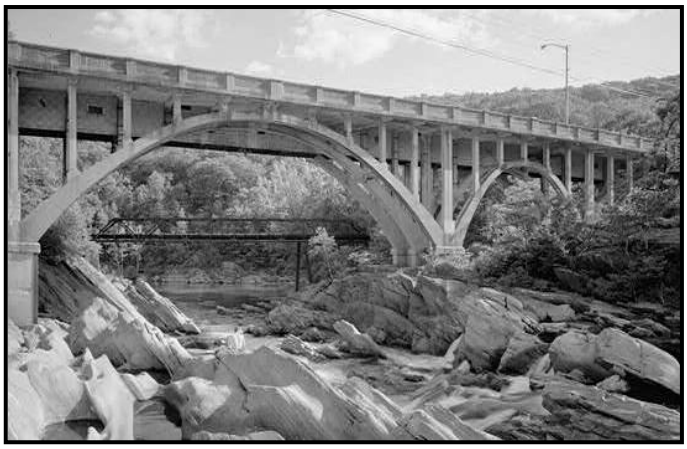

Figure 3.1 – The Woronoco Bridge showcases American open-spandrel design (photograph courtesy of HAER/Library of Congress).

The Woronoco Bridge is a reinforced concrete open spandrel bridge that was constructed in 1923. From written descriptions of the bridge (courtesy of HAER and LOC) as well as construction drawings for the bridge (courtesy of Mass Highway), the following geometric properties for the bridge were determined:

Span Length, l = 104' = 31.76 m
Deck thickness, h_G = 18" = 0.4572m
Deck width, b_G = 26'-8" = 320" = 8.128m
Arch thickness at crown, h_A = 18" = 0.4572m
Arch width, b_A = 6'-6" (3 arches at 2'-2" wide each) = 78" = 1.9812m

With these values, the simplified procedure outlined previously in Section 2.2.2 can be applied to see whether or not the arch-to-deck stiffness ratio of this existing American bridge differs significantly from that proposed by Billington for typical American bridges ($\frac{I_A}{I_G} = 1$):

$$I_A = \frac{(1.9812m)(0.4572m)^3}{12} = 0.015779m^4$$

$$I_G = \frac{(8.128m)(0.4572m)^3}{12} = 0.064732m^4$$

$$\frac{I_A}{I_G} = \frac{0.015779m^4}{0.064732m^4} = 0.24375$$

This ratio not only differs from the typical value of unity, but also is less than the critical value of 0.5. This places the bridge in the first region of the curve where an advantage to deck-stiffening is observed.

Completing the procedure outlined by Billington (assuming W=1.5 tons/meter), we can orient this bridge with regard to the curve shown in Figure 2.3**.**

$$M_A = \frac{M_G I_A}{I_G} = \frac{M}{(1+\frac{I_G}{I_A})} = \frac{M}{1+4.1024} = \frac{M}{5.1024}$$

$$M = \frac{Wl^2}{64} = \frac{(1.5\frac{tons}{m})(31.76m)^2}{64} = 23.6414mT$$

We can then find the maximum anticipated moment in the arch and the resulting maximum bending stress in the arch:

$$M_A = \frac{M}{5.1024} = \frac{23.6414mT}{5.1024} = 4.63mT$$

$$\sigma_A = \frac{M}{[2I_G(\frac{I_A}{I_G h_A} + \frac{1}{h_A})]} = \frac{23.6414mT}{[2(.064732m^4)(\frac{.015779m^4}{(.064732m^4)(.4572m)} + \frac{1}{.4572m})]} = 67.1265\frac{tons}{m^2}$$

$$\sigma_A = 6.09\frac{kg}{cm^2}$$

When this arch stress is plotted against a curve that shows the relationship between bending stress in the arch and relative stiffness of the arch, as the one Billington created for the Schwandbach Bridge, the result is Figure 3.2. Note that the general shape of the curve and the location of a critical point are the same as the curve that which Billington proposes. However, the magnitudes of bending stress in the arch are different. This is due in part to the shorter length of the Woronoco Bridge.

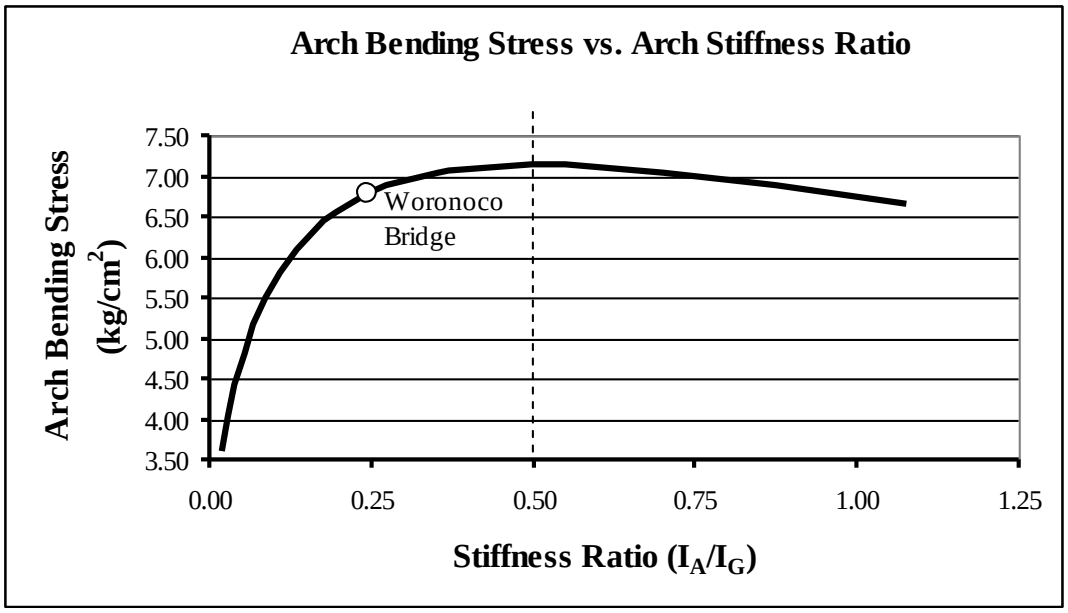

Figure 3.2 – The maximum bending stress in the arch of the Woronoco Bridge using Billington's proposed simplified procedure and actual dimensions of the bridge.

When performing this calculation on the Schwandbach Bridge, Billington found M = 32.8mT rather than 23.6414mT because the bridge span was 37.2m in length whereas the Woronoco Bridge is 31.76m in length. If we scale up the dimensions of the Woronoco Bridge such that the span would be 37.2m like the Schwandbach Bridge (for ease of comparison), and we assume that the stiffness ratio would remain the same, then the bending stress associated with this new, longer span length will be:

$$M = 32.8mT$$

$$M_A = \frac{M}{5.1024} = \frac{32.8mT}{5.1024} = 6.43mT$$

$$\sigma_A = \frac{M}{[2I_G(\frac{I_A}{I_G h_A} + \frac{1}{h_A})]} = \frac{32.8mT}{[2(.064732m^4)(\frac{.015779m^4}{(.064732m^4)(.4572m)} + \frac{1}{.4572m})]} = 93.1311\frac{tons}{m^2}$$

$$\sigma_A = 9.4\frac{kg}{cm^2}$$

Looking again at the curve proposed by Billington, we can plot the Woronoco Bridge based on its arch-to-deck stiffness ratio as well as the calculated maximum bending stress in the arch (Figure 3.3).

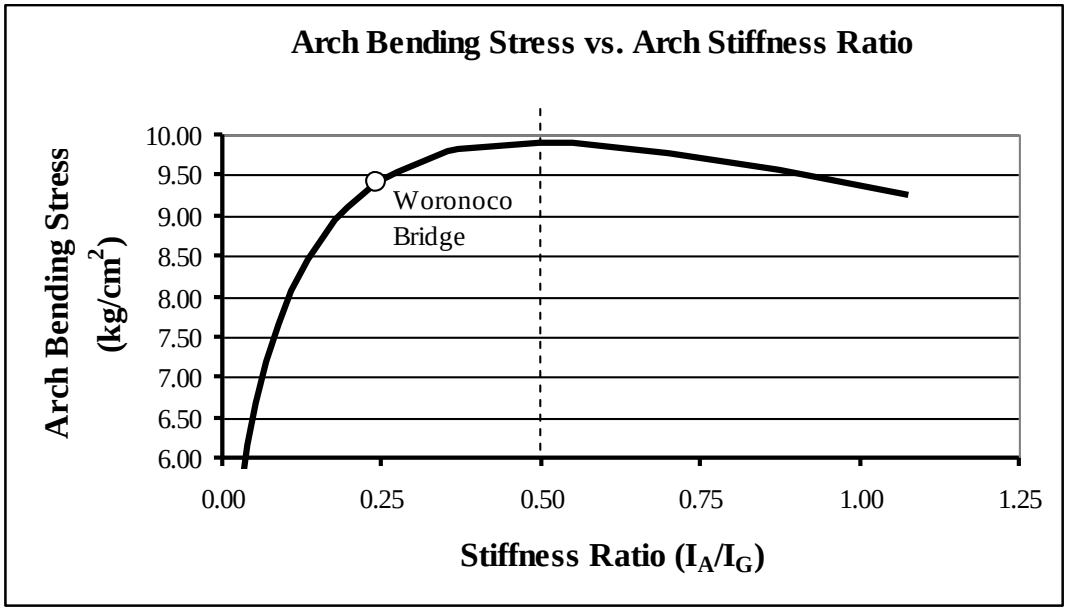

Figure 3.3 – The maximum bending stress in the arch of the Woronoco Bridge using Billington's proposed simplified procedure and scaled dimensions of the bridge.

From this figure, note that the magnitude of the stresses are different from those in Billington's curve that compares the Schwandbach Bridge and Typical American Designs of 1931. The difference in stress magnitudes can be seen visually in Figure 3.4. While the length of the bridge has been modified to agree with the length of the Schwandbach Bridge, used by Billington, the arch is ribbed and so the thickness of the arch for a given moment of inertia will be higher. The equation for stress in the arch is calculated using equation (7) from before:

$$\sigma_A = \frac{M_A \cdot c}{I} = \frac{M_A \cdot h_A}{2 \cdot I_A}$$

Since the Woronoco Bridge has three ribbed arches rather than one broad arch, it requires a thicker arch in order to achieve a given arch stiffness (and stiffness ratio). Bending stress in the arch is proportional to the arch thickness. Therefore, bending stress must increase if the thickness of the arch increases. The important point, however, is that despite the specific values of bending stress Figure 3.4 clearly shows that the Woronoco Bridge is located in the first region of the curve.

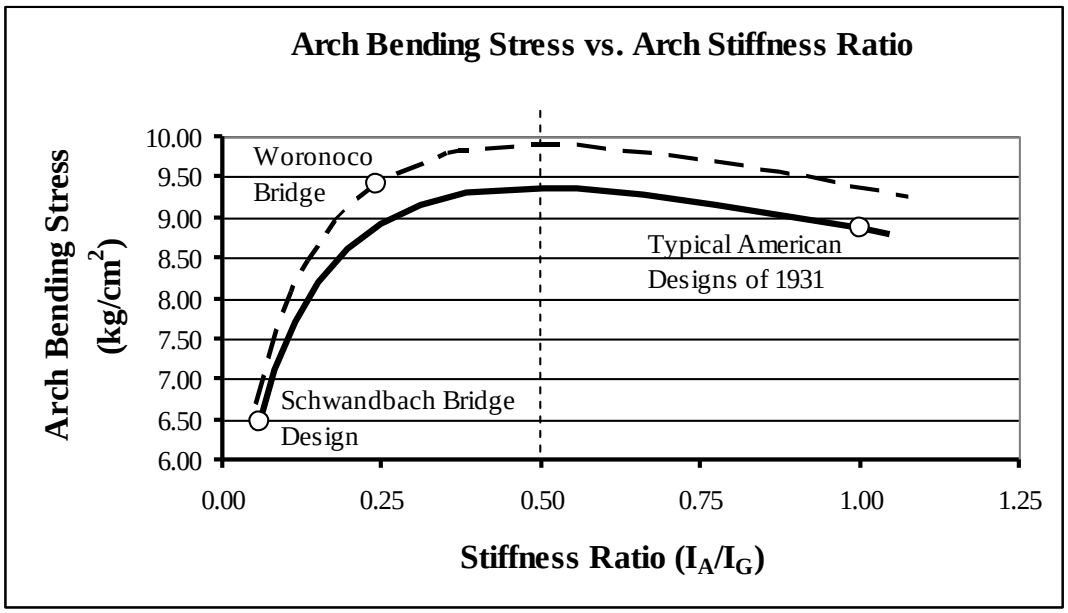

Figure 3.4 – The stiffness ratio and arch bending stress of the Woronoco Bridge plotted with reference to two curves: one accounting for the Woronoco Bridge's ribbed arch (dotted line) and one assuming a single, broad arch (solid line).

The stiffness ratio of the Woronoco Bridge differs from that which Billington anticipated for typical American reinforced concrete open spandrel bridges. While the thickness of the deck and the arch crown are each eighteen inches, the width of the deck is substantially larger than the width of the arch. In the Woronoco Bridge, the arch is divided up into three ribs, each of dimensions 2'-2" wide. This results in an arch –to-deck stiffness ratio of 0.25 rather than 1, which would be the case if the arch were a

single member whose width was the same as the width of the deck. From this, it would seem that American open spandrel designs that employ arch ribs rather than a single, broad arch reduce the relative stiffness of the arch and thus reduce the maximum bending stress in the arch. Perhaps Billington assumed that the arch width was always the same as the deck width or perhaps he did not consider these examples of American open spandrel bridges when he refers to typical American designs.

The preliminary analysis of this bridge is promising; however, the simplified procedure used is based on several assumptions that may not be entirely appropriate for this bridge. In addition to the question of whether or not typical American open spandrel bridges tend to have a relative stiffness ratio of 1 (as Billington suggests), there are questions surrounding the applicability of the assumptions involved in the simplified analysis procedure used to generate these curves. Once the appropriateness of the assumptions used in this simplified procedure are identified and evaluated, a model that accurately represents the behavior of American open spandrel bridges can be developed using modern computer-based methods. This will not only help to better preserve these structures, but will also provide justification and rationale for their design development.

CHAPTER 4

DEVELOPMENT OF WORONOCO BRIDGE MODEL

4.1 Identification of Assumptions involved in Simplified Analysis

Billington's curve was developed using the assumptions Robert Maillart employed in designing the Schwandbach Bridge rather than the principles employed by American bridge engineers. Therefore, it is possible that some of these assumptions are not applicable to American examples of reinforced concrete open spandrel bridges. This curve, however, provides a starting point for the development of a model that is based on and representative of an existing example of an American open spandrel bridge. By identifying whether or not the assumptions inherent in this curve are appropriate for an existing example of American design, each assumption can then be maintained or altered in order to create a bridge model that correctly represents the behavior of an existing American open spandrel bridge.

In order to evaluate the applicability of Billington's curve for use in describing American bridge behavior, the assumptions used in his simplified analysis procedure described in Section 2.2.1 are identified in order to evaluate the appropriateness of each in reference to the Woronoco Bridge (an existing American open spandrel bridge). In this effort, a 2D finite element model whose behavior matches that predicted using the simplified procedure was created with SAP2000. By generating a computer model whose behavior agrees with the behavior Billington proposes, the assumptions inherent in the simplified method can be identified. Using this calibration model as a starting point, whether or not each assumption is an appropriate approximation for the Woronoco Bridge can be evaluated.

To calibrate the model, a uniform live load was placed over half the span (W_L = 1.5 tons/m) as was done in the simplified analysis outlined in Section 2.2. The span of the computer model is 31.76m (the actual length of the Woronoco Bridge) and, as a result, the maximum bending moment in the arch is expected to be 4.63mT at quarter-span according to the simplified calculations shown previously (See Section 2.2.1). Figure 4.1a shows the undeformed shape of the SAP2000 model that agrees with the behavior anticipated from the simplified procedure. Figure 4.1b shows the bending moment diagram for both the arch and the deck.

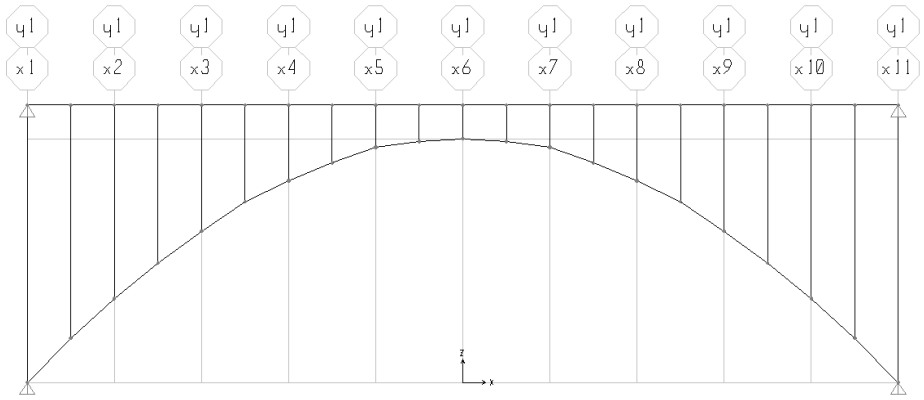

Figure 4.1a - Four pinned-supports with spandrel columns pinned at each end (moment of inertia in arch varies with $I_S \cos(\theta_S) = I_A$, where each member is the larger of the calculated values at each end).

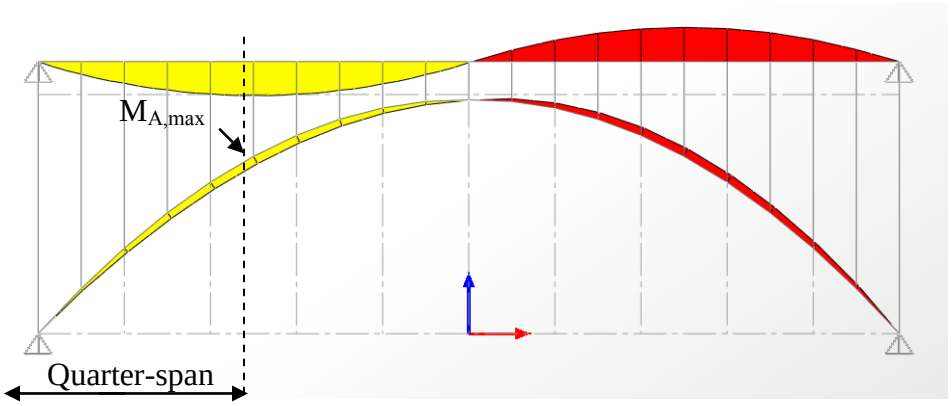

Figure 4.1b - Moment diagram for the Woronoco Bridge model with maximum moment in the arch, $M_{A,max}$ = 4.64mT, located at quarter-span.

As was predicted using the simplified procedure, the maximum bending moment in the arch is 4.64mT and it occurs at quarter-span.

From the 2-dimensional calibrated computer model, the major assumptions necessary to achieve agreement with Billington's simplified procedure have been identified and are summarized below.

1) The arch and deck supports are all pinned and cannot carry any bending moment.
2) The spandrel columns are all pinned at both ends and cannot transfer moment between the arch and the deck.
3) The arch is parabolic in shape. It is unclear if the simplified method is appropriate for other parabolic shapes (flatter parabolas).
4) The accuracy of the approximation depends on the number of columns. Increasing the number of columns improves the approximation. Also, there needs to be a spandrel column at quarter-span in order to achieve a maximum bending moment in the arch at that location.
5) The arch stiffness varies according to $I_S \cos(\theta_S) = I_A$ (with the closest agreement coming from assigning each beam element the larger of the two values).

Each of these assumptions was developed from and is appropriate for use in representing Robert Maillart's Schwandbach Bridge. Their accuracy in representing the actual behavior of the Woronoco Bridge, however, is questionable and is investigated in more detail in the following section.

4.2 Evaluation of Modeling Assumptions

To determine the validity of each assumption for use in the modeling of American open spandrel bridges, the calibration model was altered by removing one assumption at a time. This way, each assumption's affect on the bending moments in both the deck and the arch could be observed. Once the impact of each assumption is known, their appropriateness for use in describing the behavior of an existing example of an American open spandrel bridge can be evaluated.

4.2.1 Assumption 1: Pinned Bridge Supports

The first assumption made in order to achieve agreement between the computer model and the simplified analysis proposed by Billington is that the supports at either end of the deck and the arch are pinned. This allows for free rotation at either end of the deck and arch. As a result of this assumption, there cannot be any bending moment at the abutments and the bending moment distribution for both the beam and the deck is comprised of two anti-symmetric parabolas.

The appropriateness of this simplification is questionable considering the Woronoco arch is considerably thicker near the abutments than at any other point along the span (54" thick at the abutment as opposed to 18" at the crown of the arch). If the Woronoco Bridge designers sized sections in order to efficiently resist anticipated stresses, the largest members would be placed at the locations that were expected to carry the maximum stresses. If this is the case, then assuming that the arch is pinned at the abutments may not accurately represent the intended structural behavior of the bridge if the ends of the arch were sized to carry both axial forces and bending moments. To investigate how this assumption affects the bending moment distribution and to establish whether or not it is a reasonable assumption in regards to the Woronoco Bridge, the end supports of the arch were changed from fully pinned to fully fixed in the computer model (Figure 4.2).

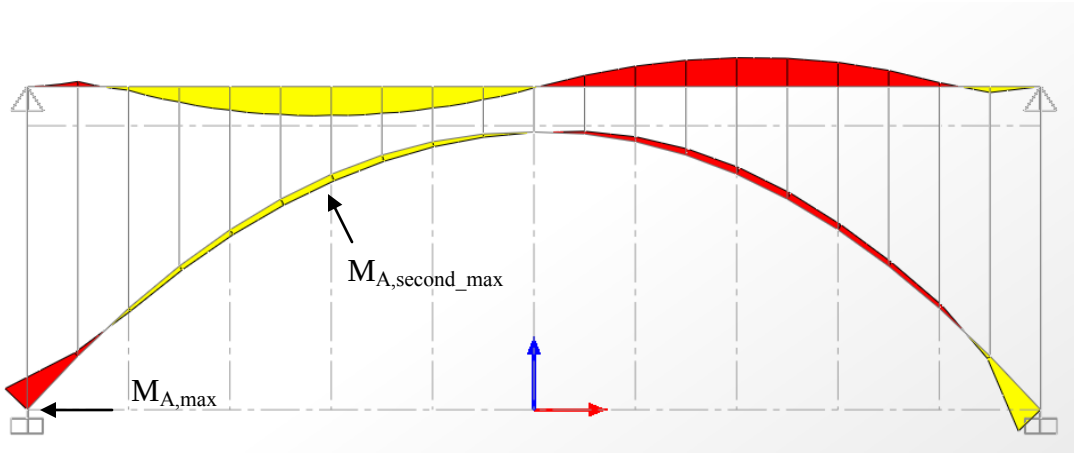

Figure 4.2 – The bending moment diagram that results from fixing the ends of the arch, but maintaining all other assumptions ($M_{A,max}$ = 14.437mT at the arch abutment).

The magnitude and location of the maximum moment differ from the calibrated model. There is a significant increase in the bending moment at the abutments where the maximum moment in the entire bridge model occurs (Figure 4.2). This behavior potentially justifies the substantial thickness of the arch at the abutments.

Aside from the jump in bending moment at the abutments, however, the shape of the bending moment diagram for the rest of the bridge model is similar to the calibrated model that agrees with Billington's results. The maximum arch bending moment within the part of the bridge that is represented by two anti-symmetric parabolic bending moment diagrams is 3.36 mT. The maximum bending in the deck of this model is 13.74 mT. Both of these relative maximum bending moments are less than those found in the calibration model (where the arch abutments were pinned). By fixing the arch at its ends, the bending moments concentrate at the abutments but then reduce throughout the rest of the bridge.

This tradeoff between the two models is an important issue to consider. Manipulating the location and magnitude of maximum stresses in the bridge is related to bridge

maintenance and performance over time. It raises the question of which reinforced concrete open spandrel elements typically need the most repair or replacement. Depending on where these types of American bridges typically need to be restored, there may be a benefit to concentrating the bending moment in different locations to reduce these characteristic repairs.

The Woronoco Bridge is currently closed and access to inspect or photograph the actual arch abutment is limited. Figure 4.3 is part of a construction plan provided by MassHighway that was used in the process of making repairs to the bridge. Note that the thickness of the arch at the abutment is provided on the drawing. Insight into the fixity of the arch abutment can be gained by comparing the construction drawing of the Woronoco Bridge with a construction drawing for the Schwandbach Bridge[4] (Figures 4.3 and 4.4, respectively).

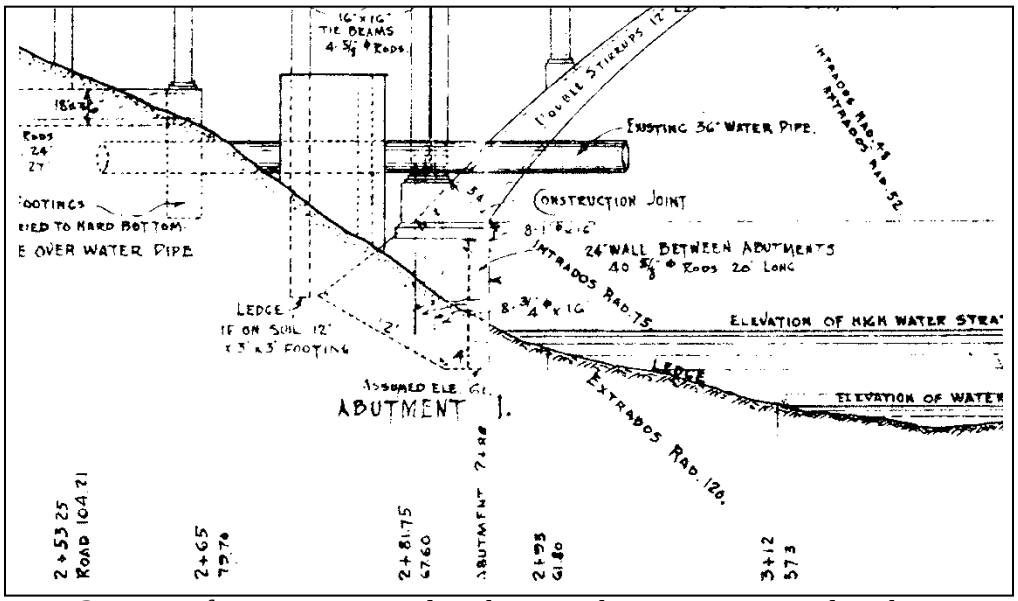

Figure 4.3 – Part of a construction plan showing the Woronoco Bridge abutment-arch connection (courtesy of MassHighway).

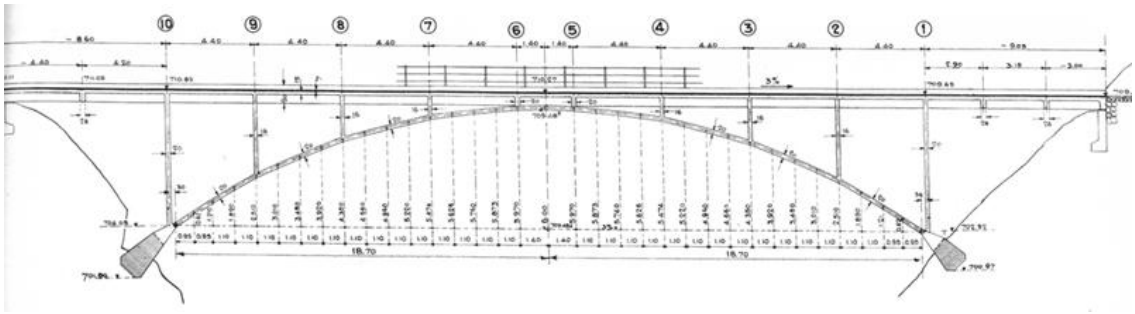

Figure 4.4 – Elevation of the Schwandbach Bridge[4].

Comparing the arch abutments of the Woronoco Bridge to those at the Schwandbach Bridge, it is clear that both abutments are not deeply imbedded into the foundation. It is known from the assumptions Maillart employed in the design of this bridge that he intended for these abutments to function as pinned supports. Because they are placed shallowly into the ground, they are relatively free to rotate.

The abutment of the Woronoco Bridge is also shallow. From this similarity, the Woronoco Bridge arch abutment is most accurately modeled as a pinned connection. In reality, though, the abutment would be partially restrained because it is not a literal "pin" connection. To capture this partially-restrained behavior, two models must be constructed: one where the arch abutments are pinned and one where the arch abutments are fixed. By creating an envelope solution to resolve this problem, the actual behavior of the bridge will be bounded within the results of the two models. However, the results for the pinned model will be primarily considered.

4.2.2 Assumption 2: Pinned Spandrel Columns

The second assumption made in the calibrated computer model in order to achieve agreement with Billington's predicted behavior was to release the fixity at both ends of each spandrel column. The spandrels in the calibrated model are assumed to be pinned at both ends. As a result, they are unable to transfer bending moments between the deck and the arch and do not carry any bending moment themselves. From photographs of the Woronoco Bridge, however, the ends of the spandrel columns get visibly larger at each end (Figure 4.5). This geometric variation could be purposeful to ensure moment transfer or it could be entirely aesthetic. Regardless of the motivation behind enlarging the spandrels at the ends, it is questionable to assume that the ends of each spandrel columns are truly pinned to the arch and the deck. To determine the importance of this assumption, a model was created in which the column end-releases were modified in order to allow for moment transfer at both ends of each column.

Figure 4.5 – Photograph of the Woronoco Bridge in which the spandrel columns are visibly enlarged where they are connected to the arch ribs (courtesy of HAER/LOC).

To investigate the appropriateness of the assumption that all spandrel columns are pinned at either end, a computer model was created where the ends of all the spandrel columns were fixed to the beam and arch. As before, all other assumptions made in order to achieve agreement with Billington's simplified analysis were maintained. The columns were fixed to the deck and arch by removing the end moment releases of each spandrel column. The deformation of this modified model is shown in Figure 4.6a and shows how each end of each spandrel maintains its original, undeformed angle with respect to the deck and the arch at the connection point. Figure 4.6b shows the resulting bending moment diagram in the structure.

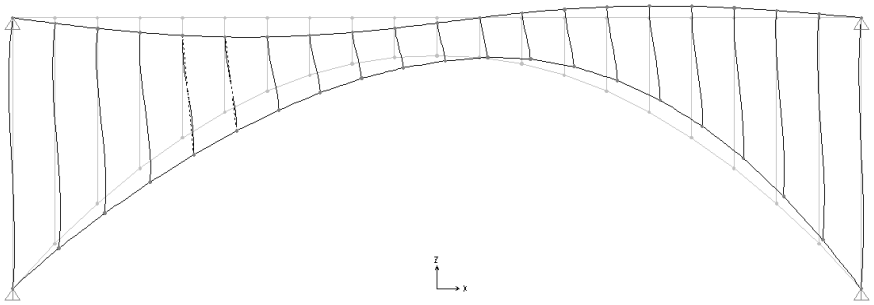

Figure 4.6a – The deformed shape of the Woronoco Bridge model when end moment releases are removed from the spandrel columns.

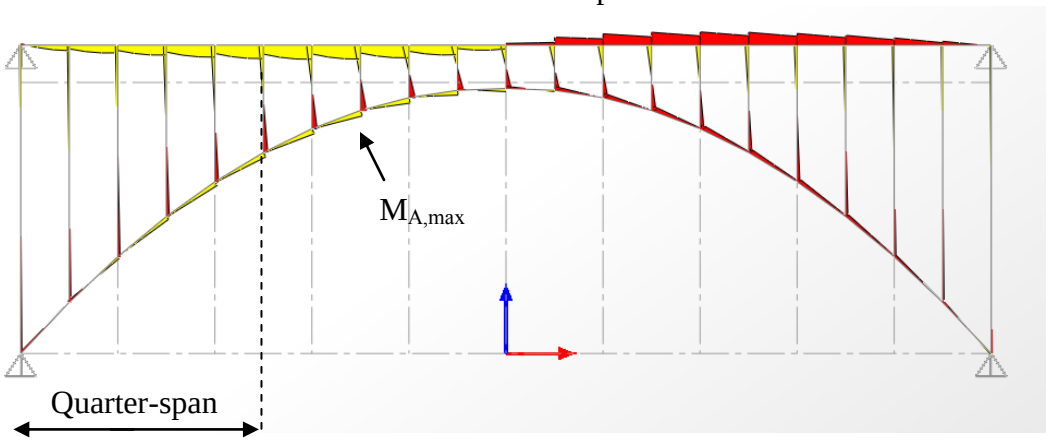

Figure 4.6b – The moment diagram of the Woronoco Bridge model when end moment releases are removed from the spandrel columns, $M_{A,max}$ = 1.71 mT (the bending moment in the deck at quarter-span is 4.15 mT and maximum bending moment in the spandrel columns at this location is 1.814 mT).

From Figure 4.6b, it is clear that there are jumps in the bending moment where a column is frames into an arch or deck element. While the general moment distribution is similar in shape to the calibration model (two anti-parabolic shapes), there are significant differences.

Not only has the location of maximum moment changed, as indicated in Figure 4.6b, but also it appears that fixing the columns at both ends significantly decreases the maximum moment in both the deck and the arch. By comparing the maximum bending moments in this model to those found in the calibration model, where columns behaved purely as axial members that did not carry any moment, the arch and deck benefit from fixing the columns at both ends (see Table 4.1). As with the issue of arch fixity to the abutment, a trade off has been identified. While fixing the columns would complicate their design in that they would now carry bending moment (the maximum column bending moment is 1.8mT), it would reduce the bending moment in both the arch and the deck. Which behavior is preferable depends on which elements typically require more maintenance over the life of the bridge.

Table 4.1 – Comparison of bending stresses when spandrels are pinned or fixed.

Maximum Bending in Arch (mT)		**Maximum Bending in Deck (mT)**	
Spandrels Pinned	Spandrels Fixed	Spandrels Pinned	Spandrels Fixed
4.64	1.71	19	4.15

The end fixity of the spandrel columns clearly has a significant impact on the bending moment distribution throughout the open spandrel bridge. Before one can accurately model the bridge and identify which elements are most susceptible to fatigue over time, one must determine whether or not the spandrel columns in the Woronoco Bridge should be modeled as pinned or fixed at either end. Since the Woronoco Bridge is still standing,

this question can be resolved through visual inspection of the columns where they connect to the deck and the arch. Any evidence of metal reinforcement, as well as the lack of significant concrete cracking at the connection, supports the decision to model the spandrels columns as fixed to both the deck and the arch. Figure 4.7 shows recent photographs of the spandrel columns condition near these connection points.

Figure 4.7a – Evidence of reinforcement in the spandrel columns that goes into the arch connection (photograph taken in June 2009).

Figure 4.7b –Lack of cracking between the spandrel columns and the arch (photograph taken in June 2009).

Figure 4.7c –Lack of cracking between the spandrel columns and the deck (photograph taken in June 2009).

The photographs provided in Figure 4.7 clearly show both the presence of metal reinforcement and the absence of significant concrete cracking in the columns. While the Woronoco Bridge columns were rehabilitated at some point after construction and these pictured may not indicate the original bridge condition, it is clear that the spandrel columns are currently fixed to both the arch and the deck. And since the overarching motivation of this paper is to better preserve existing historic structures through the employment of modern methods based on existing conditions, the Woronoco Bridge model will feature spandrels that can transfer moments between the deck and the arch.

4.2.3 Assumption 3: Parabolic Shape of Arch

The third assumption made in Billington's simplified analysis is that under uniform loading the arch will carry its portion of the total load solely through axial forces. This was a valid approximation for Maillart's deck-stiffened bridges and was one that Maillart was aware of in the selection of his arch forms[4]. However, it ceases to be an appropriate assumption for bridges in which the parabolic arch is flat enough that it begins to behave as a beam member.

To create the calibration model of the Woronoco Bridge, the height of the arch at known distances along the span were measured from scaled construction plans (courtesy of Mass Highway). These coordinates were then used to create a best fit parabolic curve in Microsoft Excel. Figure 4.8 shows the points measured from scaled construction plans, the best-fit parabolic curve, and the equation of the best-fit parabolic curve. The arch geometry of the calibrated computer model which matches the maximum bending

moment results from the simplified analysis was created using this best-fit parabolic equation rather than the measured values.

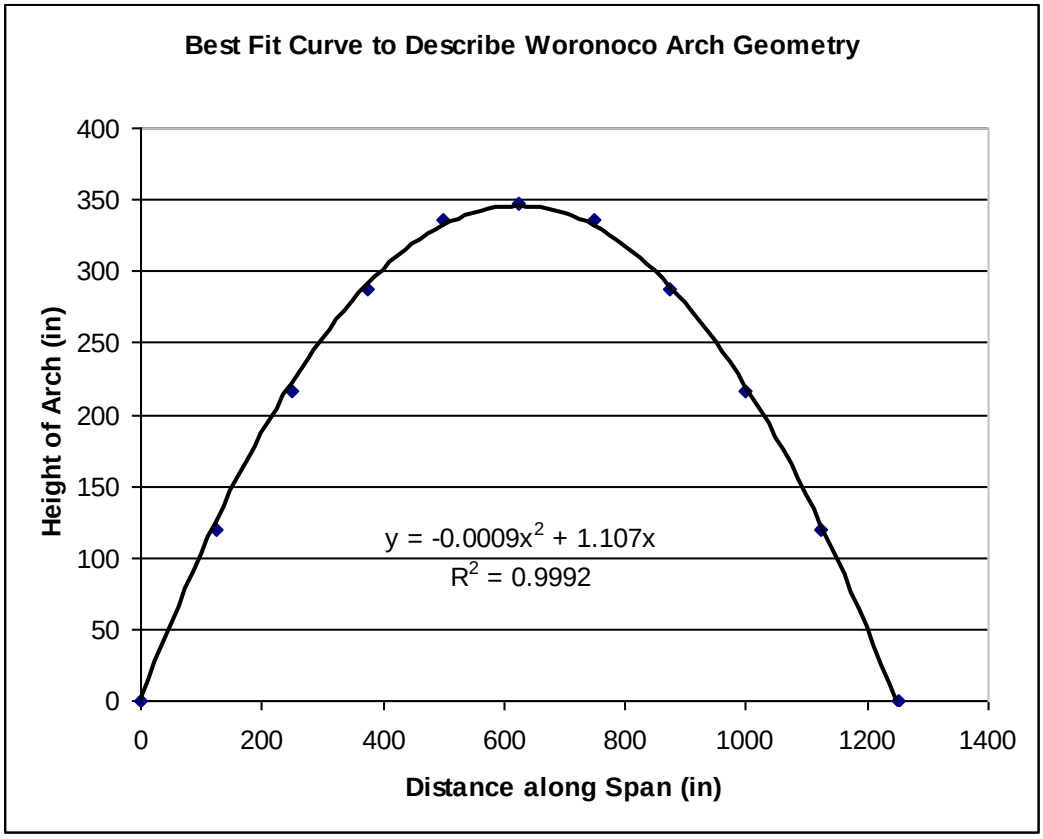

Figure 4.8 – The parabolic approximation (solid line) used to represent the existing arch geometry of the Woronoco Bridge (diamonds).

While this assumption seems to be appropriate for the Woronoco Bridge (indicated by the high R^2-value), it is of interest to investigate flatter parabolic arches. From this, the limitations of this assumption can be identified by determining when the arch of a bridge will significantly behave as a beam and have to carry some of the load through bending as well as axial forces. This can be done by incrementally scaling the parabolic curve and recording the effect on maximum bending stress in the arch.

To study the effect of flattening the arch, several models were made by scaling the heights of the arch in the calibrated model by a given factor (see Figures 4.9-4.11). The height of the spandrel columns was maintained in each modified model. The calibrated model has an aspect ratio (span/rise) = 3.67. The aspect ratio for all of the "flattened" parabolic bridge models are provided in the caption of each figure. Table 4.2 summarizes the results of varying the aspect ratio of the Woronoco Bridge model.

Table 4.2 – Summary of the relationship between aspect ratio and maximum bending in arch.

	Aspect Ratio (span/rise)	**Maximum Bending in Arch (mT)**
Woronoco	3.67	4.64
75% Woronoco	4.9	4.86
Schwandbach	6.23	5
50% Woronoco	7.35	5.1
25% Woronoco	14.7	5.56

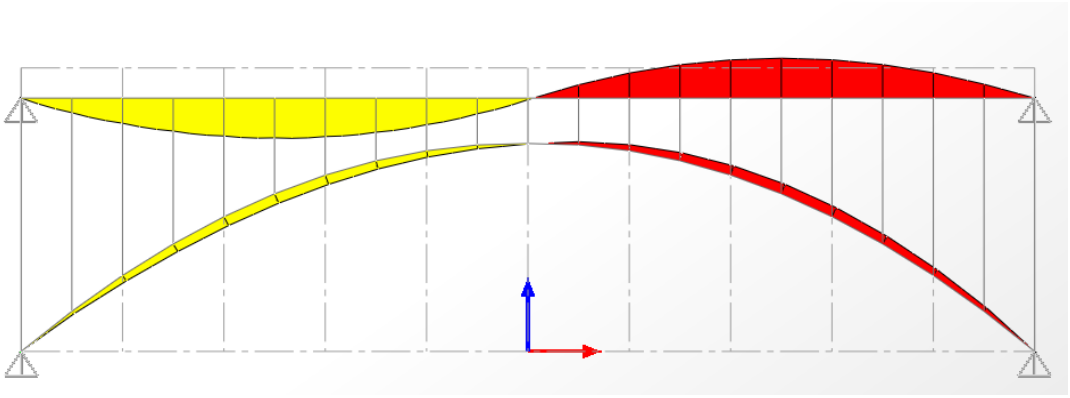

Figure 4.9 – Elevation of arch is scaled 75% and the maximum moment in the arch is 4.86mT, located at quarter-span (the moment in the deck is 18.72mT at that point, which adds up to the correct amount for total moment, and has an aspect ratio of 4.8975).

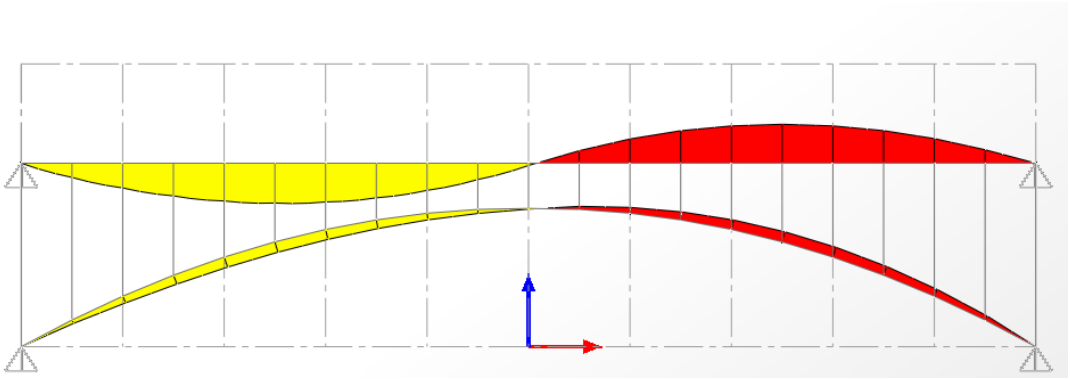

Figure 4.10 – Elevation of arch is scaled 50% and the maximum moment in the arch is 5.09mT, located at quarter-span (the moment in the deck at this point is 18.838 mT, which adds up to 23.93 mT, which is higher than the anticipated total moment, and has an aspect ratio of 7.35).

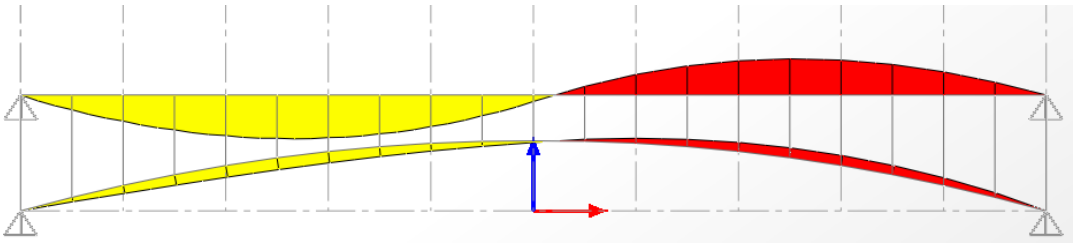

Figure 4.11 – Elevation of arch is scaled 25% and the maximum moment in the arch is 5.56mT, located at quarter-span (the moment in the deck at this point is 20.16 mT, which adds up to 25.72 mT, which is significantly higher than the anticipated total moment, and has an aspect ratio of 14.6925).

From this parametric study it is clear that as the arch is flattened, the maximum bending moment in the arch increases as one would expect. The aspect ratio for each model was calculated in order to compare them with typical aspect ratios for Maillart's deck-stiffened bridges. Billington provides a list of aspect ratios for each of Maillart's deck-stiffened arch bridges[4]. The Schwandbach Bridge, Maillart's second to last deck-stiffened bridge, has an aspect ratio of 6.23. In order to get a bridge model matching this aspect ratio, the arch elevations in the calibration model were scaled to 59% of their original value. Figure 4.12 shows the bending moment distribution for an arch bridge with an aspect ratio equal to that of the Schwandbach Bridge.

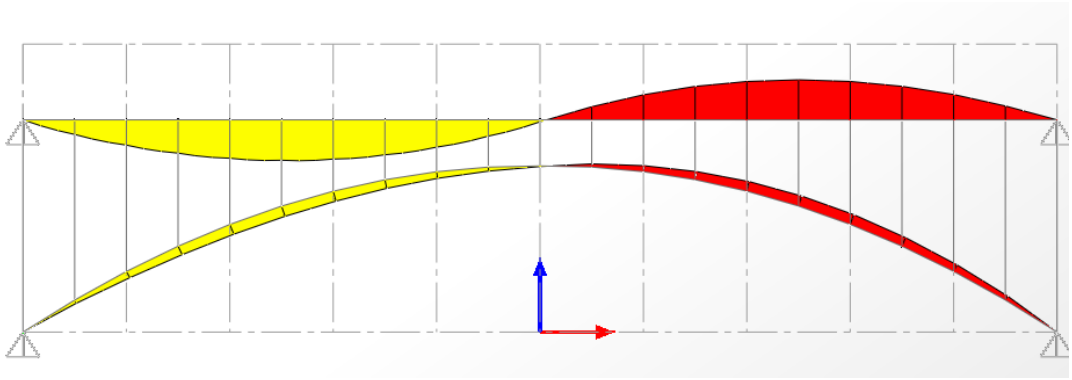

Figure 4.12 – Elevation of arch is scaled 59% and the maximum moment in the arch is 5mT, located at quarter-span (the moment in the deck at this point is 18.75mT, which adds up to 23.75 mT, and has an aspect ratio of 6.225).

For the aspect ratio of the Schawandbach Bridge, the maximum moment in the arch is 5 mT, which is 0.36 mT greater than that predicted by the simplified procedure.

It seems as though this assumption is acceptable for bridges that have an aspect ratio less than or equal to that of the Schwandbach Bridge (span/rise = 6.23). However, a significant increase in bending results if the arch is too flat. Therefore, this assumption is appropriately applied to both the Woronoco Bridge and the Schwandbach Bridge, but caution should be taken if it were applied to flatter arch bridges, such as Maillart's Spital Bridge (aspect ratio = 9.2) or Toss Bridge (aspect ratio = 10.84).

4.2.4 Assumption 4: Number of Spandrel Columns

The fourth assumption required to achieve agreement with Billington's simplified analysis is that there are enough spandrel columns to adequately simulate a uniform loading condition on the arch. In order to achieve a maximum arch moment in the calibrated Woronoco Bridge model of the predicted magnitude of 4.63mT and location at quarter-span, the number of columns had to be increased. For simplicity, a column was added midway between two existing columns. The height of the arch at every connection

point to a spandrel column was solved for using the parabolic equation provided in Figure 4.8. The resulting points were connected by linear beam elements whose moments of inertia were solved for using the equation $I_S \cos\theta_S = I_A$. As always, the remaining assumptions made in order to obtain the results in the simplified analysis were maintained.

It was observed during the development of the calibration model that in order to get the anticipated location of maximum moment in the arch, it was necessary to have a spandrel column at this location (quarter-span). To investigate the relationship among the number of columns, the maximum bending stress in the arch and the location of this maximum, several models have been generated in which the number and spacing of spandrels were varied.

To determine the effect of spandrel number on the magnitude of maximum bending moment in the arch, a model was generated using the parabolic approximation provided previously. In this model, the number of spandrel columns was decreased and the spandrel spacing was altered so that a spandrel would be located at quarter-span (the anticipated location of maximum bending moment in the arch). Figure 4.13 shows this model and the resulting moment distribution.

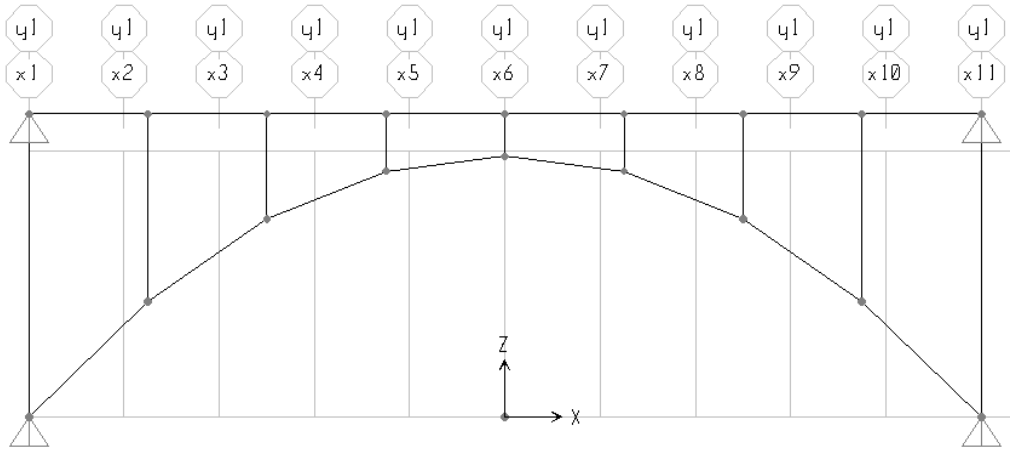

Figure 4.13a – Decreased number of spandrel columns with a spandrel located at the anticipated location of maximum bending moment located at quarter-span.

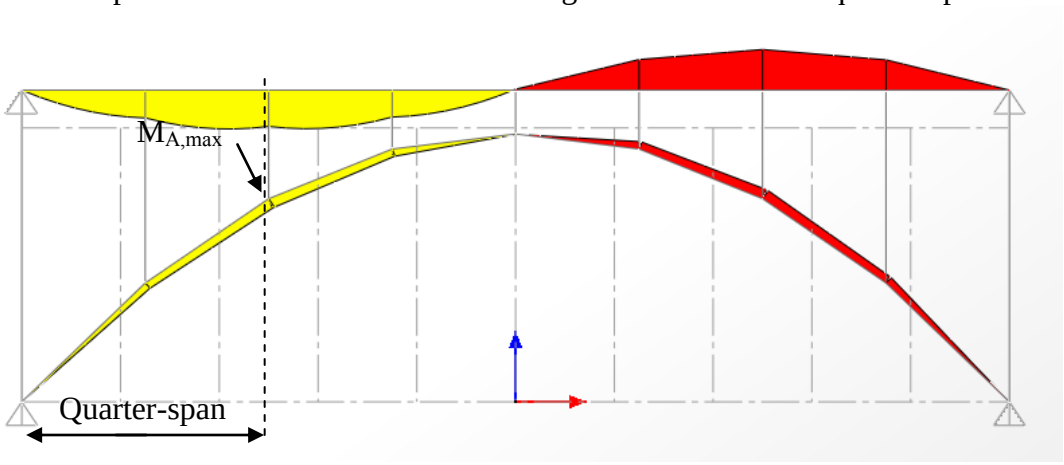

Figure 4.13b – The moment distribution with decreased number of spandrels, $M_{A,max}$ = 4.89 mT located at quarter-span.

From this model, the number of spandrels does not appear to affect the location of maximum moment as long as there is a spandrel at quarter-span. However, the magnitude of the maximum moment in the arch increases as a result of the decreased number of spandrels. To prove this further, another model was created by removing every other spandrel (Figure 4.14).

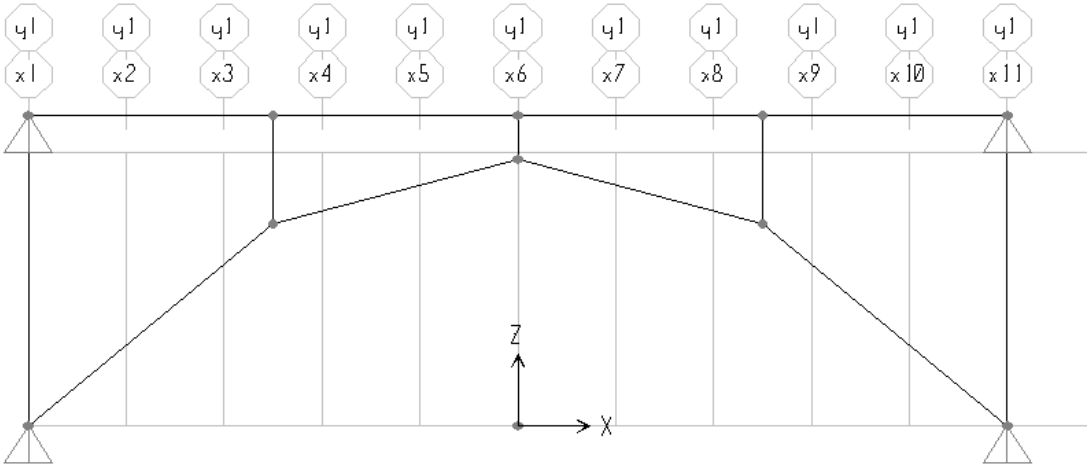

Figure 4.14a – Decreased number of spandrel columns with a spandrel located at the anticipated location of maximum bending moment (quarter-span).

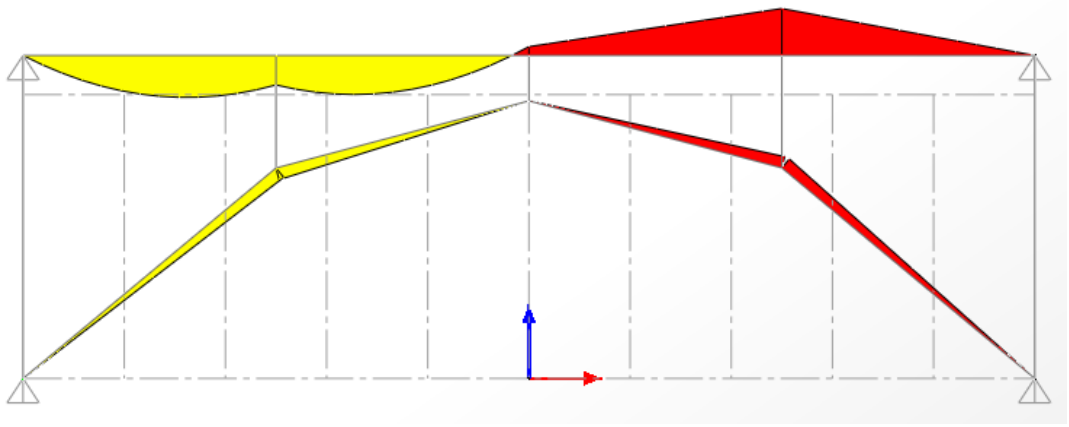

Figure 4.14b – The moment distribution with decreased number of spandrels, $M_{A,max}$ = 5.74 mT located at quarter-span, moment in the deck at this location is 13.98 mT.

While the anticipated location of the maximum moment in the arch is preserved (even with the greatly reduced number of spandrels), the magnitude of the maximum moment in the arch has increased significantly from that found in the calibration model. Table 4.3 summarizes the relationship between column number and the maximum bending in the arch.

Table 4.3 – Effect of varying column number on the maximum bending moment.

	Number of Columns	Maximum Bending in Arch (mT)
Calibration Model	21	4.64
First Variation	9	4.89
Second Variation	5	5.74

While the effect of column number is an interesting one to consider, none of the models discussed so far have the column configuration that is present in the Woronoco Bridge. Figure 4.15 represents the actual number and spacing of spandrel columns found in the Woronoco Bridge.

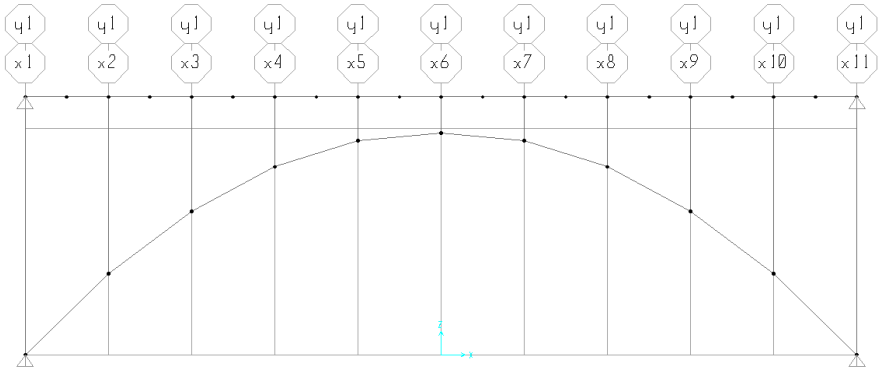

Figure 4.15a - Four pinned-supports with spandrel columns pinned at each end (moment of inertia in arch varies with $I_S \cos(\theta_S) = I_A$, where each member is the larger of the calculated values at each end).

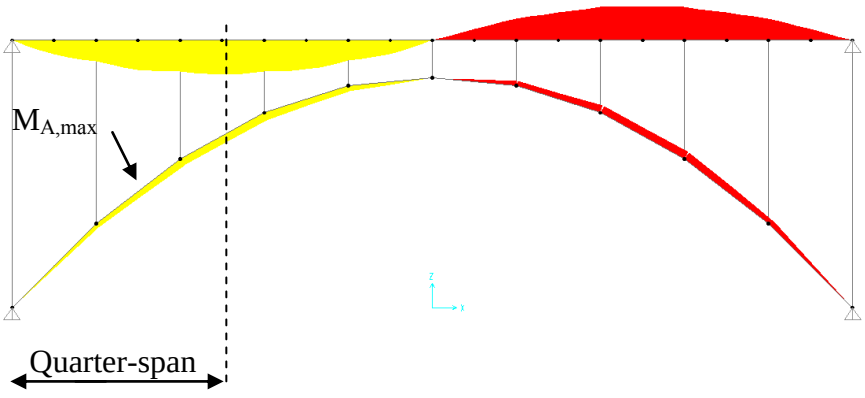

Figure 4.15b - Moment diagram with maximum moment, $M_{A,max}$ = 4.45mT.

Note that the location of spandrel columns appears to be important in order to achieve the anticipated location of the maximum bending moments at quarter-span using the simplified procedure. While the maximum bending moment in the arch only increases by 0.25mT when the Woronoco Bridge is modeled with the actual number of spandrels rather than an artificially increased number, it is clearly a better representation of the Woronoco Bridge to model it this way.

As was observed with the investigation of the effect that parabolic shape has on the maximum bending moment in the arch, it is important to be aware that there are always limitations to simplifying assumptions. While the Woronoco Bridge is not poorly represented by assuming an increased number of columns, the model created to investigate actual structural behavior and identify critical elements will use the actual number and spacing of spandrels. Therefore, the fourth simplifying assumption that Billington makes in order to perform his simplified analysis is not appropriate for the Woronoco Bridge since it requires the addition of fictitious spandrel columns.

4.2.5 Assumption 5: Variation of Arch

The fifth assumption Billington makes in his simplified analysis procedure is related to the variation in arch stiffness along the span. He assumes that the stiffness of the arch is a function of the arch angle at a given location. The relationship he assumes is repeated below for convenience:

$I_S \cos\theta_S = I_A$, where I_S is the arch stiffness at a given location, θ_S is the arch angle at a given location and I_A is the crown stiffness of the arch.

For the Woronoco Bridge, the crown stiffness of the arch, I_A, is 0.015779 m^4. Figure 4.16 provides an elevation view of the calibrated Woronoco Bridge model and the location of values used in this calculation of arch element stiffness.

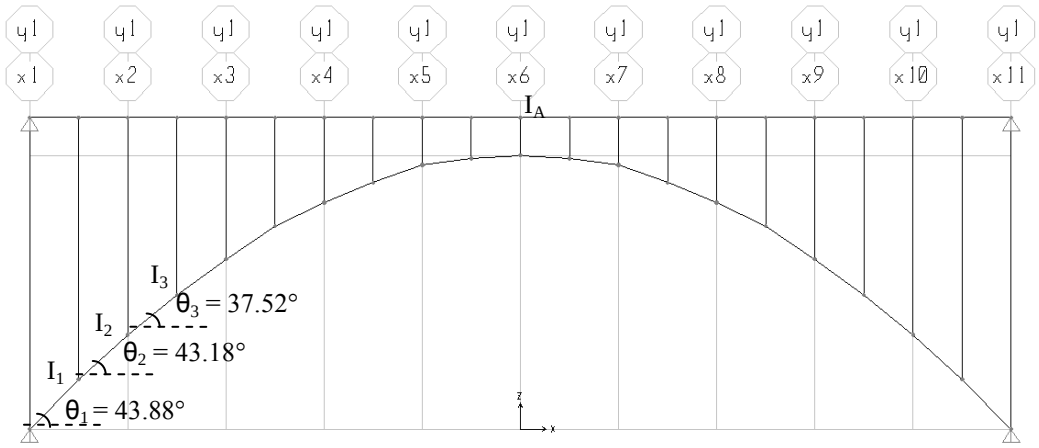

Figure 4.16 – Elevation of the Woronoco Bridge model showing three angles and the three corresponding moments of inertia.

The equation for arch stiffness was used to determine the arch moments of inertia at various locations in the calibrated computer model of the Woronoco Bridge that matched Billington's predicted bending moment behavior. Sample calculations are provided below to show how arch stiffness was determined using this proposed formula:

$$I_1 = \frac{I_A}{\cos(\theta_1)} = \frac{0.015779m^4}{\cos(43.83°)} = 0.021873m^4$$

$$I_2 = \frac{I_A}{\cos(\theta_2)} = \frac{0.015779m^4}{\cos(43.18°)} = 0.021639m^4$$

$$I_3 = \frac{I_A}{\cos(\theta_3)} = \frac{0.015779m^4}{\cos(37.52°)} = 0.019894m^4$$

While Billington notes that this formula closely approximates the arch stiffness variation in the Schwandbach Bridge[4], it is necessary to assess its accuracy in

representing American open spandrel bridges. Using this formula, the stiffness of arch element 1, I_1, is 0.021873 m^4(Figure 4.16). In reality, the thickness of the arch segment near the abutment is approximately 44 inches and the moment of inertia is 0.2305 m^4. This means that in order to apply Billington's stiffness formula, element 1 was scaled to be 8.6% of its actual value.

To determine the effect of arch stiffness on maximum moment in the arch, a computer model was made with every assumption required to achieve agreement with the simplified analysis, except for the variation in stiffness along the arch. Instead, the measured stiffness values are used. The moments that result from this alteration can be seen below in Figure 4.17.

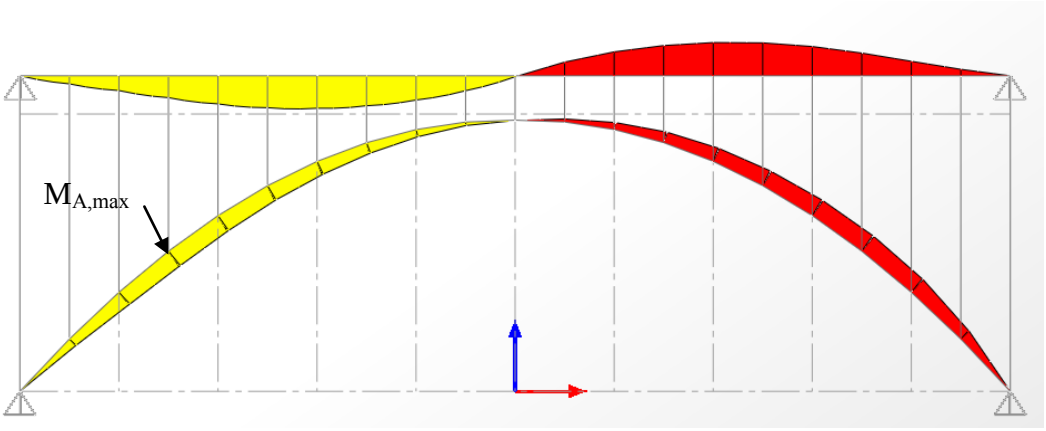

Figure 4.17 – Moment diagram resulting from changing the approximated stiffness variation to the measured stiffness variation in the arch, $M_{A,max}$ = 8.89 mT (the moment in the deck at that point is 10.55 mT).

Increasing the stiffness of the majority of the elements in the arch results in the arch carrying more of the bending moment, however, it still carries less than the deck. The predicted anti-parabolic shape of the bending moment is intact, however, it appears skewed. Because the arch is sized such that the arch elements near the abutment are the

thickest, it is reasonable to expect that the maximum moment shifts towards the abutments and away from quarter-span.

As stated previously, the actual stiffness at the ends of the arch (0.2305 m^4) had to be multiplied by 0.0863 in order to achieve Billington's assumed stiffness in the arch at that location. Similarly, the other arch elements were scaled down from the actual stiffness values in order to achieve the same results. At quarter-span, the measured stiffness of the arch is 0.0374 m^4 and this had to be multiplied by 0.45 to get Billington's assumed stiffness value. The moment diagram that results from replacing assumed stiffness values with actual stiffness values significantly affects both the location and magnitude of the maximum bending moment in the arch and the deck.

As was the case with spandrel number and spacing, it is clearly the better choice to model the Woronoco Bridge based on actual dimensions rather than approximations. Otherwise, the bridge model would underestimate the bending in the arch. Again, this raises questions related to the intention of American open spandrel bridges and the maintenance of them over time. While Maillart was attempting to reduce bending in the arch and derive an open spandrel form based on the simplified analysis outlined in Section 2.2, perhaps American engineers had different design priorities.

4.3 Assumptions Appropriate for Model of the Woronoco Bridge

From the above investigation of the five fundamental assumptions that are required in order to apply Billington's simplified analysis procedure, it is clear that while all may arguably be applicable to Maillart's bridges, several do not accurately describe the Woronoco Bridge. As a result, it is questionable as to whether or not this simplified

analysis is an accurate representation of American open spandrel bridges. If a bridge does not fall within the limitations of these assumptions, the simplified analysis should be used with caution and solely as a preliminary means of analysis. Below is a summary of the five assumptions investigated and the justification for or against their use in the representation of the Woronoco Bridge:

1) The arch and deck supports are all pinned and cannot carry any bending moment. This is based on construction drawings which do not indicate a substantial enough foundation to restrain rotation at the abutment. However, the abutment is likely to be partially restrained in reality and so a model in which the bridge abutments are fixed will be created in order to achieve an envelope within which the actual bridge behavior is captured.
2) There is continuity between the spandrel columns and the deck as well as the arch. As a result, the columns are able to transfer moment between the arch and the deck. This assumption is justified by visual inspection of the columns in which the presence of metal reinforcement and the absence of significant cracking in the columns was observed.
3) The arch is parabolic in shape. The elevations of the arch were measured from construction drawings and used to develop a best-fit parabolic shape for use in the computer model. The best-fit parabolic arch that describes the Woronoco arch is assumed to carry uniform loading solely through axial forces since it was proven to be steep enough so as not to behave significantly as a beam.
4) The number and spacing of columns is taken from construction drawings of the Woronoco Bridge. Using the existing column configuration guarantees a more accurate representation of the actual structural behavior of the historic bridge.
5) The arch stiffness varies according to measured geometric values for the arch along its span. The arch will be modeled as a series of beam elements, each spanning between two columns. The stiffness of each beam element will be the average of the actual arch stiffness found at either end of that segment. Using the average of actual measured arch stiffness values ensures that the model will accurately portray the structural behavior of the Woronoco Bridge.

CHAPTER 5

USE OF MODEL TO INVESTIGATE DESIGN CHOICES

5.1 The Effect of Column Stiffness and Spacing

The assumptions involved in modeling the Woronoco Bridge have been evaluated in Chapter 4 and only those that are appropriate for this specific example of an American open spandrel bridge are used to develop a representative computer model. This model allows for not only the investigation of the design decisions that were made by early American engineers but also the determination of the relationship between the stiffness of members and their load-carrying responsibilities. Using the Woronoco Bridge as an example of an American reinforced concrete open spandrel bridge, this chapter discusses the effects of columns stiffness and spacing on the axial forces and bending moments within the structure, as well as the overall aesthetics of the structure. By establishing how column stiffness and spacing affect the structural behavior and appearance of the Woronoco Bridge, the design priorities of early engineers can be better understood. Keeping in mind Billington's analysis of both Swiss and American open spandrel bridges, the investigation of column stiffness and spacing is performed using the same half span live load described in Section 2.2.1.

The Woronoco Bridge is an example of American reinforced concrete open spandrel bridges. It is fundamentally comprised of a deck, three arch ribs and three rows of columns that connect each arch rib to the deck. Each arch rib is connected to the deck by eleven axially rigid and evenly spaced columns. Due to the lack of cracking at the ends of the columns, as well as evidence of reinforcement within the ends of the columns, the columns are able to transfer bending moments between the arch and the deck. Since the

columns are able to carry bending moments and allow for the arch and the deck to interact with one another, it is of interest to investigate the effect that column stiffness and spacing have on the structural behavior of the bridge. Through this investigation, insight into both the structural behavior of and the design considerations for early American open spandrel bridge are gained.

5.1.1 Study of Column Stiffness in the Woronoco Bridge

The cross-section of the columns in the Woronoco Bridge is a 16-inch square. This column geometry allows for both significant moment transfer as well as a light and open appearance. The choice for 16-inch square columns, however, is not fully understood. In order to shed more light on this design decision, a parametric study was conducted in which the column stiffness was incrementally altered. The representative Woronoco Bridge model created in SAP2000 (see Section 4.3) was used for this study. The study features the representative Woronoco Bridge model (with 16-inch square columns) as well as twelve variations of this model. Table 5.1 summarizes the column cross-sectional dimensions used for each of the twelve variations in this study. Note that the moments of inertia listed in Table 5.1 are based on the cross-section of one and a half column cross-sections. This is because the representative model is a 2D frame of half of the Woronoco Bridge. Therefore, the width of the deck, arch and columns used in the representative model are one half of the total width.

Table 5.1 – Summary of the thirteen column stiffness models investigated as part of parametric study (*Actual geometric properties of the Woronoco Bridge).

Thickness of Spandrels (in)	Stiffness of Spandrels (in^4)	I_C/I_A
8	512	0.03
10	1250	0.07
12	2592	0.14
14	4802	0.25
*16	*8192	*0.43
18	13122	0.69
20	20000	1.06
21	24310	1.28
22	29282	1.54
23	34980	1.85
24	41472	2.19
26	57122	3.01
28	76832	4.05

5.1.1.1 The Effect on Maximum Bending Moment

All of the thirteen models were analyzed under the same half-span live load (W_L = 1.5 tons/meter). Figure 5.1a-c show the bending moment diagrams that result from this loading for three out of the thirteen models included in this study. While these figures do not include any numerical values, they are all scaled equally for qualitative comparison. Therefore, these figures serve as a helpful visual in recognizing the differences in the bending moment distribution as a result of changing the column stiffness. For example, when the columns are relatively thin (as in Figure 5.1a) the moment diagram is nicely shaped as two anti-symmetric parabolas. This is the bending moment behavior that Billington proposed in his simplified bridge model. This behavior makes sense given that 8" x 8" square columns are not capable of carrying any significant moment and primarily act as axial members. Thus, when the columns are not very stiff, the arch and the deck are virtually performing as pin-connected elements.

As the columns are made stiffer, the bending moment distribution continues to roughly follow the shape of two anti-symmetric parabolas. The smoothness of the distribution, however, is lost as the column stiffness increases. Significant jumps in the bending moment occur where the columns are connected to either the arch or the deck. While the arch and the deck are still interacting with one another, this interaction is no longer as clear and well-behaved as it was when the columns behaved primarily as axial members. By developing computer models in which the column's moment-carrying role can accurately be represented, the true behavior of this American open spandrel bridge can be better understood.

Figures 5.1a, 5.1b and 5.1c show the bending moment diagrams for computer models in which the columns are 8" x 8", 16" x 16" square and 28" x 28" square, respectively. Figure 5.1b represents the actual column stiffness of the Woronoco Bridge.

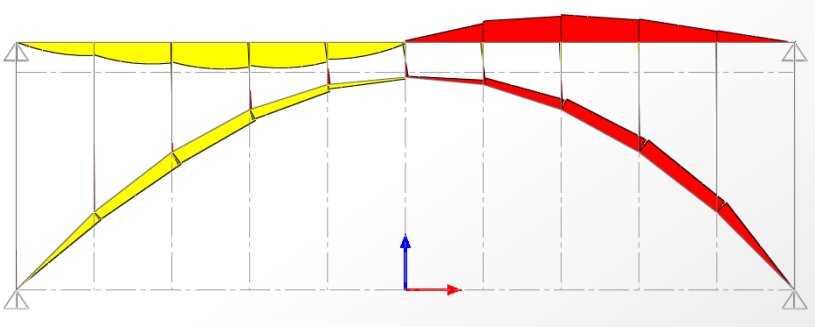

Figure 5.1a - Bending moment diagram with spandrel columns 8" x 8" square.

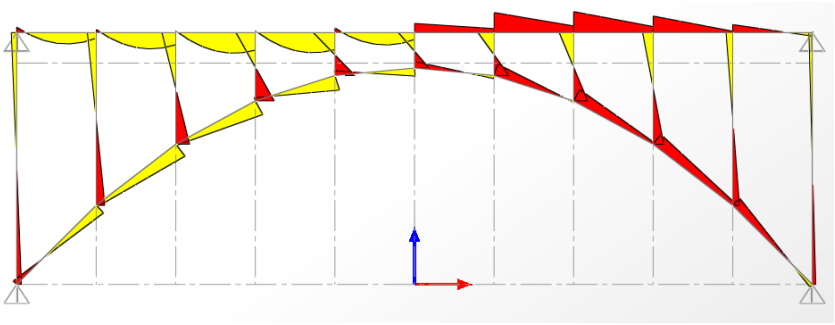

Figure 5.1b - Bending moment diagram with spandrel columns 16" x 16" square

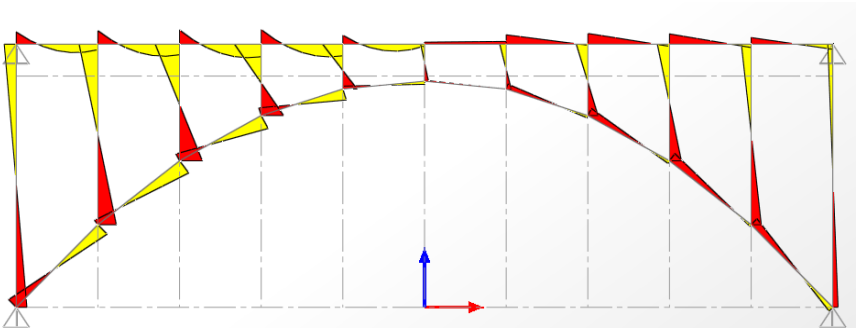

Figure 5.1c - Bending moment diagram with spandrel columns 28” x 28” square

From each bridge model, the maximum bending moment for the deck, arch and columns were recorded. These results are provided in Table 5.2**.**

Table 5.2 - The maximum bending moment results from each of the thirteen models in which the column stiffness was incrementally varied.

Thickness of Spandrels (in)	**Stiffness of Spandrels (in^4)**	**I_C/I_A**	**Maximum Arch Bending Moment**		**Maximum Deck Bending Moment**		**Maximum Column Bending Moment**	
			(k-in)	**(kN-m)**	**(k-in)**	**(kN-m)**	**(k-in)**	**(kN-m)**
8	512	0.03	552.83	62.46	965.31	109.07	155.22	17.54
10	1250	0.07	412.30	46.59	710.58	80.29	235.07	26.56
12	2592	0.14	313.61	35.43	520.79	58.84	286.21	32.34
14	4802	0.25	259.28	29.30	400.64	45.27	323.19	36.52
16	8192	0.43	243.65	27.53	327.31	36.98	341.77	38.62
18	13122	0.69	238.73	26.97	281.13	31.76	349.03	39.44
20	20000	1.06	239.11	27.02	254.43	28.75	372.66	42.11
21	24310	1.28	240.29	27.15	245.57	27.75	389.16	43.97
22	29282	1.54	241.75	27.31	238.75	26.98	405.22	45.79
23	34980	1.85	245.19	27.70	233.63	26.40	420.93	47.56
24	41472	2.19	250.06	28.25	229.93	25.98	436.40	49.31
26	57122	3.01	259.54	29.33	225.90	25.52	466.75	52.74
28	76832	4.05	268.00	30.28	225.50	25.48	496.42	56.09

Varying the stiffness of the columns has a noticeable effect on the maximum bending moment in each bridge member. When the columns are 8" x 8" square, the maximum bending moment in the arch is 552.83 kip-in (62.46kN-m). When the columns are 28" x 28" square, the maximum bending moment in the arch is 268 kip-in (30.28kN-m). The latter value is roughly half the former.

The maximum bending moment for each of the thirteen bridge models are provided in Table 5.2. These bending moment results are plotted in Figure 5.2 for ease of evaluation. Note that column stiffness has been normalized by the arch stiffness in this plot, just as Billington normalized deck stiffness (Section 2.2.1).

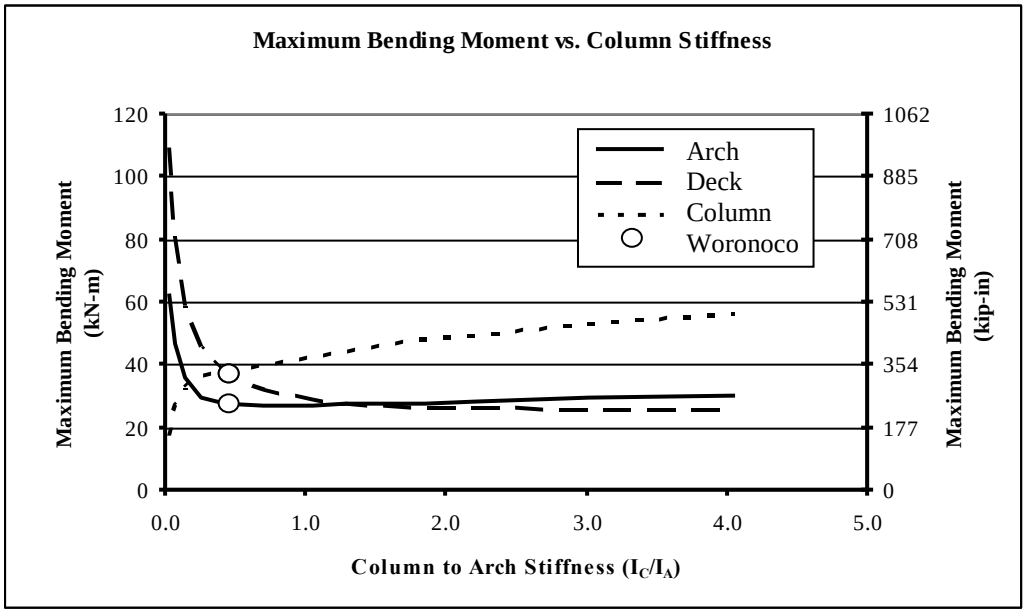

Figure 5.2 – Plot of the maximum bending moments in the arch, deck and columns as a result of varying the columns stiffness.

From Figure 5.2, it is clear that the maximum bending moment in the columns increases as the stiffness of the columns increase. On the other hand, the maximum bending moment in both the arch and the deck decrease as the column stiffness increases. These changes occur quickly while the column to arch stiffness ration (I_C/I_A) is less than

0.5. After this point, the curves that depict the maximum moment in the arch and the deck begin to level off. This behavior indicates that beyond a column to arch stiffness ratio of 0.5, there is no significant advantage to increasing column stiffness (in terms of reducing bending moment in the arch and the deck). Figure 5.2 also provides the location of the Woronoco Bridge with respect to these three curves. It is interesting to see that the Woronoco Bridge is arguably located within the region that effectively uses the column stiffness to minimize bending in both the deck and the arch.

While it is hard to see from Figure 5.2, the maximum bending moment in the arch has a local minimum. After this point, the bending moment begins to gradually increase as the column stiffness increases. To see this behavior more clearly, a plot of just the maximum bending in the arch as a result of column stiffness is provided in Figure 5.3.

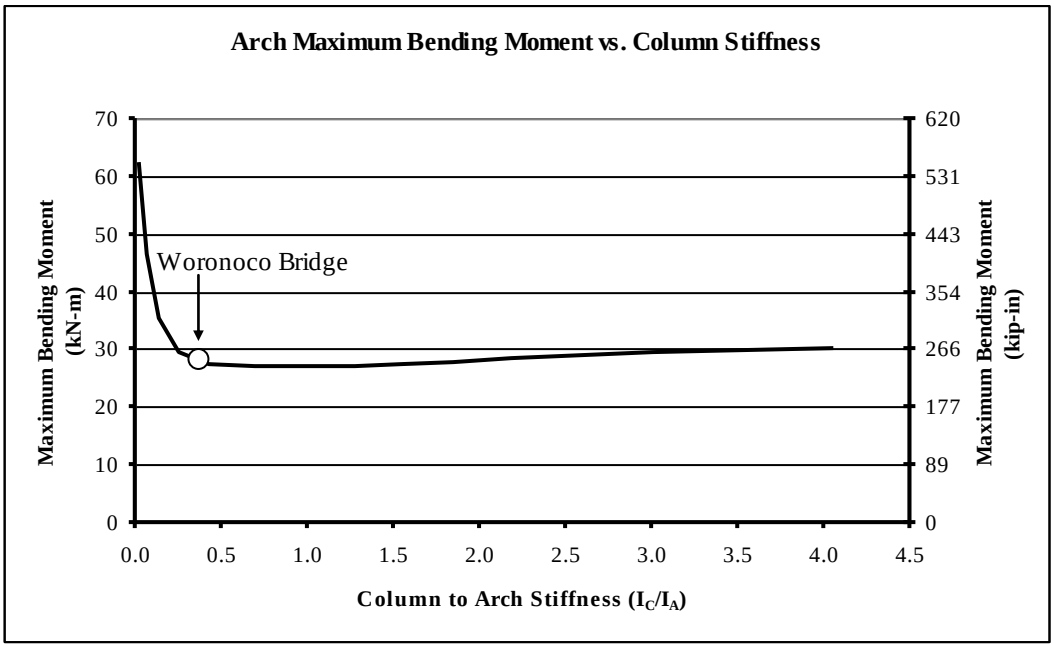

Figure 5.3 – Plot of the maximum bending moment in the arch as a result of varying the column stiffness.

Figure 5.3 not only shows that a minimum in the arch maximum bending moment exists, but also that the columns of the Woronoco Bridge are designed such that they practically achieve this minimum value. This result is significant for a variety of reasons. First, it is evidence supporting that the selection of column size, and therefore stiffness, for the Woronoco Bridge was deliberate and informed. Second, it indicates that designers of the Woronoco Bridge planned for and were aware of the interactions among the arch, deck and columns. Third, it gives rise to a structural achievement similar to Robert Maillart's "deck-stiffened" bridges: "column-stiffened" bridges.

5.1.1.2 The Effect on Maximum Axial Forces

In addition to the maximum bending moments throughout the bridge, altering column stiffness also affects the axial forces experienced by each of the three load-carrying members. As was done in Section 5.1.1.1, the representative Woronoco Bridge model was used in addition to twelve variations of this model in order to investigate the effect of column stiffness on axial forces in the bridge. The only difference in the models is the stiffness of the columns that connect the arch and deck. Figure 5.4 shows the axial force diagrams from three of the thirteen models included in this study. All of the pictures in Figure 5.4 are equally scaled and illustrate how column stiffness does significantly alter the axial force distribution throughout the bridge.

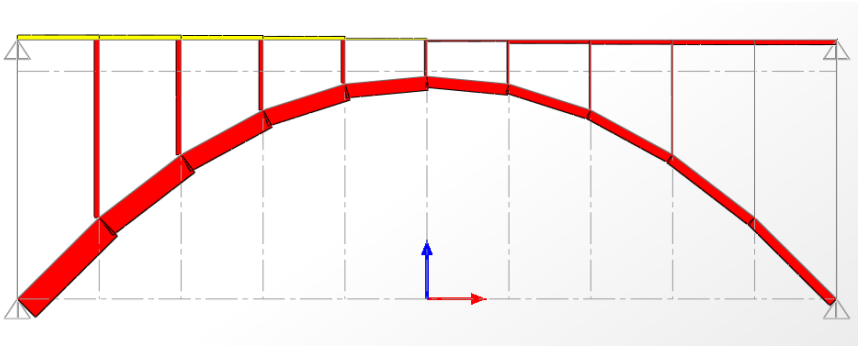

Figure 5.4a - Axial diagram with spandrel columns 8” x 8” square.

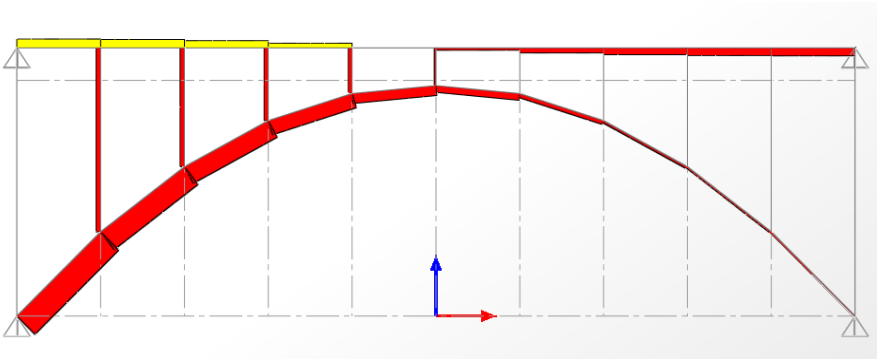

Figure 5.4b - Axial diagram with spandrel columns 16” x 16” square.

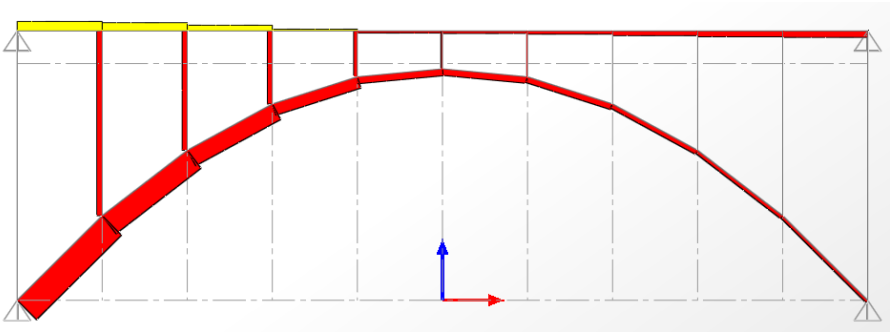

Figure 5.4c - Axial diagram with spandrel columns 28” x 28” square.

While the general shape of the axial force diagrams is similar for all three bridge models shown in Figure 5.4, it is clear that the column stiffness noticeably affects the distribution of axial forces. From each of the thirteen bridge models, the maximum axial force in the deck, arch and columns were recorded. These results are summarized in Table 5.3.

Table 5.3 - The maximum axial forces results from each of the thirteen models in which the column stiffness was incrementally varied.

Thickness of Spandrels (in)	Stiffness of Spandrels (in^4)	I_C/I_A	Maximum Arch Axial Force		Maximum Deck Axial Force		Maximum Column Axial Force	
			(kip)	(kN)	(kip)	(kN)	(kip)	(kN)
8	512	0.03	49.29	219.23	9.30	41.38	9.63	42.85
10	1250	0.07	56.30	250.42	14.76	65.65	10.26	45.64
12	2592	0.14	61.06	271.58	18.60	82.72	10.72	47.67
14	4802	0.25	63.46	282.27	20.71	92.11	11.00	48.92
16	8192	0.43	64.19	285.52	21.62	96.16	11.17	49.70
18	13122	0.69	63.88	284.14	21.81	97.02	11.28	50.19
20	20000	1.06	62.96	280.04	21.61	96.14	11.35	50.48
21	24310	1.28	62.36	277.38	21.43	95.32	11.38	50.60
22	29282	1.54	61.72	274.53	21.22	94.39	11.40	50.68
23	34980	1.85	61.04	271.51	21.00	93.40	11.40	50.71
24	41472	2.19	60.36	268.47	20.77	92.37	11.43	50.82
26	57122	3.01	59.00	262.41	20.31	90.34	11.45	50.93
28	76832	4.05	57.72	256.73	19.90	88.50	11.49	51.09

The values in Table 5.3 show that column stiffness does affect the axial forces throughout the bridge, however, this relationship is more easily observed by generating a plot of this data (Figure 5.5).

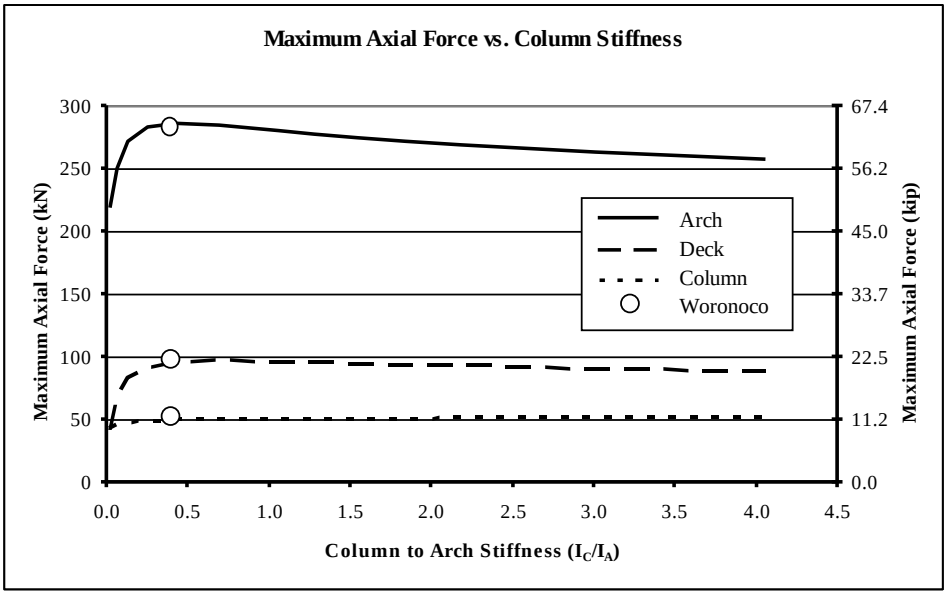

Figure 5.5 – Plot of the relationship between column stiffness and maximum axial forces in the three load-carrying members.

Figure 5.5 indicates the existence of a critical column stiffness value. It is the value associated with the peak of each curve. Before this critical region, increasing the column stiffness causes an increase in the axial forces in each load-carrying member. After this region, however, an increase in column stiffness seems to reduce the axial forces in both the arch and the deck. Since the Woronoco Bridge is located arguably within this maximum value region, it appears as though the reduction of axial forces were not a primary design concern for the Woronoco Bridge designers.

This plot does, however, clearly show that the arch is the primary axial load-carrying member, followed by the deck and then the columns. When looking at the elevation of the Woronoco Bridge, the size of these three load-carrying elements closely mirrors the axial force diagram (Figure 5.6).

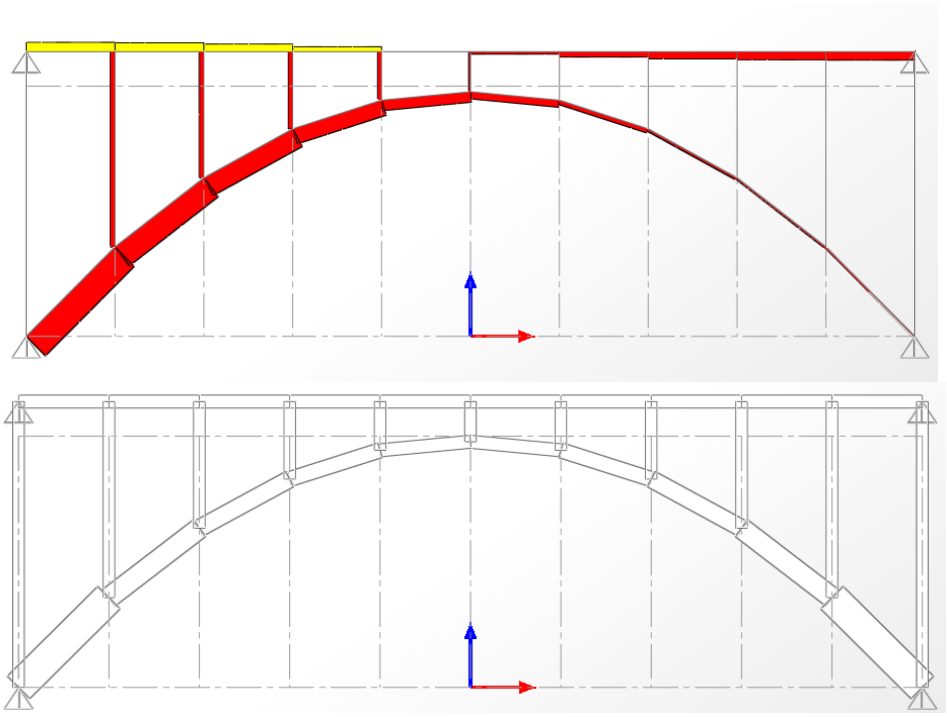

Figure 5.6 – The axial force distribution that results from a half-span live load (top) is reflected in the sizing of the three load-carrying elements, seen in the elevation of the bridge (bottom).

Note that the axial force diagram shown in Figure 5.6 is the result of a uniform live load over only the left half of the bridge. As a result, the diagram would be mirrored about the centerline if the right half of the bridge were loaded instead.

By designing the columns that reduced the maximum bending in the arch, Woronoco Bridge designers had to account for the worst-case axial force distribution. And while the Woronoco Bridge arch is not as thin and elegant as some of Maillart's arches, the form does appear to reflect the intended structural behavior.

5.1.1.3 The Influence of Aesthetics

Varying the stiffness of the columns has a noticeable effect on the maximum bending moment in each bridge member as well as the maximum axial forces throughout the bridge. However, changing the stiffness of the columns also has an aesthetic impact. Perhaps the Woronoco Bridge engineers were mindful to size the columns such that the bridge would not only reflect its intended structural behavior but also appear light and open. It has already been noted that the sizing of the arch, deck and columns was done in such a way so as to reflect the loads carried by each member of the bridge. Therefore, it is not unreasonable to propose that the designers of this bridge were conscious of the aesthetic consequences of their design choices.

From Figure 5.5, we know that increasing the column size beyond the prescribed 16" x 16" dimensions would have significantly decreased the axial forces in both the arch and the deck. However, it was decided not to increase the column size, despite these advantages. From Figure 5.3, we know that the 16" x 16" column dimensions result in a minimum bending moment in the arch. If the columns were to be stiffened more than

this, the bending moment in the deck would continue to decrease and the bending in the arch would increase only slightly. From these two figures, increasing the column stiffness beyond its current 16”-square dimensions has more structural advantages than disadvantages. It is possible, then, that another deciding factor existed and was not necessarily of a structural nature. Perhaps the appearance of the Woronoco Bridge played an important role in the sizing of the columns.

To examine this point further, consider both the appearance of the Woronoco Bridge with various column sizes, as well as the engineering atmosphere at the time the bridge was built. Looking first at the appearance of the bridge, Figure 5.7 shows three of the thirteen models that were included in the parametric study of column stiffness.

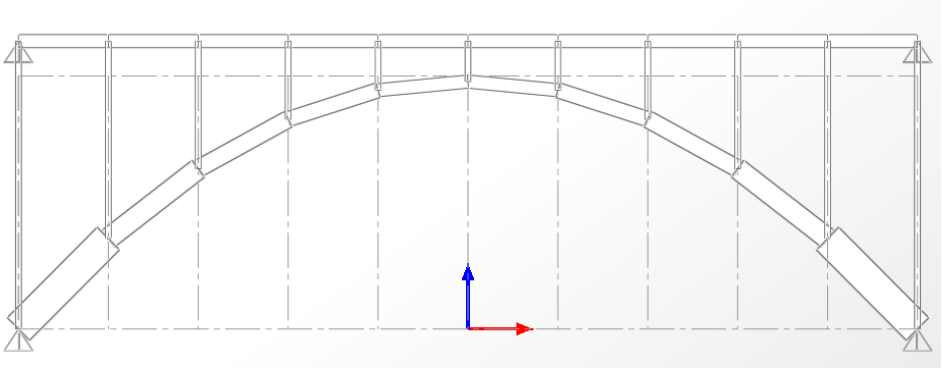

Figure 5.7a - Elevation with spandrel columns 8” x 8” square.

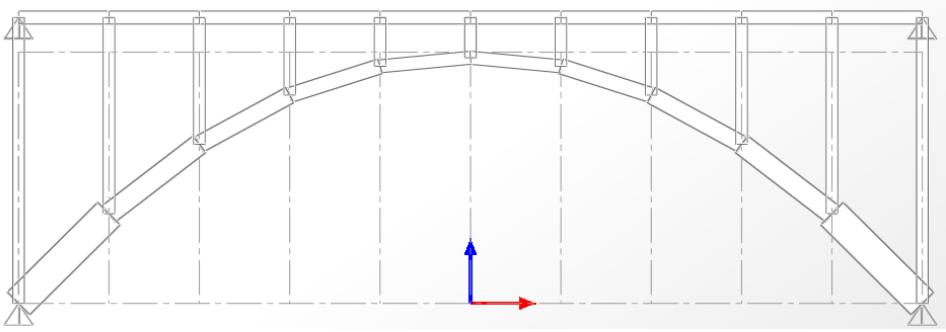

Figure 5.7b - Elevation with spandrel columns 16” x 16” square.

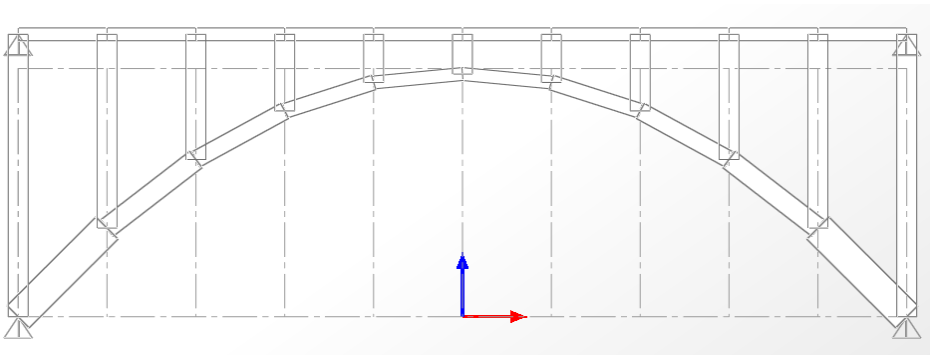

Figure 5.7c - Elevation with spandrel columns 28” x 28” square.

In the last of the three pictures, the columns are 28” x 28”. This is as thick, if not thicker, than the arch at every location except nearest the abutments. It was previously observed that the silhouette of the Woronoco Bridge closely mirrored the load-carrying responsibilities of the bridge members. The arch was significantly thicker than both the deck and the columns because its axial load-carrying responsibility was greater. The decision for stiffer 28” x 28” columns would falsely portray the columns to be equal load-carrying members as the arch. While stiffer columns decrease axial forces in the arch, as well as bending in both the arch and deck, it would inaccurately represent the structural behavior of the bridge.

5.1.1.4 Justification for Design Choices

Looking now at the design mentality in which the Woronoco Bridge was designed, it was highly desirable to create as much open space between the arch and the deck as possible. The Woronoco Bridge was built in 1923. Prior to the mid-nineteenth century, all concrete bridges were looked upon as massive arches that resembled ancient masonry bridges. With the advancement and standardization of concrete reinforcement prior to the construction of this bridge, however, came a race to design a more elegant reinforced

concrete arch bridge while also minimizing the structure's self weight. Texts written between 1910 and 1930 promoted the open spandrel design and applauded its aesthetic appearance, claiming it could be fit into any landscape without taking away from its natural beauty.[2] Considering the progressive attitude of structural designers of the time, as well as the widespread popularity of and confidence in reinforce concrete during the time of the Woronoco Bridge construction, it is reasonable to assume that aesthetics were a priority in the design of the structure.

Reinforced concrete open spandrel bridges of this time period helped to redefine the image associated with concrete structures in America. It would have been odd to have designed a reinforced concrete open spandrel bridge during this time period that did not strive towards a light and open aesthetic quality. In addition, the fact that the Woronoco Bridge dimensions reflect the load-carrying behavior of the bridge is proof that the designers wanted to create a form that reflected function. Despite the method used for analysis and design, the creators of the Woronoco appeared to be aware of the effect column stiffness had on the internal moments and axial forces. They stiffened the columns just enough to minimize bending moment in the arch and significantly reduce bending moment in the deck. And while the axial forces could have been reduced by further stiffening the columns, the Woronoco Bridge designers were most likely mindful of the aesthetic sacrifices this would require.

5.1.2 Study of Column Spacing in the Woronoco Bridge

During the design of the columns that connect the arch and the deck, Woronoco Bridge designers not only chose the size (and thus stiffness) of each column, but also decided upon the number of columns to use. In a similar attempt to better understand the design choices made in the Woronoco Bridge, a parametric study was conducted in which the number of columns was varied and the resulting structural behavior was observed. The model variations were created by first selecting a range of spandrel numbers to evaluate. Given the number of spandrels, the spacing between them was easily calculated. The elevation of the arch at each spandrel location was then determined using the spandrel spacing and parabolic equation that was determined to accurately describe the Woronoco Bridge geometry in Section 4.2.3.

5.1.2.1 The Effect on Maximum Bending Moment

Similar to the analysis conducted in order to investigate the structural effects of column stiffness, all of the bridge models used to evaluate the effect of column spacing were subjected to a half-span live load (W_L = 1.5 tons/meter). Figure 5.8a-c show the bending moment diagrams that result from this loading for three out of the seven models included in this study. While these figures do not include any numerical values, they are all scaled equally. These figures show the differences in the bending moment distribution as a result of changing the column spacing and number. As the number of columns increases, the moment diagram looks more and more like two anti-symmetric parabolas. The maximum bending moments in the arch, deck and columns were recorded for each model and are provided in Table 5.4.

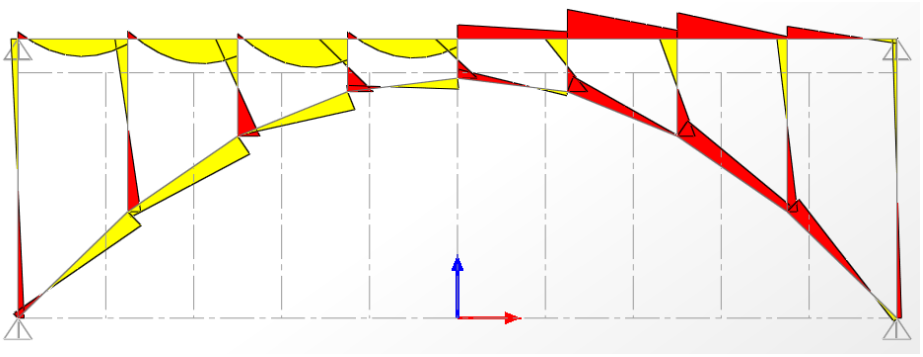

Figure 5.8a - Bending moment diagram for nine columns.

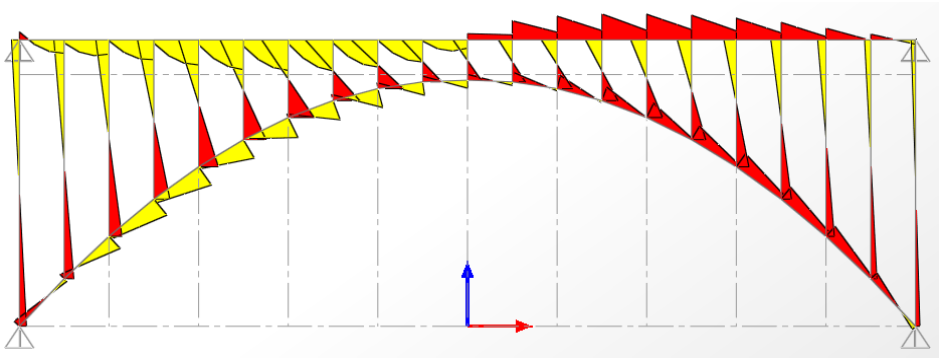

Figure 5.8b - Bending moment diagram for twenty-one columns.

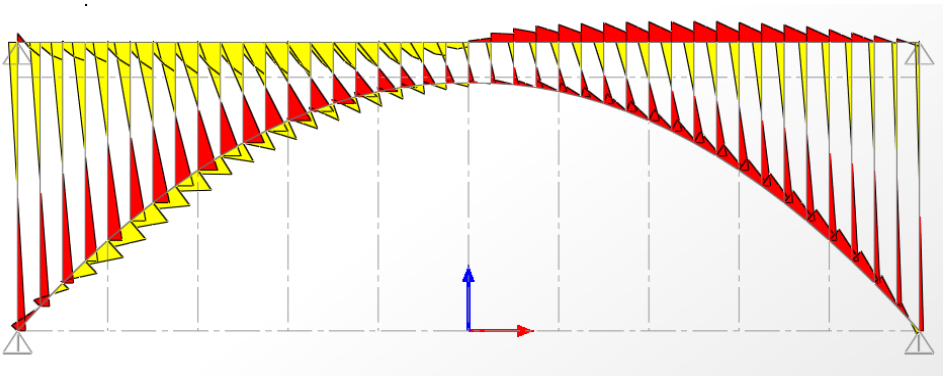

Figure 5.8c - Bending moment diagram for forty-one columns.

Table 5.4 - The maximum bending moment results from each of the seven models in which the column spacing was incrementally varied.

Number of Spandrels	Spandrel Spacing (in)	Maximum Moment in Arch		Maximum Moment in Deck		Maximum Moment in Columns	
		(kip-in)	(kN-m)	(kip-in)	(kN-m)	(kip-in)	(kN-m)
6	250	580.265	65.56	635.43	71.80	502.68	56.80
9	156.25	303.30	34.27	409.95	46.32	402.58	45.49
11	125	243.65	27.53	327.31	36.98	341.77	38.62
15	89.3	192.66	21.77	260.39	29.42	263.44	29.77
21	62.5	155.4	17.56	219.94	24.85	192.78	21.78
26	50	139.30	15.74	192.22	21.72	160.34	18.12
41	31.25	112.79	12.74	152.71	17.25	109.67	12.39

The values in Table 5.4 show that column spacing does significantly affect the bending moments throughout the bridge, however, this relationship is more easily observed by generating a plot of these data (Figure 5.9).

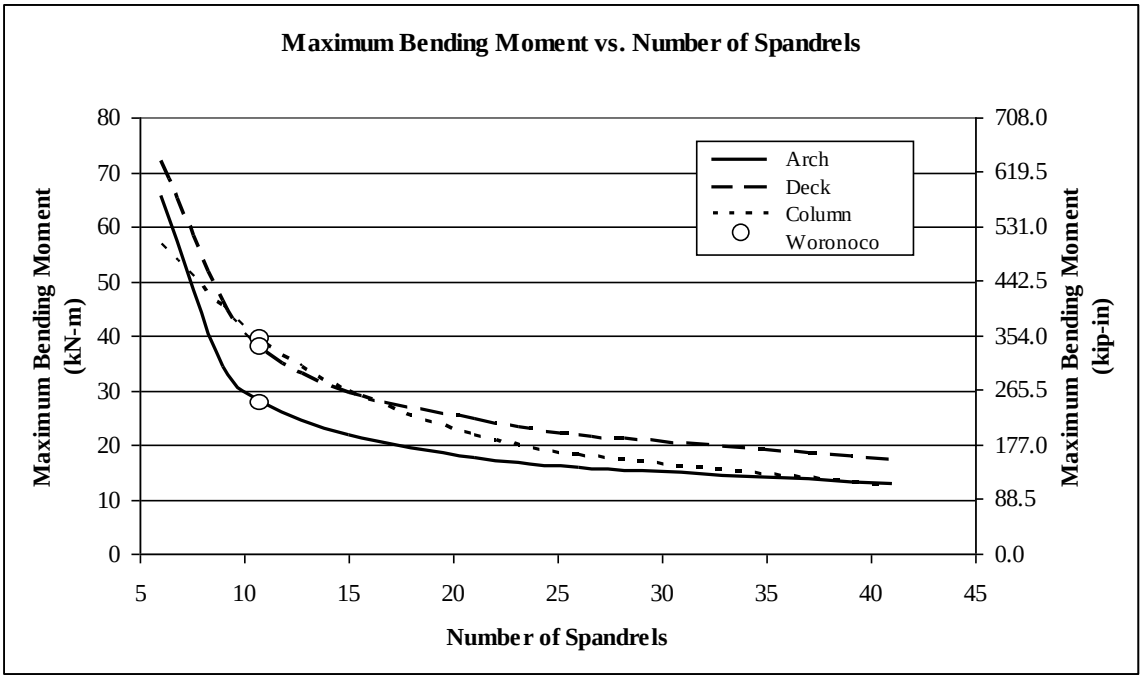

Figure 5.9 – Plot of the maximum bending moments in the arch, deck and columns as a result of varying column number.

From Figure 5.9, it is clear that as the number of columns increases, the maximum bending moment in the arch, deck and each column decreases. This is similar to the relationship between column stiffness and maximum bending moment except that there is no observed minimum value. Instead, the relationship between column number and maximum bending moments appears to level off when there are 15 to 25 columns. Beyond this region, the advantage of increasing the number of columns further is minimal. The Woronoco Bridge is located before the curve starts to level off, however, is arguably not taking full advantage of the reduction in moments that result from increasing the columns number. To perhaps justify this decision of only eleven columns, the aesthetic implications of adding more columns is discussed in the next section.

5.1.2.2 The Influence of Aesthetics

The Woronoco Bridge's location in Figure 5.9 alone does not alone justify the choice for eleven columns. However, it does explain why designers may have ruled out using fewer columns. To explain why Woronoco Bridge designers did not choose to increase the number of columns further (and reduce bending moments further), the aesthetic consequences of such a choice can be considered. As was stated in the discussion of spandrel stiffness, the engineering atmosphere during the Woronoco Bridge's construction was one of innovation and experimentation with reinforced concrete forms. The recent standardization of and confidence in reinforced concrete provided designers the tools to create lighter and more open concrete structures. Figure 5.10 shows three of the seven models that were included in the parametric study of column number and spacing.

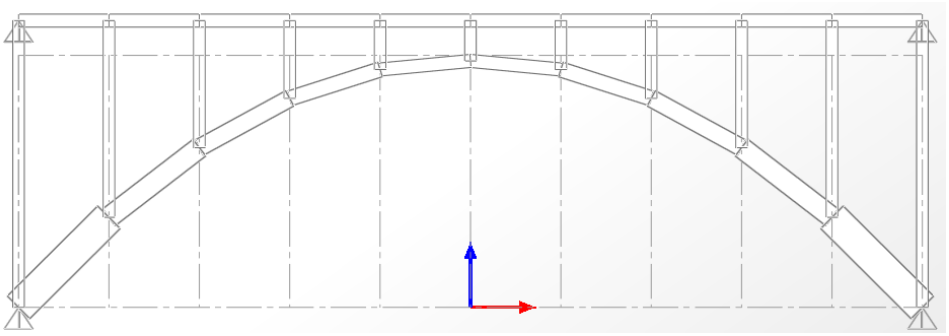

Figure 5.10a - Elevation with eleven columns (actual elevation of the Woronoco Bridge).

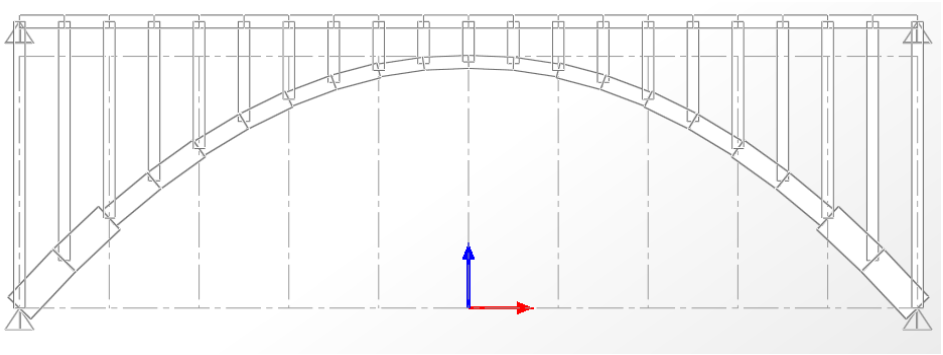

Figure 5.10b - Elevation with twenty-one columns.

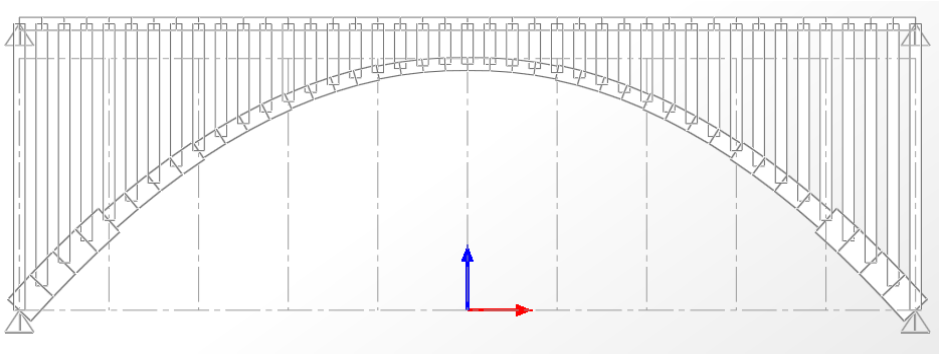

Figure 5.10c - Elevation with forty-one columns.

When viewing these elevations in conjunction with the plot of maximum bending moments (Figure 5.9), a trade-off is presented. Clearly, increasing the number of columns will reduce moments throughout the bridge. However, as the number of columns exceeds twenty to twenty-five, the reduction in bending moment begins to level-

off. At the same time bending moment is being reduced, the appearance of the bridge is becoming less and less open. From Figure 5.10c, it is clear that attempting to minimize bending moments will eventually result in a form that is nearly equal to a filled concrete arch. Even the employment of twenty-one columns, shown in Figure 5.10b**,** may not have been appealing to designers given the innovative forms and advancements in reinforced concrete that had been developed prior to the Woronoco Bridge's construction. One of the primary design considerations for the Woronoco Bridge may have been the maximization of open space between the arch and the deck. If so, trade-offs between reducing internal moments and increasing open space between the arch and deck were likely considered.

5.1.2.3 The Effect on Maximum Axial Forces

For completeness, the effect that column number has on axial forces throughout the bridge was also investigated. Using the same seven models, the maximum axial forces were recorded based on the same half-span live load (W_L = 1.5 tons/meter). The results are provided in Table 5.5 and are plotted in Figure 5.11.

Table 5.5 - The maximum axial forces results from each of the seven models in which the column number was incrementally varied.

Number of Spandrels	Spandrel Spacing (in)	Maximum Axial Force in Arch		Maximum Axial Force in Deck		Maximum Axial Force in Columns	
		(kip)	(kN)	(kip)	(kN)	(kip)	(kN)
6	250.00	57.49	255.72	17.67	78.60	22.67	100.84
9	156.25	62.58	278.36	20.58	91.54	14.40	64.05
11	125.00	64.19	285.52	21.62	96.16	11.17	49.70
15	89.30	65.41	290.94	22.50	100.08	8.12	36.12
21	62.50	65.79	292.63	22.91	101.90	6.15	27.36
26	50.00	65.68	292.14	23.03	102.44	5.04	22.42
41	31.25	64.53	287.03	22.97	102.17	3.21	14.28

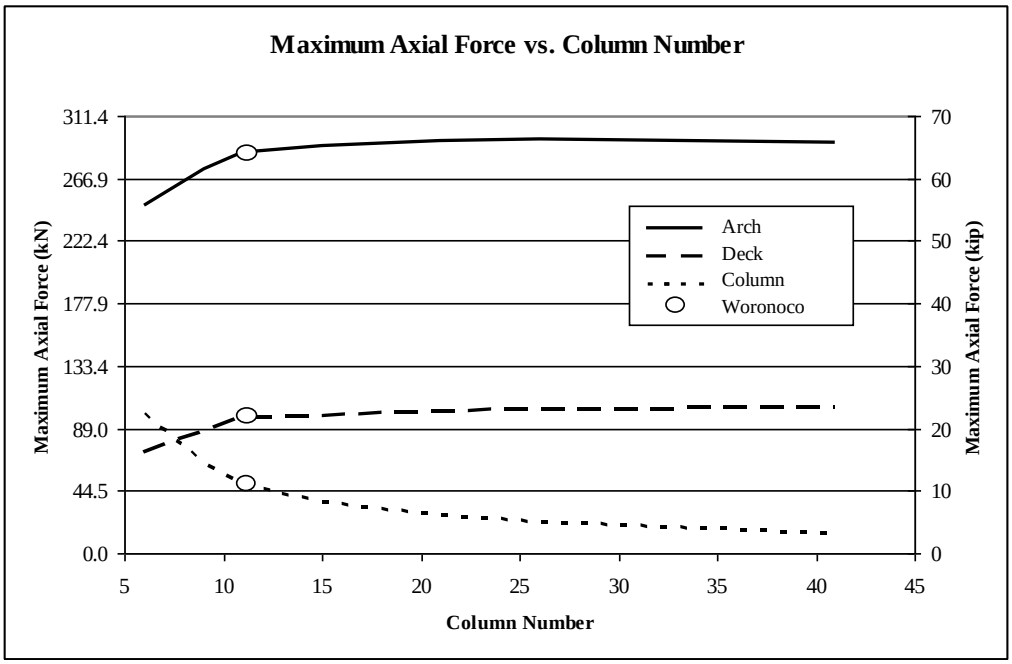

Figure 5.11 – Plot of the relationship between column number and maximum axial forces in the three load-carrying members.

From Figure 5.11, it is observed that the maximum axial force in each column continually decreases as the number of columns increases. This makes sense given that increasing the number of columns must then decrease the column spacing and the percentage of the total load each column is responsible for carrying. The maximum axial force in the arch and deck, however, increases, reaches a maximum value and then gradually decreases as the number of columns increases. The Woronoco Bridge is shown on Figure 5.11 to the left of these maximum axial force regions, which appear to fall between fifteen and thirty columns. As was observed with the parametric study of column stiffness, the designers of the Woronoco Bridge do not seem to have been as concerned with the minimization of axial forces as they were with both the minimization of bending moments and the creation of a light and open appearance.

5.2 The Effect of Deck Stiffness

Maillart's theory behind the design of his deck-stiffened bridges and its possible application to American open spandrel bridges is partly the motivation behind the creation of a representative computer model. According to David Billington's summary of Maillart's work, there is a theoretical point up until which increasing the stiffness of the deck, relative to the arch, will decrease the maximum bending moment in the arch. Beyond this theoretical point, where the arch stiffness at the crown is half of the deck stiffness, decreasing the stiffness of the deck, relative to the arch, will decrease the maximum bending in the arch. As a result, it is of interest to examine the effect of deck stiffness on the structural behavior of the representative Woronoco Bridge model. As with the investigation of column stiffness and spacing in the previous section, this study will aid in the understanding of design choices made by the original Woronoco Bridge engineers. In addition, it may be determined whether or not the Woronoco Bridge can be classified as a "deck-stiffened" open spandrel bridge.

5.2.1 Study of Deck Stiffness in the Woronoco Bridge

Both the deck of the Woronoco Bridge and the crown of the arch are 18 inches thick. The deck is 26'-8" wide. The arch, however, is divided into three ribs that are each only 2'-2" wide. As a result, the deck is approximately four times stiffer than the arch (at the crown of the bridge). Since many examples of American open spandrel bridges feature an arch and a deck that have practically the same stiffness at the crown of the bridge, it is not fully understood why the Woronoco Bridge engineers decided to divide the arch into ribs and thus reduce the arch's overall stiffness.

The representative Woronoco Bridge model created in SAP2000 (see Section 4.3) was used for this study. The study features the representative Woronoco bridge model (with an 18-inch thick deck) as well as eight variations of this model. Table 5.6 summarizes the deck cross-sectional dimensions used for each of the eight variations in this study. Note that the moments of inertia listed in Table 5.6 are based on the cross-sections of half of the bridge. This is because the representative model is a 2D frame of half of the Woronoco Bridge. Therefore, the width of the deck, arch and columns used in the representative model are half of the total width.

Table 5.6 - Summary of the nine deck stiffness models investigated as part of parametric study (*Actual geometric properties of the Woronoco Bridge).

Deck Thickness (in)	Deck Stiffness (in4)	IA/IG
9	9841.5	1.93
12	23328	0.81
14	37044	0.51
16	55296	0.34
*18	78732	0.24
20	108000	0.18
22	143748	0.13
24	186624	0.10
32	442368	0.04

5.2.1.1 The Effect on Maximum Bending Moment

All of the nine models were analyzed under the same half-span live load (W_L = 1.5 tons/meter). Table 5.7 summarizes the maximum bending moments found in each of the three load-carrying members for all nine deck-stiffness models. From this table, it is clear that as the deck is stiffened, the maximum bending moment in both the arch and columns decrease while the maximum bending moment in the deck increases. In order to more easily analyze the relationship between deck stiffness and the maximum moment in

each of the three load-carrying members, the results in Table 5.7 have been plotted versus the arch to deck stiffness ratio in Figure 5.12.

Table 5.7 - The maximum bending moment results from each of the nine models in which the deck stiffness was incrementally varied.

Deck Thickness (in)	Deck Stiffness (in4)	IA/IG	Max. Bending in Arch		Max. Bending in Deck		Max. Bending in Column	
			kip-in	kN-m	kip-in	kN-m	kip-in	kN-m
9	9841.5	1.93	304.96	34.46	232.70	26.29	368.18	41.60
12	23328	0.81	279.78	31.61	194.13	21.93	348.30	39.35
14	37044	0.51	266.73	30.14	219.05	24.75	351.48	39.71
16	55296	0.34	254.86	28.80	266.30	30.09	348.55	39.38
18	78732	0.24	243.65	27.53	327.31	36.98	341.77	38.62
20	108000	0.18	232.13	26.23	399.87	45.18	332.23	37.54
22	143748	0.13	220.34	24.90	481.49	54.40	320.63	36.23
24	186624	0.10	210.45	23.78	570.64	64.48	307.53	34.75
32	442368	0.04	167.90	18.97	966.65	109.2	248.39	28.07

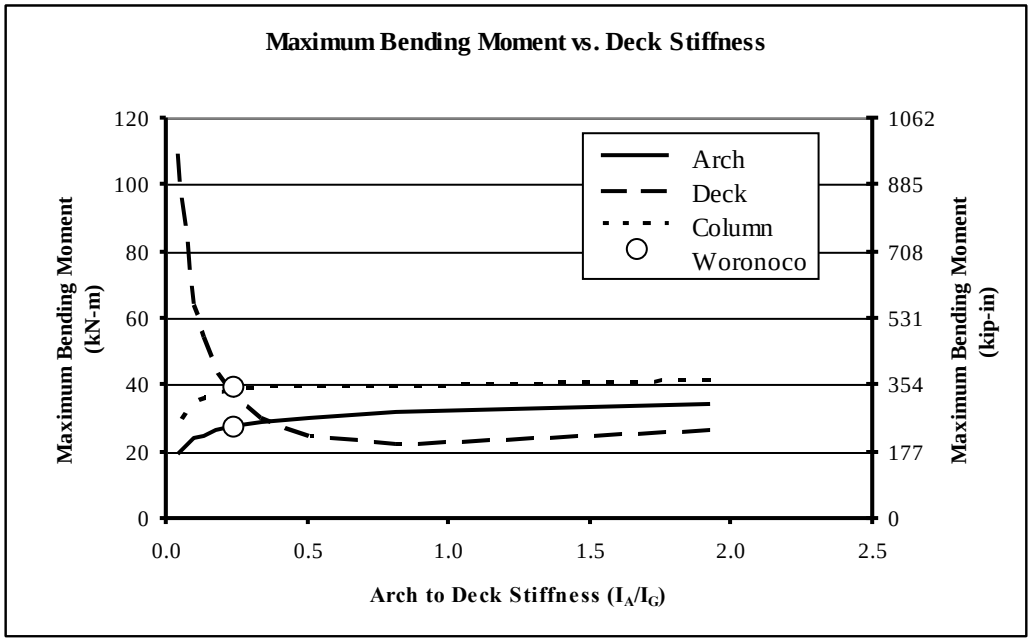

Figure 5.12 – Relationship between the maximum bending moment in each element and deck stiffness, based on the all-pinned computer model.

From Figure 5.12, varying the deck stiffness has a dramatic effect on the maximum moments in each load-carrying member up until a relative stiffness of approximately 0.5 (this stiffness ratio results from a 14”-thick deck). After this point, the effect of decreasing the deck stiffness relative to the arch is less noticeable.

It is important to discuss briefly that the maximum bending in the deck appears to have a local minimum at a ratio of 0.81 (a deck thickness of 12 inches). This is due to the nature of the bending moment distribution in the deck at different values of deck stiffness. Figure 5.13a-c is a series of pictures of the moment distribution for three of the nine model variations. For deck thickness greater than 12 inches, the positive moment in the deck provides the maximum moment. When the deck is thinner than 12 inches, however, the negative moment in the deck controls and gradually increases as the deck thickness decreases.

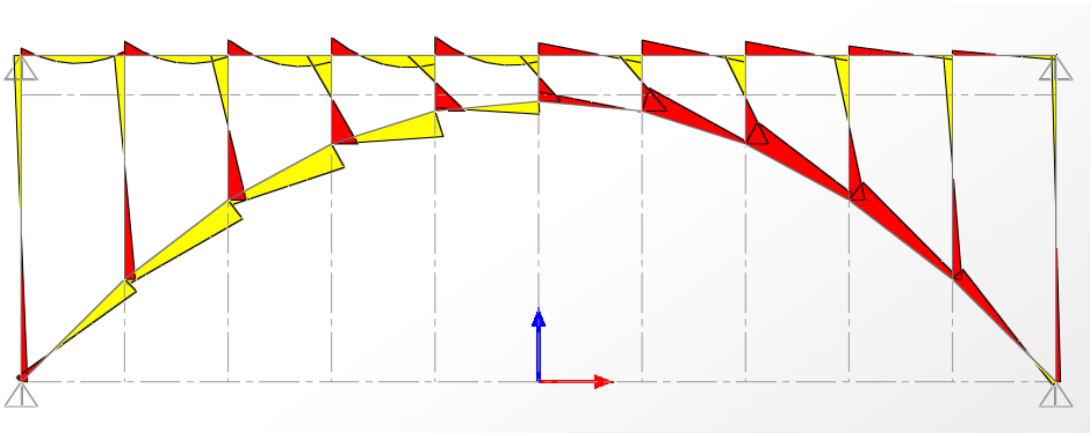

Figure 5.13a – Bending moment distribution for nine inch deck, all-pinned model.

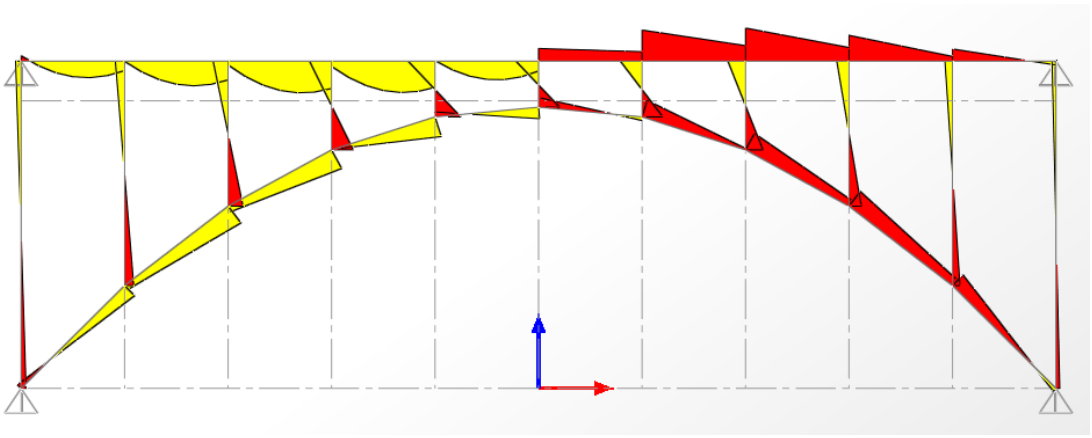

Figure 5.13b – Bending moment distribution for eighteen inch deck, all-pinned model (Woronoco).

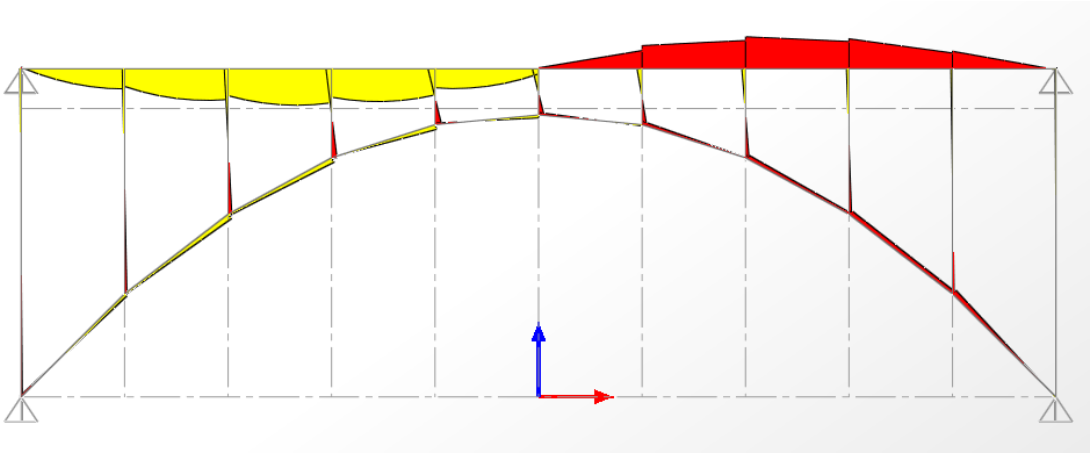

Figure 5.13c – Bending moment distribution for thirty-two inch deck, all-pinned model.

Returning again to Figure 5.12, insight into the design choice of Woronoco Bridge engineers can be gained. When the arch to deck stiffness ratio is less than 0.5 (the deck is thicker than 14 inches), the maximum bending moment in the deck decreases rapidly as the deck stiffness is reduced. Therefore, in this region there is a significant advantage gained from decreasing deck stiffness in terms of reducing the maximum bending in the deck. As the deck stiffness decreases, however, the bending in both the columns and arch increases. Similar to the study of column stiffness and spacing, a trade-off is presented.

Knowing now how deck stiffness affects the bending in each member, the deck size used in the Woronoco Bridge can be evaluated. The results for the representative Woronoco Bridge model which uses the actual bridge dimensions are indicated by circles in Figure 5.12. It appears as though the ideal region within which to design is from a ratio of about 0.24 to 0.5. Before this region, bending in the deck is dramatically higher than in either the columns or the arch. After this region, the advantage of increasing the deck thickness is minimal.

The Woronoco Bridge falls just within this ideal region. This suggests that the bridge engineers were aware of the relationship between deck stiffness and bending throughout the members. Had the Woronoco Bridge engineers chosen a thicker deck, and thus a smaller arch to deck stiffness ratio than 0.25, the maximum bending in the deck would quickly rise with little advantage in terms of reducing the bending in the columns and the arch. Had the Woronoco Bridge engineers chosen a much thinner deck and thus a greater arch to deck stiffness ratio than 0.5, it would suggest that deck-stiffening was not a design concern, but instead, arbitrary. It is puzzling, though, why the bridge engineers did not select a thinner deck that would result in a stiffness ratio of approximately 0.5 (14-inch thick deck). This choice would almost halve the bending in the deck while barely increasing the bending in either the columns or the arch.

In order to determine whether or not the Woronoco Bridge can be classified as "deck-stiffened", the arch results from the parametric study were isolated and plotted in Figure 5.14. In Billington's plot, bridges were "deck-stiffened" if they fell within the first region of the curve in which increasing deck stiffness decreased bending in the arch. From Figure 5.14, it is questionable whether or not the Woronoco Bridge is "deck-

stiffened". While it is obvious that by increasing deck stiffness the maximum bending in the arch will be reduced, this is true regardless of the arch to deck stiffness ratio. The existence of a critical point is not observed.

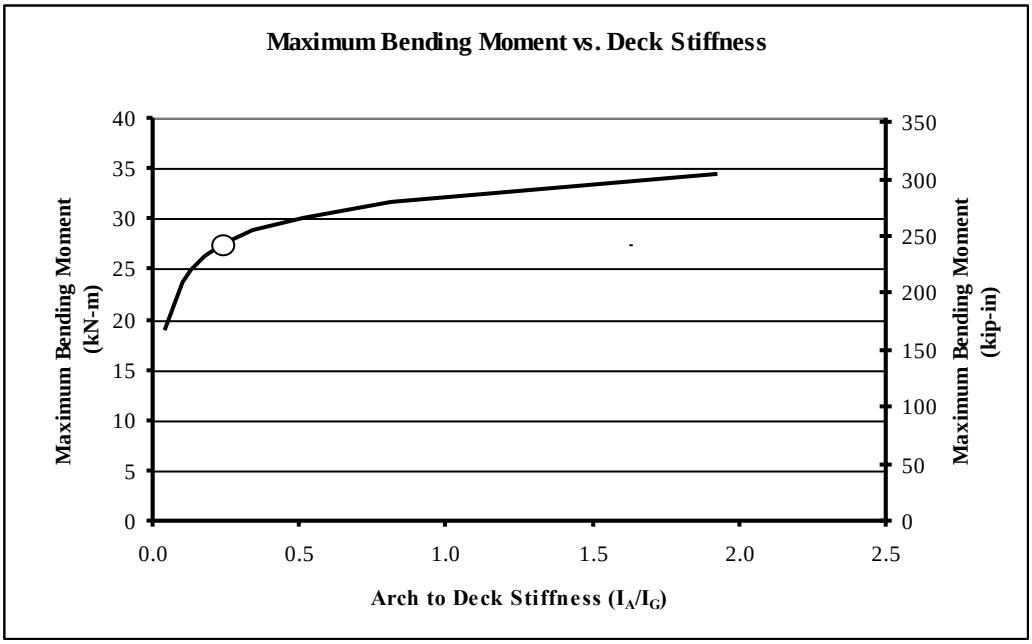

Figure 5.14 – Relationship between the maximum bending moment in the arch and deck stiffness, based on the all-pinned model.

In order to explain the absence of a critical point, the differences between Billington's assumptions and the assumptions used in the creation of the Woronoco Bridge computer model must be evaluated. The first major difference between these two analysis methods is the fixity of the spandrel columns to the arch and deck. While Billington considered the columns to be pinned at either end, the computer model recognizes continuity between the columns and both the arch and the deck. However, when the deck stiffness models are re-evaluated with the fixity at the ends of the spandrels released there is still no critical point. Figure 5.15 is a plot of the maximum bending moment in the deck and the arch in the deck stiffness models with pin-ended columns.

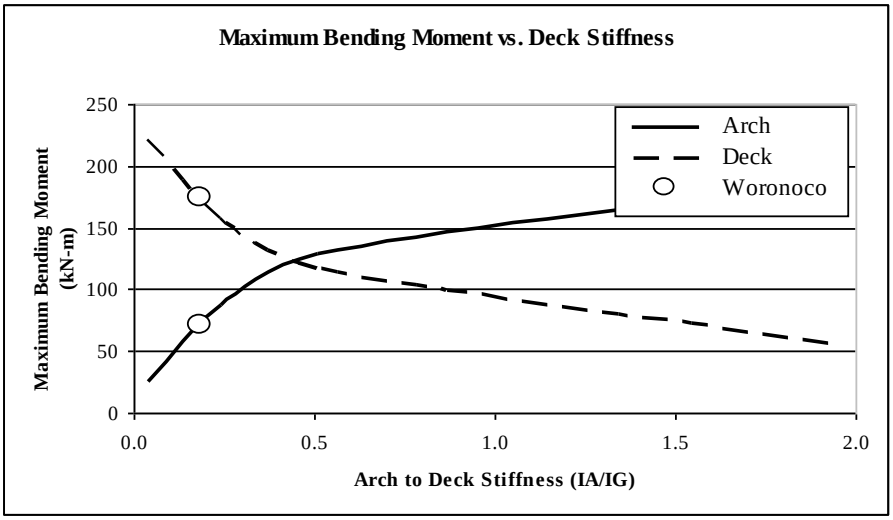

Figure 5.15 – Relationship between deck stiffness and the maximum bending moment, based on the all-pinned model in which the column ends are unable to transfer moment.

The second major difference in the two methods is the assumed geometry of the arch. Billington assumes a certain arch geometry that is accurate when applied to Maillart's deck stiffened bridges, but is much thinner than the actual arch geometry of the Woronoco Bridge. This difference, however, should only affect the accurateness of the arch to deck stiffness ratio. It would not affect the general shape of the curve and the absence of a critical point.

Another assumption involved in the creation of the representative computer model was that all of the abutments are most accurately modeled as fully pinned. This assumption is in line with Billington's method; however, it is of interest to evaluate the effect this assumption has on the bending moment distribution throughout the bridge. Figure 5.16 is a series of pictures that show how the bending moment distribution changes as a result of increasing the deck stiffness relative to the arch. While the maximum moment is at the ends of both the arch and the deck rather than at quarter-span, they follow a similar curve to that of the all-pinned model.

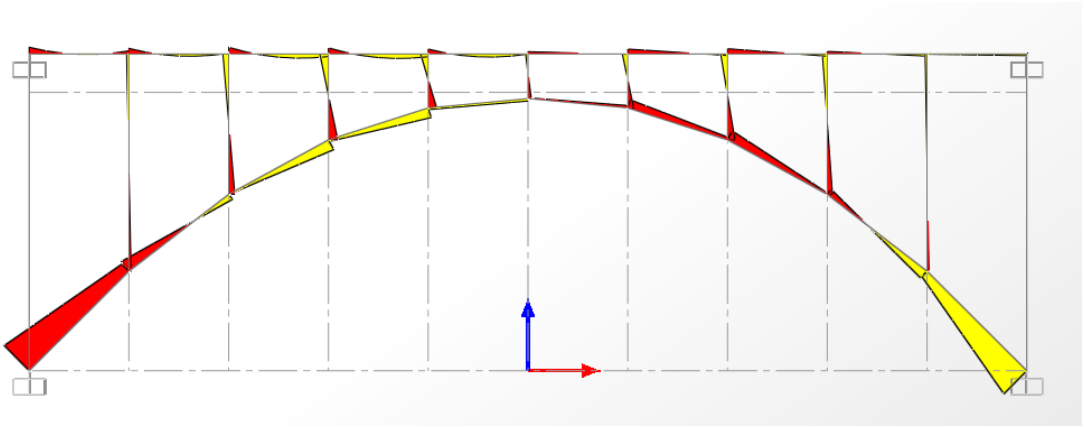

Figure 5.16a – Bending moment distribution for nine inch deck, all-fixed model.

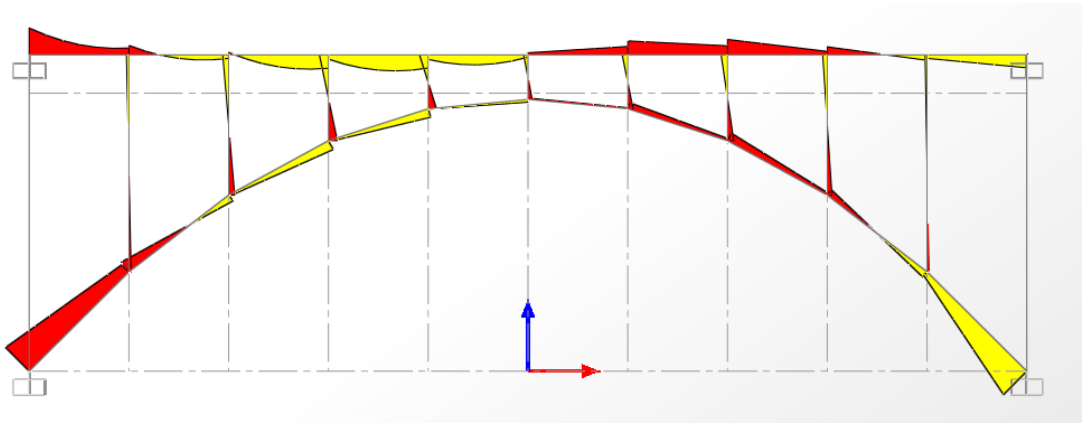

Figure 5.16b – Bending moment distribution for eighteen inch deck, all-fixed model (Woronoco).

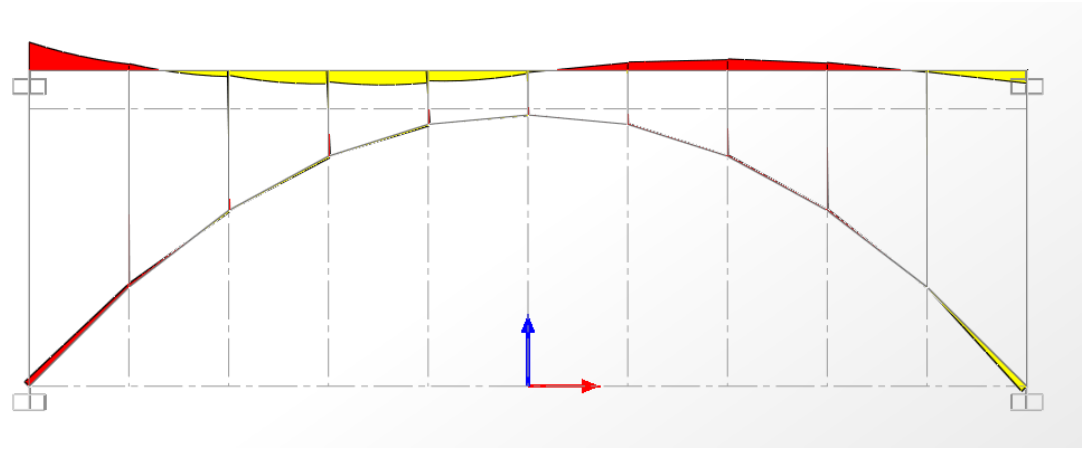

Figure 5.16c – Bending moment distribution for thirty-two inch deck, all-fixed model.

5.2.1.2 The Effect on Maximum Axial Forces

For completeness, the effect of deck-stiffening on the distribution of axial forces in each of the three load-carrying members was also evaluated. The results are summarized in Table 5.8. As in each of the previous sections, the results shown in this table were plotted in order to assist in the evaluation of design choices made for the Woronoco Bridge (Figure 5.17).

Table 5.8 - The maximum axial force results from each of the nine models in which the deck stiffness was incrementally varied.

Deck Thickness (in)	Deck Stiffness (in^4)	IA/IG	Max. Axial in Arch		Max. Axial in Deck		Max. Axial in Column	
			kip	kN	kip	kN	kip	kN
9	9841.5	1.93	66.32	294.99	22.80	101.41	11.69	52.00
12	23328	0.81	66.26	294.72	22.90	101.86	11.64	51.77
14	37044	0.51	65.82	292.77	22.65	100.75	11.53	51.29
16	55296	0.34	65.12	289.65	22.22	98.83	11.37	50.57
18	78732	0.24	63.99	284.64	21.54	95.83	11.03	49.06
20	108000	0.18	63.06	280.49	20.88	92.87	10.94	48.66
22	143748	0.13	61.67	274.31	20.03	89.09	10.68	47.50
24	186624	0.10	60.32	268.30	19.09	84.91	10.39	46.21
32	442368	0.04	53.93	239.88	14.92	66.36	9.28	41.28

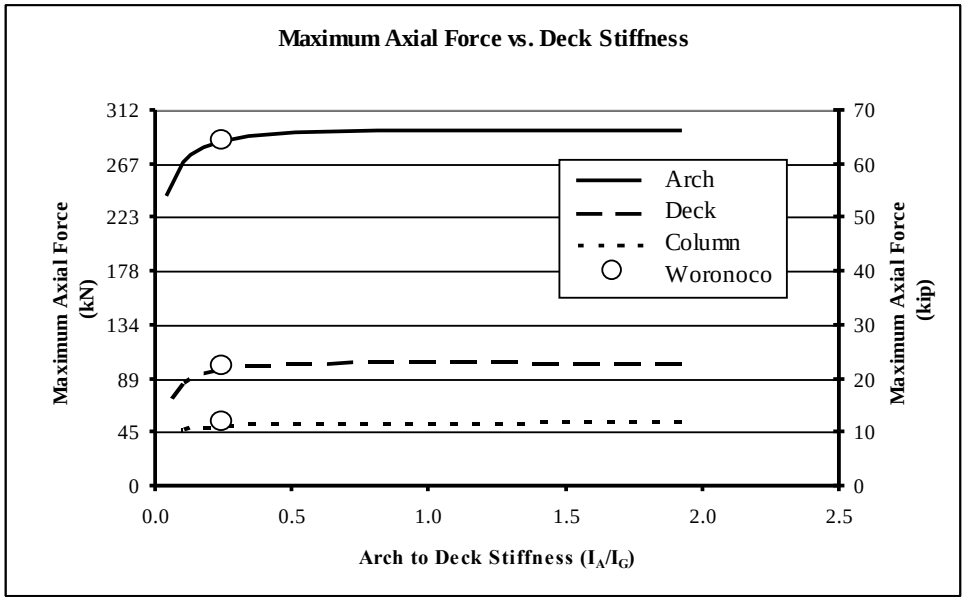

Figure 5.17 – Relationship between maximum axial force and deck stiffness, based on all-pinned model.

From Figure 5.17, it is clear that the arch is the primary axial load carrying member, regardless of the deck stiffness. When the deck stiffness is less than 18 inches and thus the stiffness ratio is greater than 0.25, the maximum axial force in each member is practically unchanged. When the deck stiffness is greater than 18 inches and thus the stiffness ratio is less than 0.25, the maximum axial force in each member is reduced. Since Woronoco Bridge engineers selected a deck thickness that results in a stiffness ratio of 0.25, it seems as though reducing axial forces throughout the structure was not a primary design concern. One must also consider, however, the aesthetic implications of thickening the deck in terms of accurately representing the load carrying responsibilities of each member.

5.2.1.3 The Influence of Aesthetics

Figure 5.18a-c is a series of pictures that show the axial force distribution from three of the nine deck-stiffness models. It is clear from Figure 5.17 that the arch is the principal axial load-carrying member. At the crown, the Woronoco Bridge is the same thickness as the deck. From Figure 5.18, the axial force at the crown of the arch and ends of the deck appear to be similar in magnitude. Therefore, sizing them equally makes sense in terms of reflecting the internal forces being resisted. If, however, the deck were to be thicker in order to reduce axial forces in all three members, the axial load carrying responsibilities would not accurately be portrayed. Additionally, as was discussed in Section 5.2.1.1, increasing the deck thickness would quickly increase the bending moment in the deck without a significant decrease in arch and column maximum bending moment.

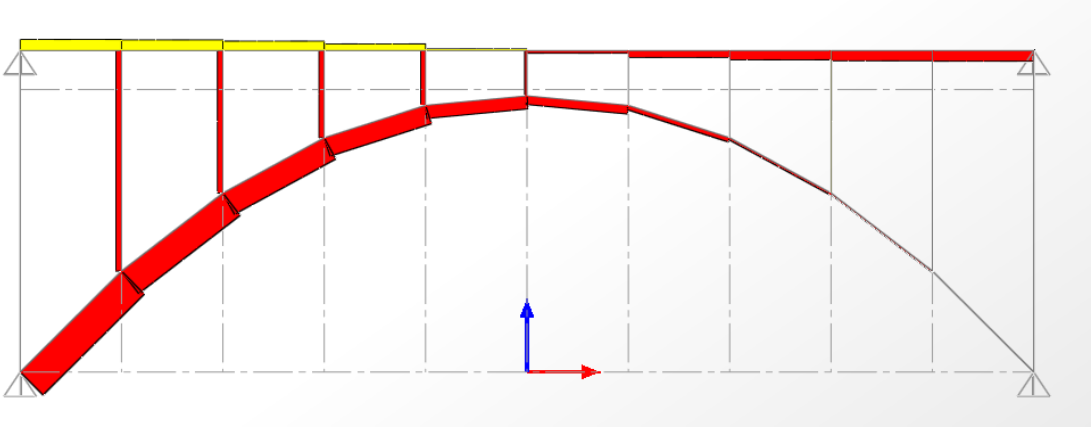

Figure 5.18a – Axial force distribution for nine inch deck, all-pinned model.

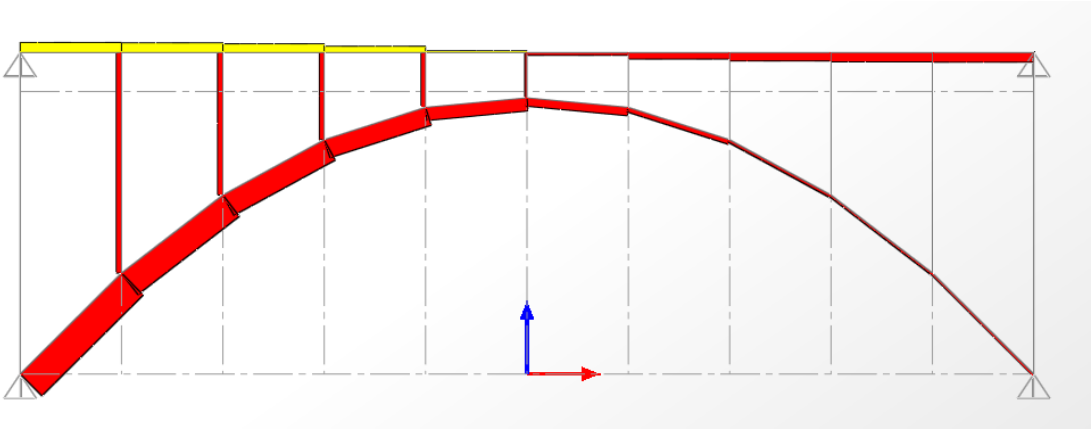

Figure 5.18b – Axial force distribution for eighteen inch deck, all-pinned model (Woronoco).

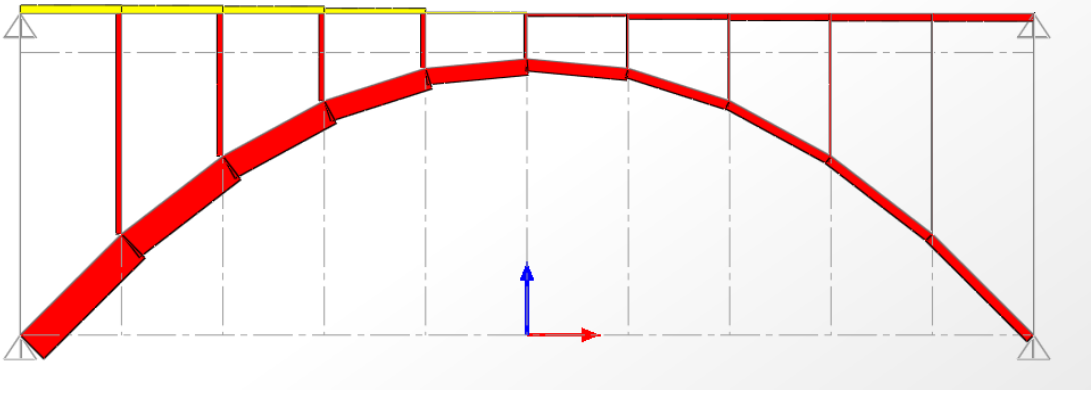

Figure 5.18c – Axial force distribution for thirty-two inch deck, all-pinned model.

Regardless of the deck stiffness, the arch dominates resisting axial forces. If the deck thickness were increased much beyond the thickness of the arch at the crown, not only

would it be wasteful from the standpoint of the material required to resist axial forces, but also it would misrepresent the role of the deck in resisting axial forces. Figure 5.19 provides the elevations of the existing Woronoco Bridge and a version of the bridge in which the deck thickness was increased to 32 inches. Comparing each elevation to the bending moment diagrams in Figure 5.18, it is clear that the existing Woronoco Bridge dimensions most accurately represent the distribution of axial forces throughout the structure.

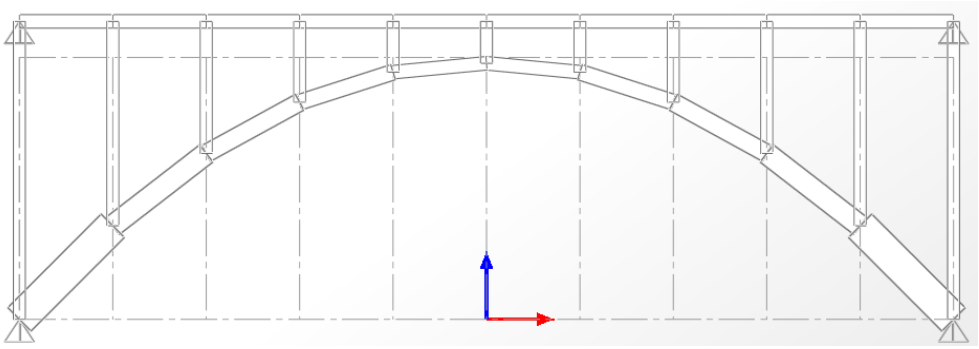

Figure 5.19a - Elevation of representative Woronoco Bridge model with eighteen inch deck.

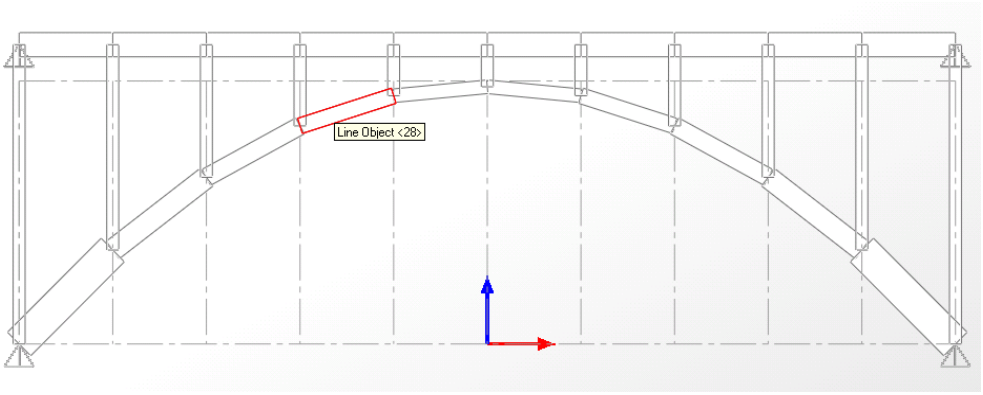

Figure 5.19b - Elevation of the thirty-two inch deck model.

5.2.1.4 Justification for Design Choices

From the parametric study investigating the effect of deck stiffness on the maximum bending moment, maximum axial forces and aesthetics of the Woronoco Bridge, several observations can be made. First, the existing arch to deck stiffness ratio of 0.24 falls within the ideal design region in terms of the maximum bending moment in each of the three load-carrying bridge members. While this location suggests that the bridge designers were aware of the relationship between deck stiffness and bending moment, it is questionable to what extent this relationship was understood. An arch to stiffness ratio of 0.5 appears to be a better choice in terms of minimizing the maximum bending in the deck while barely increasing bending in the other bridge members. Because it is suggested throughout literature that early American engineers relied heavily on experimental methods, it is possible that this relationship was evident, even if not fully understood.

Second, the issue of whether or not the Woronoco Bridge can be categorized as "deck-stiffened" is unclear. While the design of the bridge falls within a region in which an increase in deck stiffness would reduce the bending moment in the arch, there is not critical point at which this behavior is not observed. Third, the minimization of axial loads does not appear to have been a major design concern for the Woronoco Bridge engineers. The arch is the primary load carrying member and the sizing of each of the three members seems to reflect their respective responsibilities in resisting axial loads. As was discussed in the study of column stiffness and spacing, the appearance of the bridge is likely to have been an important design consideration.

CHAPTER 6

DISCUSSION OF RESULTS

The Woronoco Bridge is an existing example of an American reinforced concrete open spandrel arch bridge. Due to the ever-decreasing number of this type of bridge in America, as well as the aesthetic resemblance this bridge bares to the deck-stiffened arch bridges of Robert Maillart, there is a strong desire to better understand and more accurately model historic structures such as the Woronoco Bridge. In this effort, a computer model of the Woronoco Bridge was developed by first determining the assumptions that most closely represented the actual characteristics of the bridge. The investigation of assumptions pertaining to the computer model began with a proposed theoretical model of Robert Maillart's deck-stiffened bridges. In creating a computer model that agreed with this simplified theoretical model, the assumption inherent in the theoretical model could be identified and then adjusted to represent the Woronoco Bridge.

Each of the five major assumptions identified during the development of a computer model whose behavior matched the simplified theoretical model inspired investigation of the impact each assumption had on the distribution of bending moment within the structure. Four of the five major assumptions identified in the simplified theoretical analysis were resolved by construction drawings courtesy of HAER/Library of Congress and the use of a series of parametric studies:

- The arch and deck supports are all pinned and cannot carry any bending moment. This is based on construction drawings which do not indicate a substantial enough foundation to restrain rotation at the abutment.
- The best-fit parabolic arch that describes the Woronoco arch is assumed to carry uniform loading solely through axial forces since it was proven to be steep enough so as not to behave significantly as a beam

- The number and spacing of columns is taken from construction drawings of the Woronoco Bridge.
- The arch stiffness varies according to measured geometric values for the arch along its span.

One of the five assumptions, however, was less clear. This assumption dealt with the fixity at the ends of each column and, therefore, it was necessary to determine whether or not to treat the columns as pinned or fixed to both the arch and the deck. The simplified theoretical analysis assumes that columns are solely axial members whose ends are pinned and cannot transfer any moment. From photographs, however, evidence of metal reinforcement and the absence of cracking near the ends of the columns indicate that the columns are in fact all capable of significant moment transfer. This further differentiates American open spandrel bridges from those of Robert Maillart. Instead of the arch and deck combining to resist axial forces and bending moments, there are three load-carrying members: the arch, deck and a series of columns. In the creation of a representative model for the Woronoco Bridge, it was observed that American open spandrel bridges appear to use continuity between the columns, arch and deck to share moment carrying responsibilities.

Having identified a substantial difference between the design of American open spandrel bridges and the deck-stiffened bridges of Robert Maillart, it was of interest to investigate the effect of column stiffness and spacing in more detail. Parametric studies were performed for both column stiffness and spacing in order to determine the influence that columns have on the distribution of axial forces and bending moments throughout the bridge, as well as the aesthetics of the bridge. From these studies, a better understanding of the design priorities of early American engineers was gained. Among

the observations made from these studies, it was clear that not only do columns relieve the maximum bending in the arch but also the selection of column stiffness and spacing play a vital role in minimizing bending in the arch.

From the parametric studies of both column stiffness and spacing, it is reasonable to assume that the methods used by early American engineers made them aware of the advantages provided by a careful selection of columns size and spacing. From Figure 5.2 in Section 5.1.1.1 it is clear the maximum bending moment in the columns increases as the stiffness of the columns increase. The maximum bending in both the arch and deck, however, decrease rapidly as the column size is increased within the column to stiffness ratio range of 0 to 0.5. After the ratio of 0.5, the curves that represent the bending in the arch and deck begin to level off. Therefore, beyond this ratio of 0.5 there is little advantage to increasing the columns stiffness in terms of reducing bending moment in the arch and the deck.

The curve representing bending moment in the arch was then isolated and shown independently in Figure 5.3. This plot not only illustrated that a minimum in the bending moment in the arch exists but also that the columns of the Woronoco Bridge are designed such that they virtually achieve this minimum value. This result is important for a variety of reasons. First, it is evidence that supporting that the selection of column size, and thus stiffness, for the Woronoco Bridge was both informed and deliberate. Second, it indicates that the original designers of the Woronoco Bridge planned for and were aware of the interactions among the arch, deck and columns. Third, it proposes a structural achievement in American open spandrel bridges similar to Robert Maillart's "deck-stiffened" bridges: "column-stiffened" bridges.

The parametric studies of column stiffness and spacing also investigated the effect that column design has on the axial force distribution and aesthetic quality of the bridge. Figure 5.5 shows the relationship between column stiffness and the maximum axial forces in each of the three load-carrying members. Since the Woronoco Bridge is arguably located within the region of maximum axial force, it appears as though the reduction of axial forces were not a primary design consideration for the Woronoco Bridge engineers. And while the axial forces could have been reduced by further stiffening the columns, the Woronoco Bridge designers were most likely mindful of the aesthetic sacrifices this would require. By designing columns that significantly reduced bending in the arch, Woronoco Bridge designers had to account for the worst-case axial force distribution.

While the arch of the Woronoco Bridge is not as thin and elegant as some of Maillart's concrete arches, the form does accurately reflect the intended structural roles of each member. From Figure 5.5, it is obvious that the arch is the primary axial load carrying member. When one looks at a profile of the Woronoco Bridge side by side with the plots of axial force distribution throughout the bridge, it seems that the sizing of the arch, deck and columns were done in such a way so as to reflect the percentage of loads carried by each member. In light of this comparison, it is not unreasonable to propose that the designers of the Woronoco Bridge were conscious of the aesthetic consequences of their design choices.

In addition to the possible desire of early American engineers to have form reflect function, there was societal pressure to create light and open structures. With the advancement and standardization of concrete reinforcement prior to the construction of

the Woronoco Bridge came a race to design more elegant bridges that minimized the structures self-weight. Considering the progressive attitude of the time, as well as the widespread popularity of and confidence in reinforced concrete around the time of the Woronoco Bridge construction, it is reasonable to assume that aesthetics were a priority in the design of the structure.

From Figure 5.2, however, it is clear that while aesthetics were likely considered in the sizing of columns, they were not considered over the reduction of bending in both the arch and deck. Otherwise, the column size would have been reduced further. This would have increased bending in the arch and deck but decreased the material required for the bridge, thus creating a more open appearance. Given the choice of the column size in the Woronoco Bridge, it is reasonable to say that the design concerns of the original engineers in order of importance were 1) Reduction of bending in the arch and deck, 2) Create a light and open aesthetic quality that reflects the structural performance of the bridge, and 3) Resist axial forces.

It appears that aesthetics played an important role, in the selection of not only column stiffness but also column number. A parametric study was performed in which the number of columns was varied between six and forty-one. The resulting maximum bending moments in each of the three load-carrying elements are plotted versus column number in Figure 5.9. The Woronoco Bridge, with eleven columns, is indicated by circles in Figure 5.9. The Woronoco Bridge's location on this curve does not achieve a minimum value and, therefore, does not clearly justify the choice of eleven columns. It does, however, explain why engineers ruled out using fewer columns despite the desire to make an open appearance.

In an attempt to understand why Woronoco Bridge engineers did not increase the number of columns to further reduce the bending in each of the three load-carrying members, consider the aesthetic consequences of such a choice. Comparing the different elevations provided in Figure 5.10, it is easy to see that as the number of columns increases, the structure approaches the appearance of a traditional closed arch. This closed and bulky form was abundant prior to the birth and widespread acceptance of reinforced concrete. With this new material that could compensate for concrete's weakness in tension, however, came the ability to reduce the material required to withstand bridge loads. Therefore, an increased number of spandrels and closed form would not reflect the advantages of reinforced concrete and would go against the innovative atmosphere of the time. While column stiffness appears to have been a decision based on reducing bending moments first and creating a light, open appearance second, column number appears to have been a decision made by balancing the two considerations with similar weight.

This paper began with a theoretical analysis that was then adapted to represent an existing example of an American reinforced concrete open spandrel bridge. Since this theoretical model was developed to illustrate the structural achievement of "deck-stiffening," it is of interest to use the computer model developed in this paper to investigate the effect of deck stiffening in the Woronoco Bridge. Performing a parametric study in which the deck stiffness of the representative model was incrementally varied the relationship between bending moment and deck stiffness was observed. This relationship is shown visually in Figure 5.12.

From this plot, it appears as though the ideal region within which to design is from a ratio of about 0.24 to 0.5. Before this region, bending in the deck is dramatically higher than either the columns or the arch. After this region, the advantage of increasing the deck thickness is minimal. The Woronoco Bridge falls just within this ideal region. This suggests that the bridge engineers were aware of the relationship between deck stiffness and bending throughout the members.

To determine whether or not the Woronoco Bridge is "deck-stiffened", one must return to the theoretical model that first proposed this structural advantage. In Billington's plot, bridges were "deck-stiffened" if they feel within the first region of the curve in which increasing deck stiffness decreased bending in the arch. From Figure 5.12, it is questionable whether or not the Woronoco Bridge is "deck-stiffened." While it is true that by increasing the deck stiffness the maximum bending in the arch is reduced, this is true regardless of the arch to deck stiffness ratio. The existence of a critical point is not observed. Even when the computer model is revised such that the columns are pinned at each end, there is not critical point at which the bending in the arch is no longer increased as the deck stiffness is reduced.

Despite this difference in behavior, Figure 5.12 indicates that engineers of the Woronoco Bridge intended the deck to be the primary bending moment-carrying member. The arch, on the other hand, was intended to be the primary axial load-carrying member. This is illustrated yet again in Figure 5.17. Again, the minimization of axial forces does not seem to be a design concern in terms of deck stiffness. However, the aesthetic consequences of stiffening the deck would not only take away from the light appearance but also misrepresent the axial load-carrying responsibilities of the bridge.

The three design considerations investigated in this paper, reducing bending moments, axial forces and the material required to withstand loads, all seemed to play a role in the sizing of the Woronoco Bridge columns and deck. For the selection of column size, the minimization of bending moment in the arch and deck was the primary consideration, followed by the creation an open aesthetic form. For the selection of column number, the minimization of bending moment in the arch and deck was balanced with the creation of a light form to achieve a compromise between the two priorities. And finally for the decision of deck stiffness, the Woronoco Bridge designers appear to have been similarly balancing the reduction of bending moment in the arch with the aesthetic consequences of structural advantage.

Each of these parametric studies suggests that the designers of the Woronoco Bridge were aware of certain structural and aesthetic advantages to their design choices. The bridge was built in a time of great pressure to make structures thinner and also represent the load carrying responsibilities of each member in the final form. It is reasonable to assume that aesthetics played a role in the design of the bridge, or else structural advantages of stiffening certain elements would have been made. In addition to the creation of a pleasing form, the design intentions of the deck to primarily resist bending, the arch to primarily resist axial forces and the columns to connect the arch and deck through fixed ends is clearly observed in the parametric studies. The structural advantage of column fixity in terms of minimizing bending moment in the arch is one that is similar to the theory developed by Robert Maillart for the design of his "deck-stiffened" bridges. While it is uncertain as to whether or not the Woronoco Bridge is a surviving example of

an American "deck-stiffened" bridge, it is certainly a living model of a "column-stiffened" bridge.

The model developed in this paper could be used to evaluate the strength of specific open spandrel bridges and its performance under different loading conditions. Since the Woronoco Bridge is currently closed to traffic, the model could be used to load rate the bridge and determine the capacity with the goal of providing a safe weight posting and reopening the bridge. It is an elegant bridge that is not visible from the surrounding area. By reopening it to local traffic, perhaps an interest in incorporating it back into the landscape would be ignited. Additionally, the model used in this paper serves as a starting point from which similar parametric studies can be performed under more different loading conditions. Non-uniform loads, for example, could be applied to this model in order to determine how the stiffness of different elements effect how the load-carrying responsibility is shared among the deck, arch and columns. With both practical and theoretical applications, it is hoped that the observation made in this paper will aid in better understanding and, ultimately, preserving the ever-decreasing number of surviving historic bridges in America.

PART II: IRON LENTICULAR TRUSS BRIDGES

CHAPTER 7

BACKGROUND

7.1 Development of American Lenticular Truss Bridge

Lenticular trusses are an intriguing part of early bridge engineering history in America. From 1880 to just before the turn of the century, these bridges dominated the modest-span bridge market in New England and surrounding areas. Despite many engineer's disapproval of the design, the leadership of Charles M. Jarvis and the ambitious sales force of the Berlin Iron Bridge Company were able to design and construct on the order of 400 to 700 lenticular trusses.[5,6] Unfortunately, only 50 examples of this truss design are known to still exist nationally.[2] The innovative form combines an arch and a suspension bridge into a single structure (Figure 7.1). Like many historic bridges, however, it is quickly disappearing. More detailed research of lenticular trusses is required to preserve and better understand the few remaining built examples of this remarkable design that overcame heavy criticism and dominated the New England area at the end of the nineteenth century.

Figure 7.1 – Bardwell's Ferry Bridge illustrates the two structural forms integrated in lenticular bridges: the arch (red) and suspension cable (blue) (photograph courtesy of HAER/Library of Congress).

Lenticular bridges are singular in that they combine an arch and a suspension bridge into a single structure. The thought behind curving the upper and lower chord comes from the parabolic moment diagram that results from uniform loading of a horizontal span. By curving the load bearing chords, "stresses in all the segments of a parabolic chord are equal (the stress in the chords of a parallel chord truss increase toward mid-span). Additionally, there are no stresses in the diagonal web members of a parabolic truss under uniform load. A moving load, however, requires a counter in each panel."[5] Because arches and cable action alone cannot easily carry non-uniform or concentrated loads,[7,8] it is common to see them accompanied by truss forms in bridge design (Figure 7.2). Two bridges in one, the lenticular truss is a fascinating part of America's engineering history.

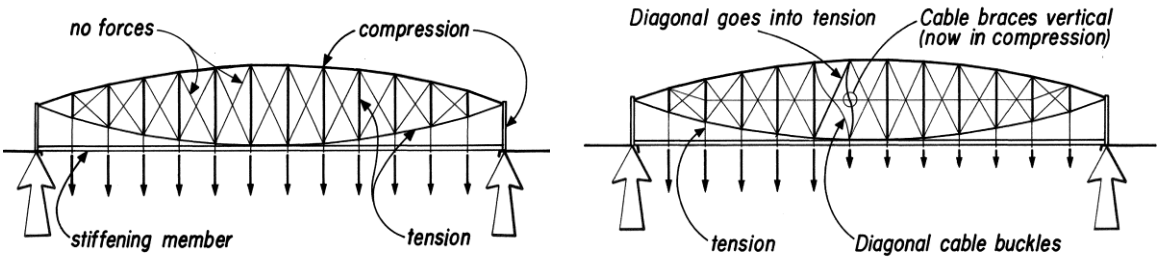

Behavior under a full load **Behavior under a partial load**

Figure 7.2 – The truss system is not engaged until there is a non-uniform load acting (courtesy of HAER/Library of Congress).

Although the origin of lenticular bridges has been traced back to Europe as early as the 1820s with designs drawn by Debia Laves and trusses built by George Stephenson, their presence in America was first documented with James Barnes' 1849 patent. This patent united "the two chords, the upper and lower, of an ordinary truss into one elliptical or oval curve." [U.S. Patent 26,230 (1849)]. Following in the footsteps of Barnes, several

other individuals received patents for bridge designs which featured elliptical, parabolic, or curved upper and lower chord arrangements and were often accompanied by a truss configuration of some kind. While various patents were obtained, there is limited documentation that proves whether or not these early patented designs were ever built. In fact, it was not until William Douglas' first patent in 1878 (Figure 7.3), that a patented design for a lenticular truss is known to have actually been constructed in America.[5]

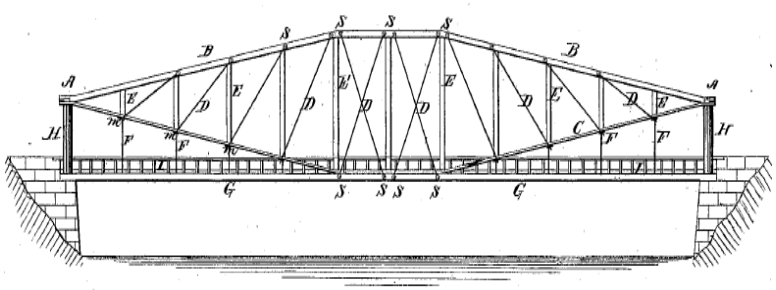

Figure 7.3 – One of three deck configurations provided in Douglas's 1878 patent [U.S. Patent 202,526].

Lenticular-shaped iron trusses were built in America almost exclusively by the Berlin Iron Bridge Company and dominated bridge construction in New England and the surrounding areas between the early 1880s and the turn of the century. The company's predecessor, The Corrugated Metal Company, had struggled until Charles Jarvis joined the firm. Jarvis was a young graduate who had studied engineering at Yale University. He modified Douglas's truss and headed an immense sales force that promoted lenticular trusses throughout the northeast, despite many engineers having denounced the design.[5] It is estimated, although no exact number can be determined, that this company built something on the order of 400 to 700 lenticular trusses in America.[5,6]

Adding to the momentum that Jarvis' leadership and insight provided, Douglas received a second patent in 1885 which improved upon his original design (Figure 7.4).

This is the design that is typically associated with the Berlin Iron Bridge Company. The primary differences between the two patents included the addition of a tensile deck-level chord and a strut brace in the end panels for longer spans. These alterations are speculated to have been in response to vibration concerns and were the result of field experience rather than rigorous theoretical analysis. Despite the improvements, however, it was still not considered by engineers of the time to be an equal to other truss forms, such as the Pratt truss.[5]

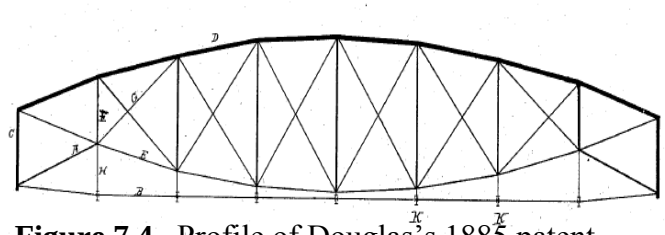

Figure 7.4– Profile of Douglas's 1885 patent [U.S. Patent 315,259].

There are several criticisms of the lenticular truss design that led engineers to claim it was inferior to other truss forms that were available at the time. Because the height of the lenticular truss tapered down from mid-span to the supports, the design often left little headroom to provide lateral bracing at any point except the center of the bridge. In addition to insufficient lateral support, many claimed that the fabrication of the lenticular bridge was more expensive than that required for parallel chord trusses. After all, the lengths of the diagonals varied in each panel due to the tapered nature of the lenticular shape. Aside from bracing and fabrication concerns, there were also issues regarding the bridge's deck. Not only was it more difficult to attach a deck to a curved chord than to a horizontal chord, but also the deck rarely contributed any stiffness to the bridge because it was often suspended on hangers entirely below the lower chord. These factors, when combined with the fact that the lenticular truss continued to be built out of iron during a

time when steel was becoming the material of choice, prevented the ultimate success of Berlin Iron Bridge Company's and its novel design.[5]

Even though many looked down on the design, however, there were benefits to the bridge's peculiar arrangement. Specifically, the combination of the suspension and arch form had a noteworthy benefit during construction. Because the arch acts in compression and the suspension cable acts in tension, the horizontal forces of the bridge are balanced (Figure 7.5). In typical arch bridges, however, the net horizontal force that results from the arch being compressed is transferred to and resisted by the supports in order to achieve equilibrium. This transfer requires that most arch bridges be constructed in place. Lenticular bridges, on the other hand, may be constructed without the presence of horizontal supports. Because they could be constructed on the ground and later lifted into place, lenticular bridges were easier to construct than many other arch bridges of the time.[2]

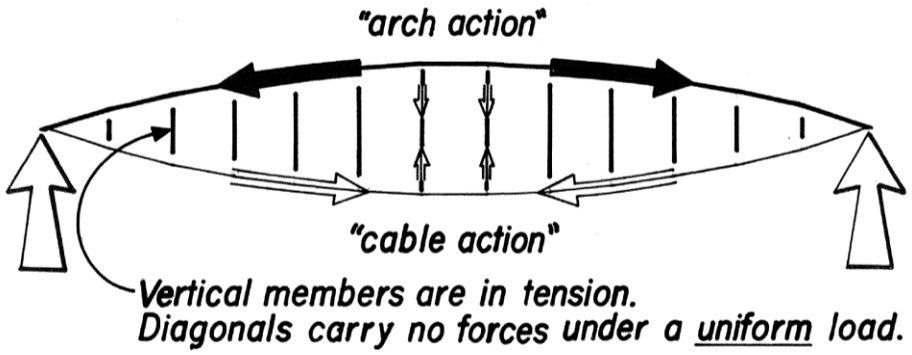

Figure 7.5 – The opposition of compression and tension forces result in zero net horizontal force at the abutments, which only need to provide vertical support (courtesy of HAER/Library of Congress).

Although an estimated 400 to 700 lenticular iron trusses were built by the Berlin Iron Bridge Company, only 50 still exist nationally.[2] Of the 50 surviving examples, nine are

located in the Commonwealth of Massachusetts. Only three of the nine are currently open to vehicular traffic.[6] As is the case with most historic bridges, there is an enormous call to evaluate the strength and behavior of these rare structures in order to better preserve and rehabilitate the few remaining examples of our nation's early engineering history. Lenticular trusses stand out in the crowd of historic bridges as an innovative design that came and went quickly, and yet dominated all other modest span bridge forms in New England for a little over a decade, despite being labeled as poor bridge design.[5]

CHAPTER 8

FINITE ELEMENT ANALYSIS OF BARDWELL'S FERRY BRIDGE

8.1 Identification of Critical Connection

In the attempt to evaluate prove the structural merit of the lenticular truss bridge, several computer models of an existing lenticular truss bridge were created and used to investigate the behavior of a critical connection under a rolling live load. The following sections outline the procedure that was used to identify the location of a critical connection and to create representative computer models. The maximum stresses that result in the connection due to this load are reported and used to estimate the fatigue life of the existing lenticular truss bridge. By better understanding the structural behavior of a specific lenticular truss bridge it is hoped that the few remaining examples will remain as physical examples of our nation's bridge building history.

One of the three lenticular truss bridges in Massachusetts that is still servicing vehicular traffic is the Bardwell's Ferry Bridge located in Shelburne, MA (Figure 8.1). Bardwell's Ferry Bridge was selected for use in this study because its design is representative of the lenticular trusses that were mass-produced by the Berlin Iron Bridge Company in the late 1880s. The dimensions for Bardwell's Ferry Bridge were obtained from original drawings and plans that were collected by the Historic American Engineering Record (HAER), available publicly on the Library of Congress website.[2]

These plans and drawings were used to first create a global, 2-dimensional model of the Bardwell's Ferry Bridge with SAP2000 software. This model was subjected to a moving truck load in order to identify a critical connection and also provide the maximum axial forces that result from a moving truck load in each member of the

connection. The connection of interest was then investigated in more detail by creating local models using ADINA finite element software and applying these maximum loads (explained in more detail below).

Figure 8.1 – Photograph of Bardwell's Ferry Bridge.

The majority of the connections on the Bardwell's Ferry Bridge are assumed to be pinned. This is an appropriate assumption given the engineering practices at the time of construction and visual inspection of connection (Figure 8.2). Thus, to replicate the actual behavior of the lenticular truss, connections in the SAP2000 model were pins that allowed rotation around an axis perpendicular to the plane of the connection elements. As a result, no bending moments are transferred at connection sites. However, significant axial and shear forces are transferred through the connections.

Because the effect of stresses caused by axial forces acting on the connection is the focus of this analysis, it was important to accurately model the geometry of load-carrying

members of the Bardwell's Ferry Bridge. When possible, the elements of the Bardwell's Ferry Bridge were recreated in SAP2000 exactly as they are described in HAER records (Figure 8.3). In certain cases where members were comprised of built-up, irregular members, care was taken to replace them with an equivalent member that maintained the same cross-sectional area and a similar moment of inertia. Again, because the effect of axial forces is the focus of the research, it was critical to maintain the correct cross-sectional area of each member. Material properties for wrought-iron were taken as those reported by Boothby[8], and are summarized in Table 8.1 below for convenience.

Table 8.1 – Material property data used for wrought iron models.

Specific Weight	490 lb/ft^3
Modulus of Elasticity	28,000 ksi
Shear Modulus	10,800 ksi
Poisson's Ratio	0.3

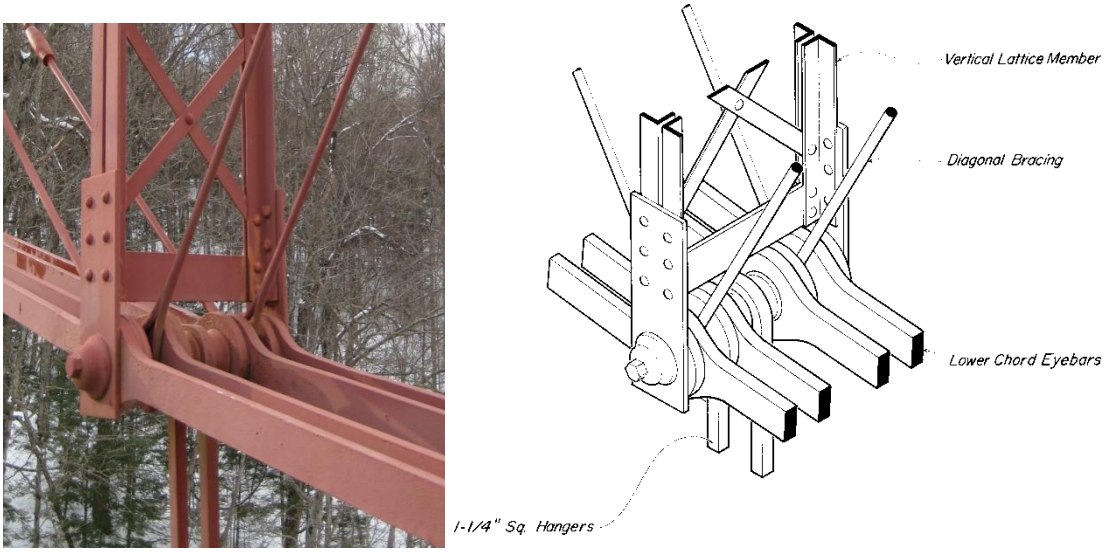

Figure 8.2 – Lower chord connection at Bardwell's Ferry Bridge (courtesy of HAER/Library of Congress).

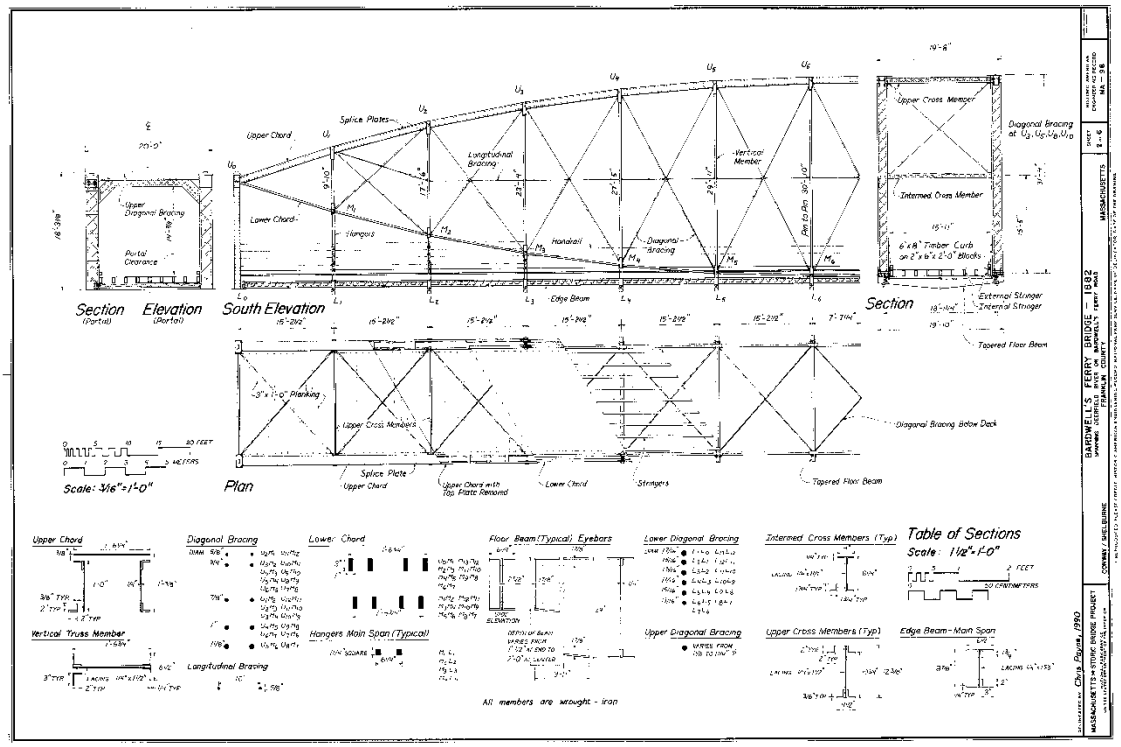

Figure 8.3 – Elevation drawing of the Bardwell's Ferry Bridge with geometries of load-carrying elements (courtesy of HAER/Library of Congress).

Figure 8.3 shows the actual dimensions of all the members which make up the lenticular truss. With the exception of the upper chord, vertical truss chords and the edge beam, all members were modeled in SAP2000 using these specifications exactly. The upper chord, vertical truss members and the edge beam were slightly modified. In the Bardwell's Ferry Bridge, the upper chord is made up of three rectangular plates and four angles. Rather than replicate this built-up shape exactly, an equivalent box-section with a total cross-sectional area is 17.4 in^2 was used. The vertical truss members are comprised of a rectangular plate that is sandwiched between two pairs of angles. This geometry was replaced by a double channel section with a total cross-sectional area of 9.4in^2. The edge beam was similarly modeled as a double channel section with a total area of 5.2in^2. All

members that serve as lateral-bracing or secondary load-carrying elements were not included in the 2-dimensional SAP2000 model.

After creating the 2-dimensional frame model of Bardwell's Ferry Bridge in SAP2000 (Figure 8.4), the model was subjected to a moving truck load in order to identify the critical connection. The Bardwell's Ferry Bridge currently has a posted weight limit of ten tons. This means that no truck over 10 tons (20 kips) is allowed to pass over the bridge without applying for and receiving an overweight permit from the state. Therefore, in order to evaluate the stresses generated in a critical connection of the bridge under realistic loading conditions, HS truck loads that were similar to this posted limit were applied to the 2-dimensional frame model. Note that since the model is only of one truss frame, the posted 10 ton capacity becomes five tons per frame in the analysis. As a result, the truck loads used in this analysis varied between HS-1 and HS-6 trucks.

The vehicle loads used in this analysis were scaled HS-44 trucks. One example is an HS-2, with a total load of approximately 7.2 kips (a leading point load of 0.8 kips and two trailing point loads of 3.2 kips each). It is important to point out that standard practice in load evaluation of bridges is to use either an HS-20 or HS-25 truck. This is because these are the live load standards that are required for current bridge design. However, the only difference between these trucks and an HS-44 is the magnitude of the point loads at each of the three axles. And since the bridge is currently posted at a 10 ton limit (20 kips), neither an HS-20 (total weight of 72 kips) nor an HS-25 (total weight of 90 kips) would be permitted to cross the Bardwell's Ferry Bridge. Therefore, any truck over a total load of 10 tons (20 kips) would need to be scaled and reduced significantly in order to be a realistic live load for this posted, historic bridge.

As a result, HS-44 truck loads were scaled down to solve for a variety of loads that fall within or just above the Bardwell's Ferry Bridge posted capacity. These truck loads were then assigned as a moving load to create an envelope of maximum and minimum axial forces in every member throughout the bridge. Figure 8.5 shows two pictures of the axial force envelope that result from this loading. Table 8.2 summarizes the maximum axial forces in each load-carrying element as they relate to the truck load. Note that truck load is given as a percentage of the posted bridge capacity (10 tons total, therefore 5 tons per frame).

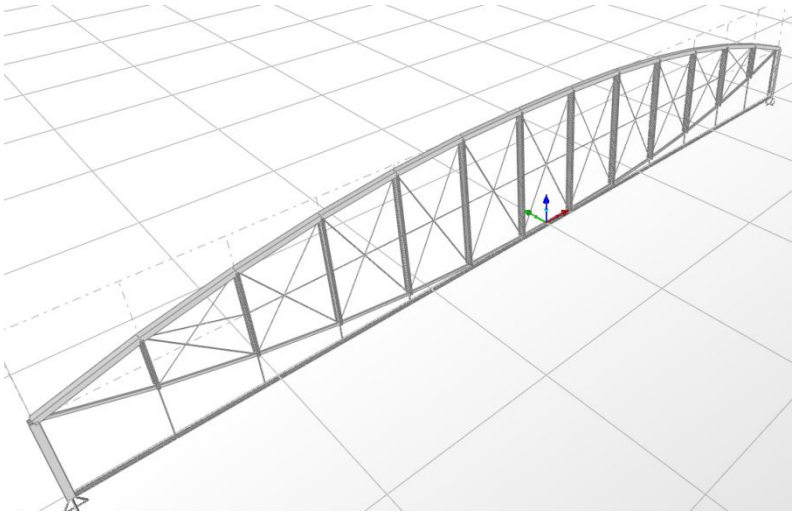

Figure 8.4 – View of 2-dimensional frame built in SAP2000 (this model determined both the location and axial forces in the critical connection).

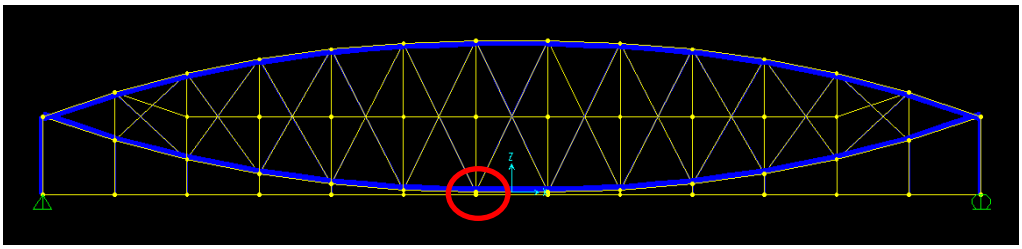

Figure 8.5a – Axial force envelope that results from a moving truck load (global view, red circled area shown magnified in Figure 8.5b).

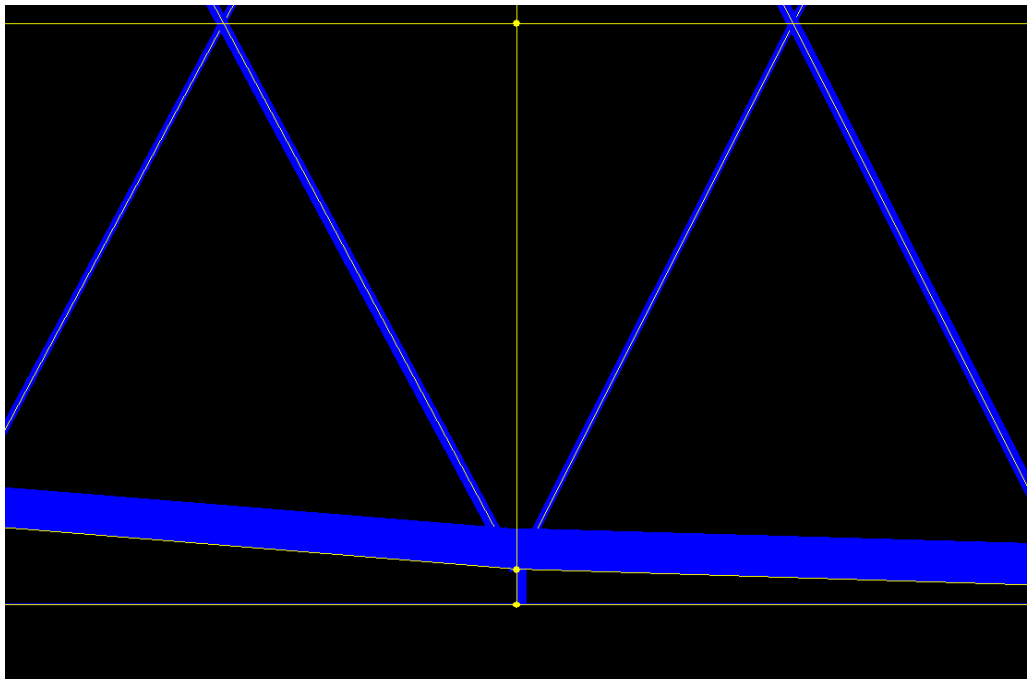

Figure 8.5b – Axial force envelope that results from a moving truck load (close up of red circled area in Figure 8.5a).

Table 8.2 – Maximum axial forces resulting from various truck loads.

Truck load (% of single frame capacity & HS Equivalent)	Max. Axial Force in Lower Chord (kips)	Max. Axial Force in Eye bar (kips)	Maximum Axial Force Per Node (kips)
33% (~HS0.9)	10	2.5	0.3125
36% (HS-1)	10.353	2.588	0.3235
52% (~HS-1.5)	15	3.75	0.46875
67% (~HS-1.9)	20	5	0.625
72% (HS-2)	20.705	5.176	0.647
108% (HS-3)	31.058	7.765	0.97
200% (~HS-5.8)	60	15	1.875
216% (HS-6)	62.116	15.529	1.94
400% (~HS-11)	120	30	3.75

It is clear from Figure 8.5 that the primary axial load-carrying elements in this connection are the lower truss chords. All of the other local maxima are significantly less than that observed in the eye bars that make up the lower truss chord. As a result, there may be

significant tensile stresses in the eye bars as well as significant shear stresses in the pin around which eye bars are pulling in opposite directions.

8.2 Maximum Stresses in Critical Connection

To investigate these stresses in more detail, second and third, more detailed models were created using ADINA finite element software. The goal of the second model is to accurately represent the connection, describe the stress distribution within the connection, and ultimately prove its ability to withstand heavy truck loads over time. And if this cannot be proven, then the model will identify the critical points within the connection that should be monitored closely to prevent unexpected fatigue and failure (areas of high stress concentrations).

8.2.1 Development of ADINA Models

The eye bar and pin geometries were determined from field measurements and entered into ADINA manually. Measurements were taken in the spring of 2009 at the Bardwell's Ferry Bridge in order to accurately represent the geometry of the pin and the eye bars. The pin was measured to be three and a half inches in diameter and the outer diameter of the eye bar was measured to be nine inches. The portion of the eye bar that is not curved is a one by three inch rectangular bar.

Although the lower chord in the Bardwell's Ferry Bridge is made up of four eye bars and every lower chord connection joins eight eye bars at a single pin, not all of the eye bars were modeled. The reason for this is that the eye bars are arranged around the pin in four similar, symmetric sets (Figure 8.2). Each set is comprised of two eye bars, each

pulling in opposite directions. Models were made for a single eye bar set in order to investigate the behavior of eccentric eye bar connections (Figure 8.6). Additionally, a model in which three eye bars are connected by a single pin was also created to investigate the behavior of concentric eye bar connections (Figure 8.7). By modeling both connections, much is learned about stress transfer from one member to another as well as critical locations within both the pin and the eye bars. Using the concentric, three-bar model as an example, the process for developing each ADINA model for the lower chord truss connection is summarized below.

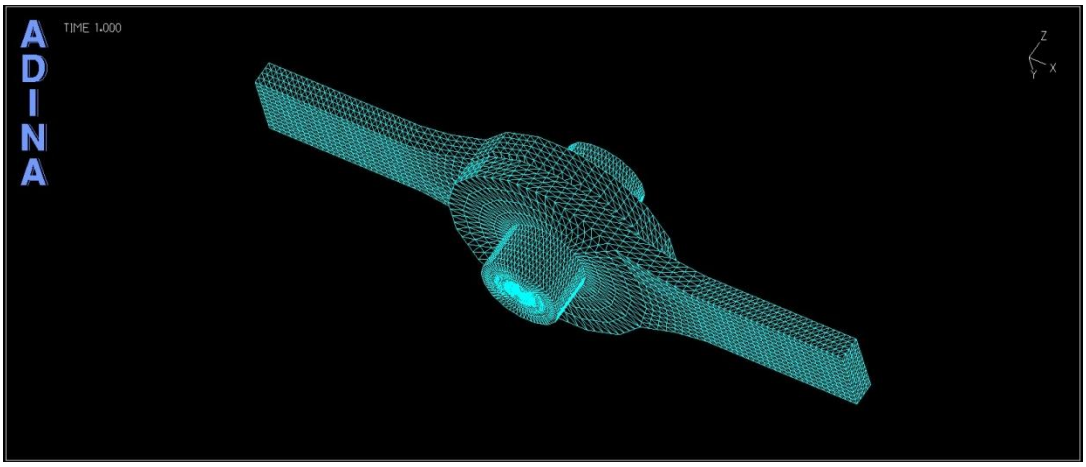

Figure 8.6 – ADINA model of eccentric eye bar connection.

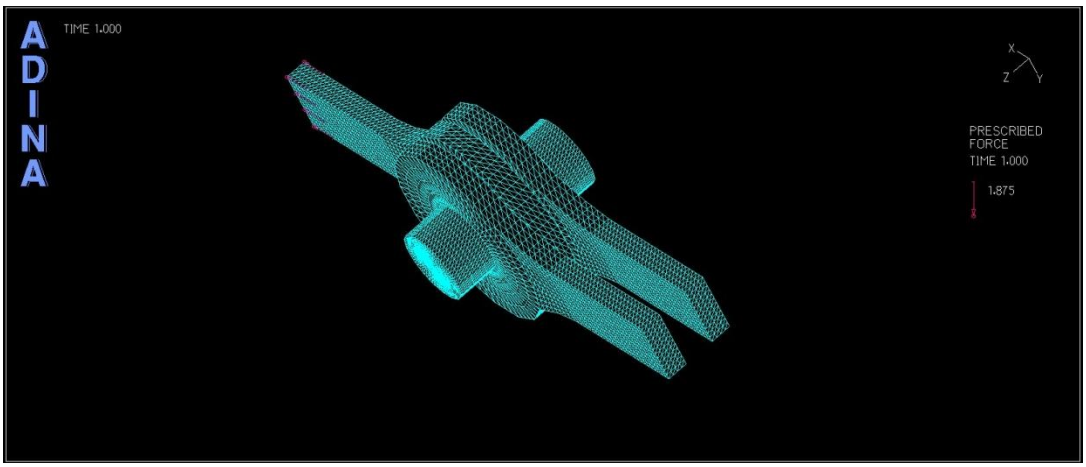

Figure 8.7 – ADINA model of concentric eye bar connection.

8.2.1.1 Concentric Model (Three Bars)

Since the eye bars are curved near the connection, the circumference of the eye bar was broken into sixteen segments. Using the equation for a circle, the coordinates for all of the points that make up these sixteen segments were found. These coordinates were then entered into ADINA manually. The points were then used to create 3D solid elements. Material properties for these elements were taken from the article, "Engineering Investigations of Lenticular Truss Bridges" and are summarized in Table 8.1. The eye bars are entirely made up of rectangular solid elements, while the pin is made up of sixteen trapezoidal elements. Figure 8.8 is a picture of the concentric model after solid elements were created using the manually entered points.

With the connection created and divided into solid elements, a mesh was formed. This was accomplished in slightly different ways for the pin and the eye bars. All of the solid rectangular elements in the eye bars were meshed by dividing each solid into four segments in all directions. The pin was divided into four segments in two of the three directions. However, the pin elements were divided into thirty one segments in the Z-direction (Figure 8.9). This was done because the pin elements were quite long in this direction and required more subdivisions in order to keep mesh size relatively consistent. Figure 8.10 shows the resulting mesh that was created from these solid element subdivisions.

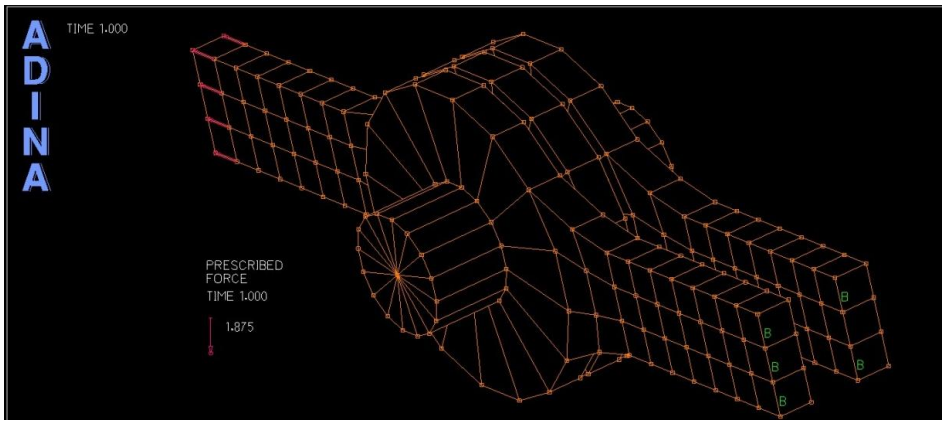

Figure 8.8 – Concentric eye bar connection uses rectangular solids to create each eye bar and trapezoidal solids to create the pin around which all eye bars are connected.

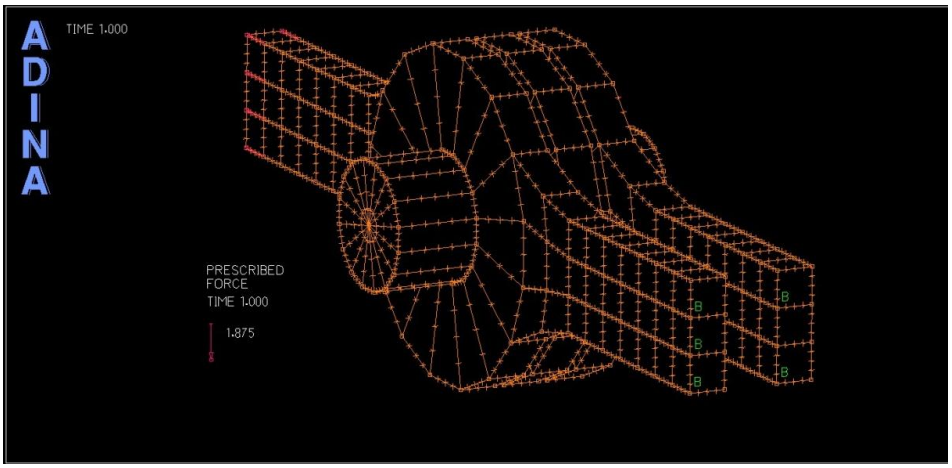

Figure 8.9 – Each solid was subdivided in order to create meshes of relatively similar size.

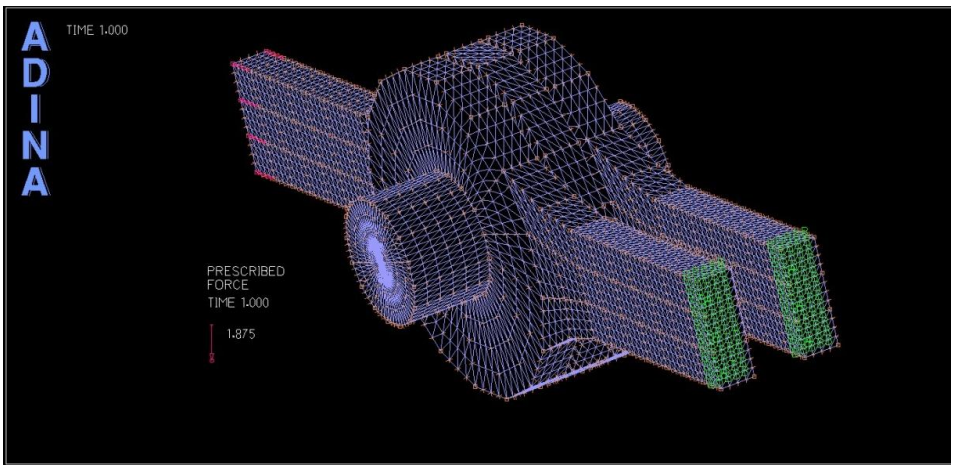

Figure 8.10 – Final mesh of concentric connection model, created from subdivision of solid elements.

Once the solid elements of the model were meshed, boundary conditions were assigned. The two outer bars were fixed at the end and the center bar was pulled by tensile forces that were determined from the SAP2000 rolling truck load analysis. Figure 8.10 is a picture showing the application of end fixity (shown in green) and tensile forces (shown in red). Since there are eight nodes at the end of each bar, the tensile load is distributed equally among the eight nodes. In addition, Figure 8.10 shows the application of 1.875 kips at each node, which corresponds to the Bardwell's Ferry Bridge being loaded at 200% of its maximum posted capacity (refer to Table 8.2).

Recall that this historic truss connection is intended to act as a pin connection. If the analysis were run at this point, the program would treat the entire connection as one solid, rather than four solids that are interacting. Therefore, the pin needs to be separated from the eye bars by creating surface interactions between them. This is done in ADINA by defining separate surfaces and then assigning a coefficient of friction between them. The outer surface of the pin was assigned to be "Surface 1" and each eye bar's inner surface was assigned to be "Surface 2", "Surface 3" and "Surface 4". The Coulomb coefficient of friction used was 0.35. This selection was based on the value suggested in the American Institute of Steel Construction (AISC) Steel Construction Manual for rough steel on steel[9]. Figure 8.11 contains two pictures in which the contact surfaces created for the outer surface of the pin and the inner surfaces of each eye bar can be seen. The lighter color meshing indicates where contact surfaces were created and defined.

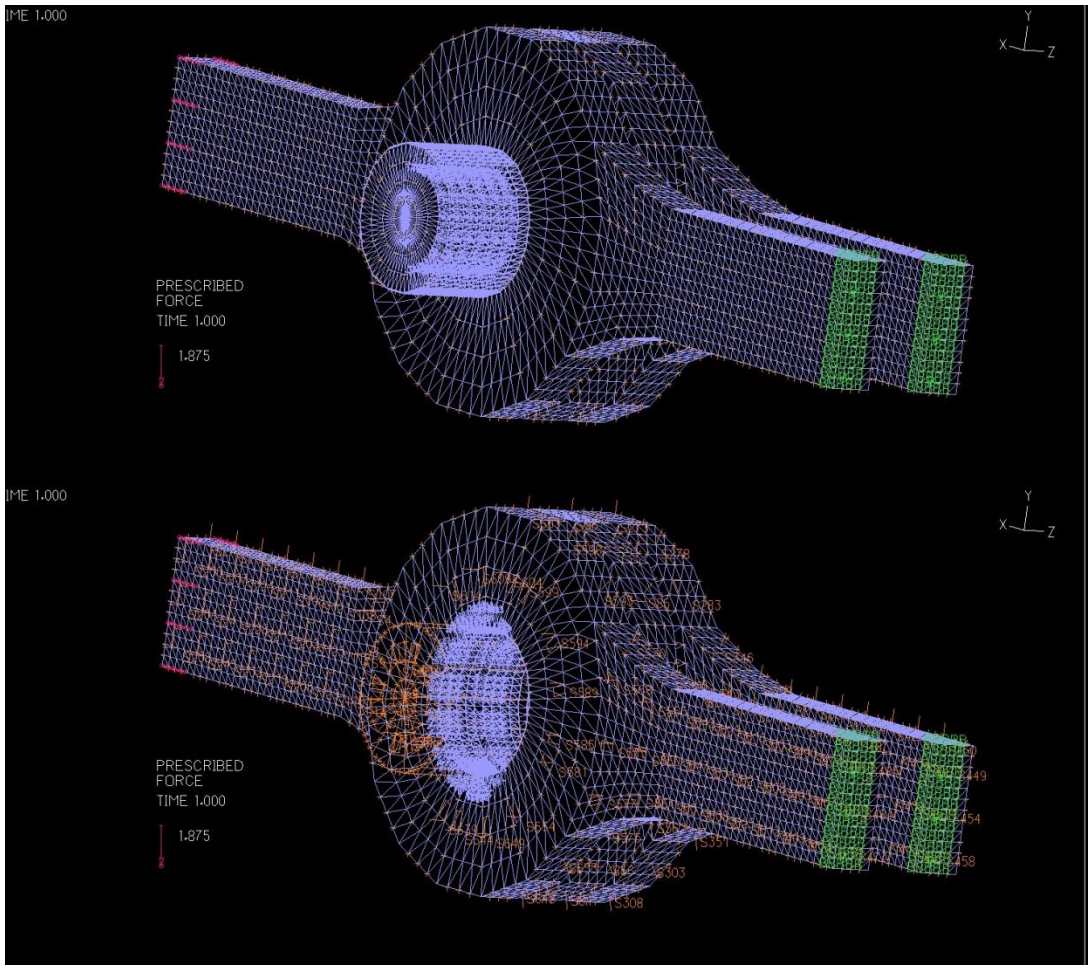

Figure 8.11 – In order to create a pin connection in the connection models, separate surfaces were defined (shown by the light colored meshing).

Pictures taken of the eccentric model illustrate the effect of defining surfaces between the eye bars and the pin. Figure 8.12 shows the axial force distribution in the eccentric connection prior to the definition of separate surfaces. The compressive stress shown in dark blue continues from the eye bar all the way through to the end of the pin, where it is fixed. The reason for pin fixity at ends in eccentric model is discussed in Section 8.1. This suggests that there is complete continuity between the eye bar and the pin. Similar behavior was found in the axial force distribution of the concentric connection model prior to the creation of contact surfaces.

Figures 8.13 and 8.14, however, show the axial force distribution in the eccentric connection and concentric models, respectively, after the definition of separate surfaces. While the dark blue still continues from the eye bar to the pin, it is centralized around the point of contact. This is a more reasonable representation of the behavior of a pinned truss. In a pinned connection, the elements fit together such that they are in contact with one another and interacting through frictional forces. Engineers often idealize these types of connections as truly pinned, in which the coefficient of friction between elements is zero. This model, however, accounts for the bearing forces these elements are capable of applying to one another. The model in which no surfaces are defined does not accurately model an actual pinned connection, but rather a completely fixed connection. Therefore, the definition of contact surfaces is critical in the accurate representation of historic lenticular truss connections.

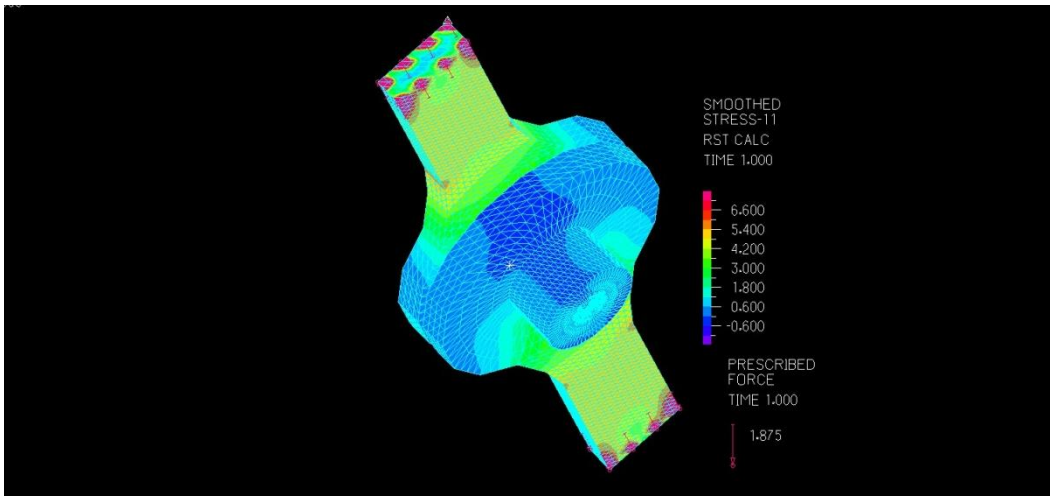

Figure 8.12 – Axial force distribution in eccentric model prior to definition of separate surfaces.

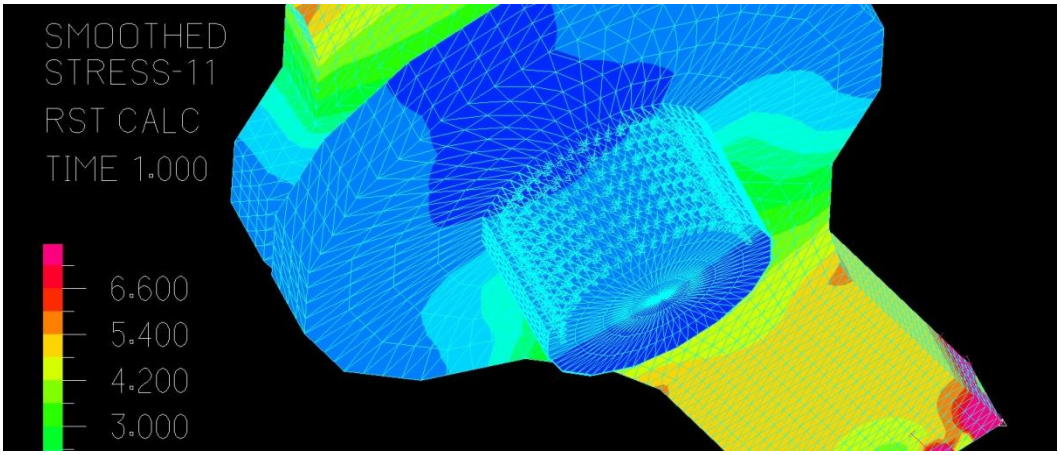

Figure 8.13 – Axial force distribution in eccentric model after definition of separate surfaces.

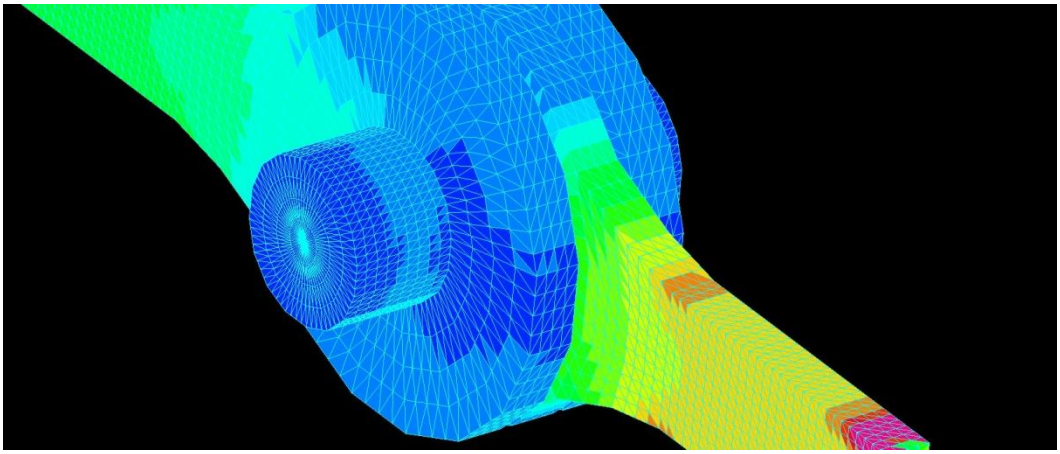

Figure 8.14 – Axial force distribution in concentric model after definition of separate surfaces.

8.2.1.2 Eccentric Connection Model (Two Bars)

The procedure outlined in Section 8.2.1.1 was used for the development of both the eccentric and concentric lenticular truss connection models. The only difference between the models is the assignment of boundary conditions. The concentric model fixes the ends of two eye bars on one side of the connection and applies a tensile load to the end of the eye bar on the other side of the connection. When this same arrangement was attempted on the eccentric model, significant bending occurred in the fixed eye bar (Figure 8.15). This result does not accurately represent the actual behavior of the pinned

lenticular truss connection. It is clear from literature of these and other historic truss types that both the lower and upper chords are intended to only withstand tensile and compressive forces. In addition, it is expected that both eye bars display similar stress distributions.

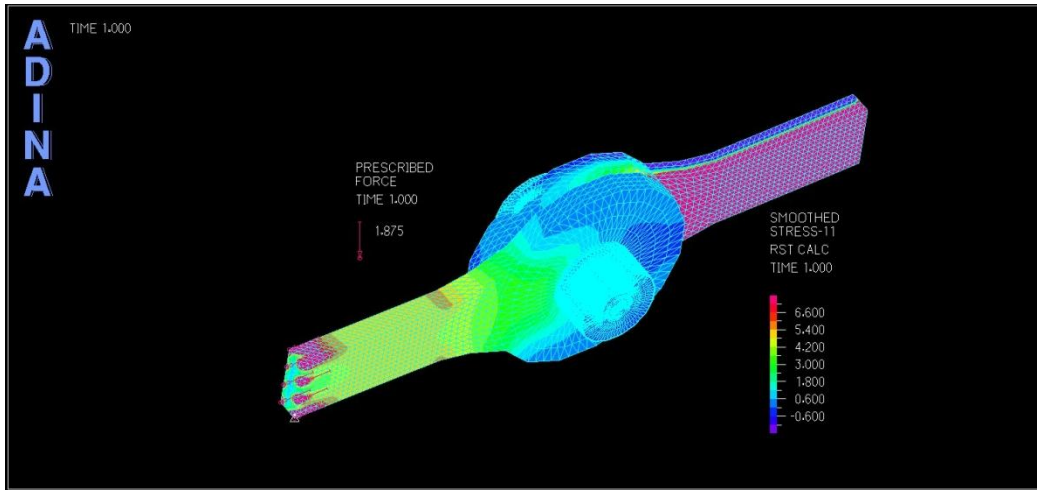

Figure 8.15 – Bending occurs in the fixed eye bar of eccentric model when the right end is fixed and tensile force is applied to left end.

As a result, the eccentric model boundary conditions were altered in order to achieve anticipated behavior under a tensile force. Figure 8.16 and 8.17 show the model boundary conditions and axial force distribution of the eccentric model in which both ends of the pin are fixed and the ends of each bar are subjected to the same tensile load. The behavior of each bar is similar and there is no sign of significant bending in either eye bar. It is important to note that while this more accurately describes the behavior of a pinned lenticular truss connection, the pin in an actual bridge is not fixed. It is for this reason that the concentric model was created. The results from each model are discussed in more detail in the following sections.

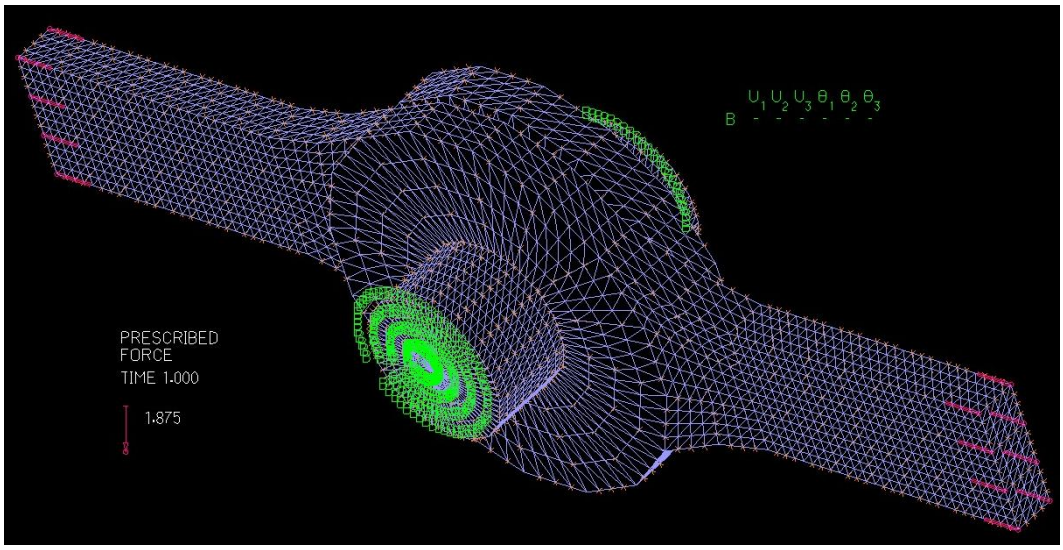

Figure 8.16 – Eccentric model in which both ends of pin are fixed and each eye bar is subjected to an equal and opposite tensile force.

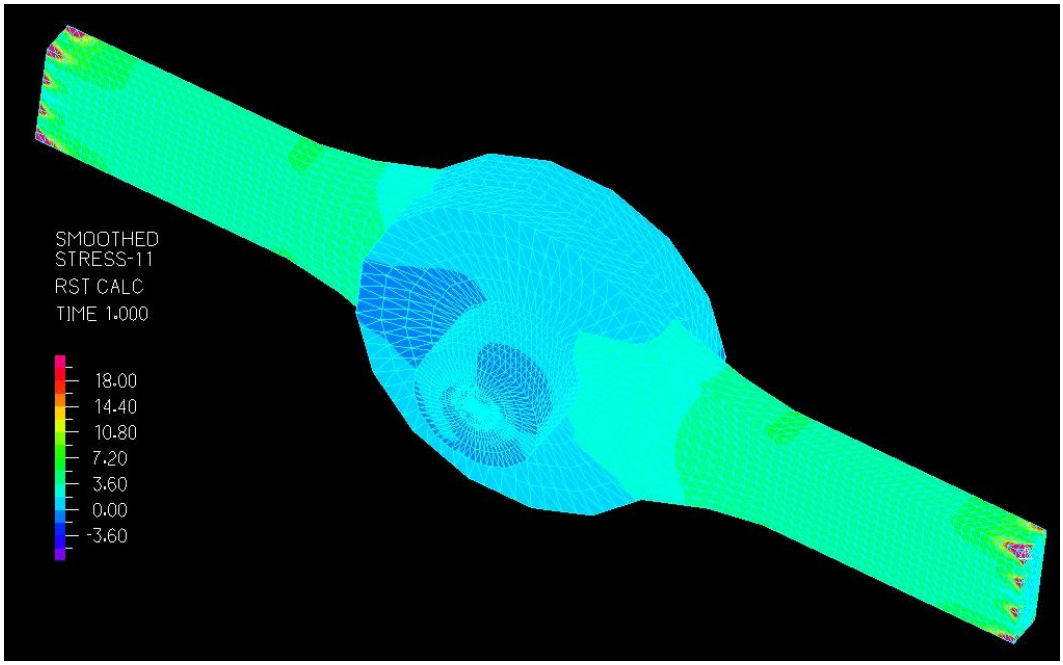

Figure 8.17 – Axial force distribution of eccentric model in which both ends of pin are fixed and each eye bar is subjected to an equal and opposite tensile force.

8.2.2 Evaluation of Axial Stress Distribution

In the concentric model (three eye bars), the ends of the two bars on one side of the connection are fixed while the load is applied to the end of the opposite eye bar. The pin

is only restrained by the contact it has with each eye bar. The axial force distribution resulting from the concentric model was similar to that seen in the second eccentric model in which the ends of the pin were fixed and each eye bar was pulled (Figure 8.18). The maximum axial stresses in the eye bars from the second eccentric model are summarized in Table 8.3.

Note that the axial force results shown in Figure 8.18 are similar to that seen in the eye bar which is not fixed in the original eccentric model (Figure 8.19). Thus, the two models yield similar results if one only uses half of the eccentric model. The original eccentric model has the advantage of not fixing the pin and thus shear stresses throughout the pin are more accurately represented. A similar axial stress distribution is observed in the concentric connection model (Figure 8.20). From these three models, the maximum tensile stress in the eye bars is consistently observed to occur at the top and bottom surface of the eye bar where the geometry transitions to its smallest cross-sectional dimensions. The stresses at this location are those provided in Table 8.3 for the maximum tensile stresses under different truck loads.

Table 8.3 – Maximum axial force in connection at different percentages of posted capacity.

Truck Load (% of Frame Capacity)	Maximum Tensile Stress (ksi)	Maximum Compressive Stress (ksi)
33%	1.06	0.256
67%	2.13	0.512
100%	3.18	0.768
200%	6.3	1.537
400%	12.6	3.074
500%	15.8	3.84

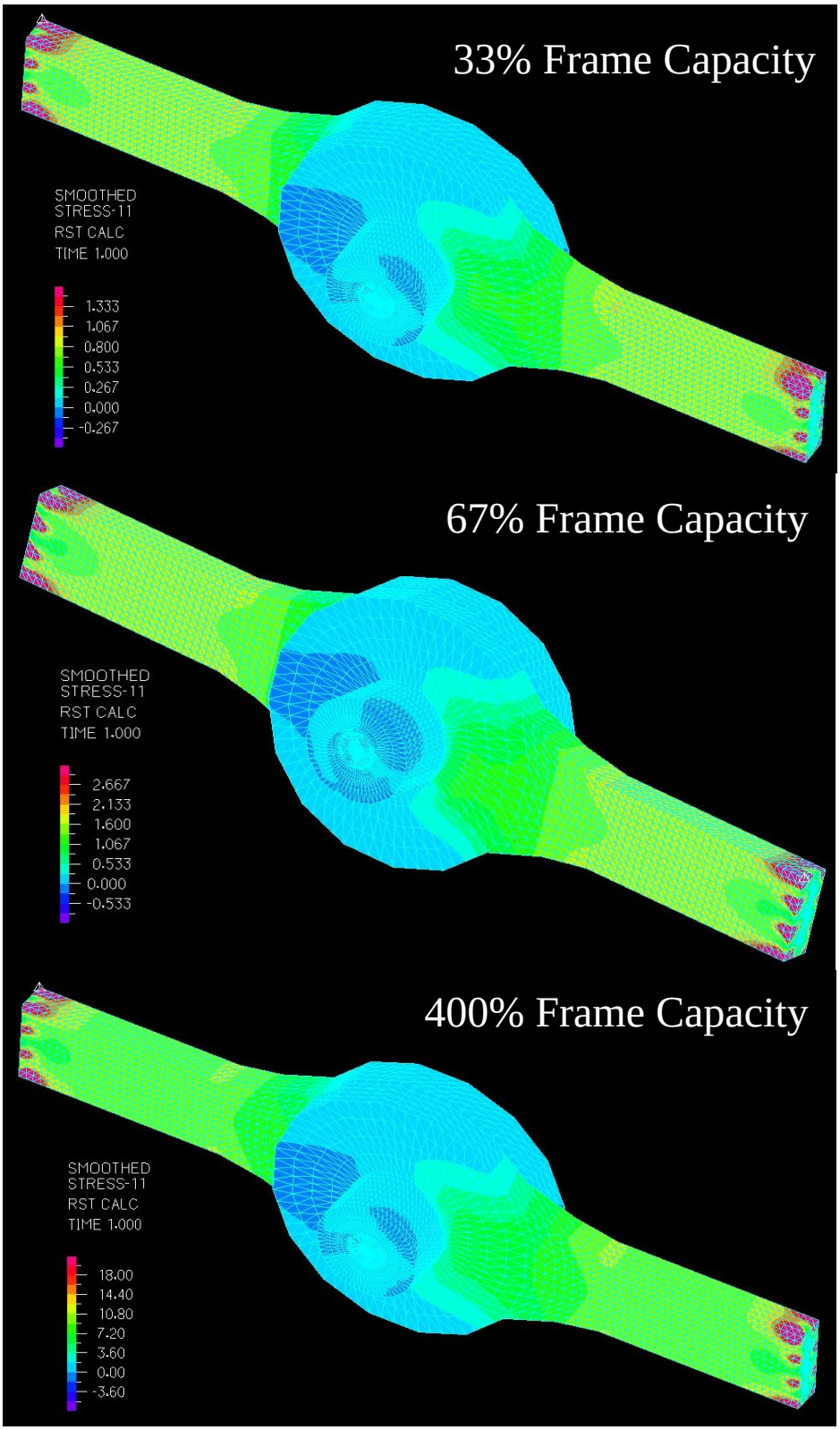

Figure 8.18 – ADINA model of critical eye bar connection with axial stress distribution (for varied truck loads that are different percentages of the bridge frame capacity).

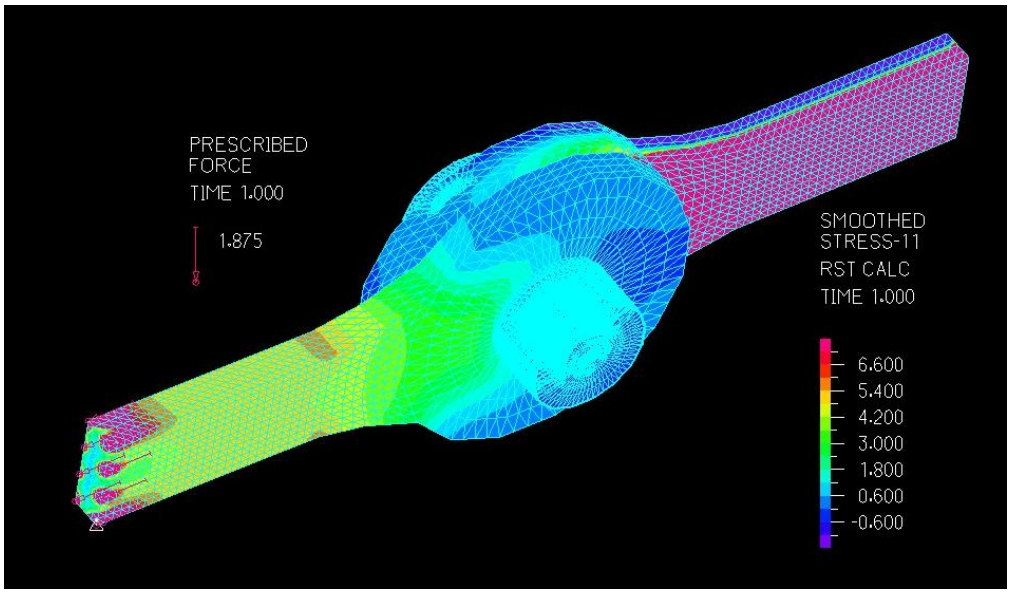

Figure 8.19 – The axial stress distribution of the front eye bar is similar to the results from the revised two- eye bar model in which the pin is fixed.

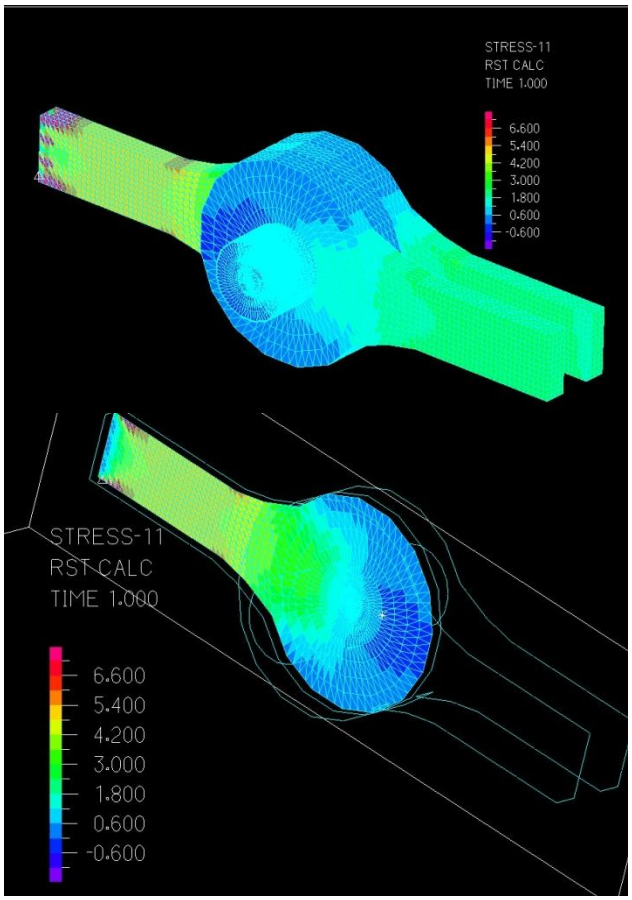

Figure 8.20 – Axial force distribution of three-bar concentric model is similar to previous two models.

8.2.3 Evaluation of Shear Stress Distribution

The concentric model more accurately describes the distribution of shear forces in the connection and, specifically, in the pin. Since the pin is fixed in the second eccentric connection, the transfer of forces from one eye bar to another through the pin is not accurately captured. The concentric model which only restrains the pin through frictional interaction with each eye bar, however, provides significant results. The shear distribution results from the concentric model are reported in this section.

In order to evaluate the stresses at a significant yet realistic overloading condition, a loading that corresponds to 200% the posted capacity (per frame) was used in the model. This means that 1.875 kips was applied to each node (Figure 8.21). The shear stresses resulting from this load case are shown in Figures 8.22 through 8.23. In order to identify the critical locations of the eye bars as well as the pin itself, cross sections of the connection were created in ADINA. This allows the investigation of the stress distributions on both the interior and exterior of the connection.

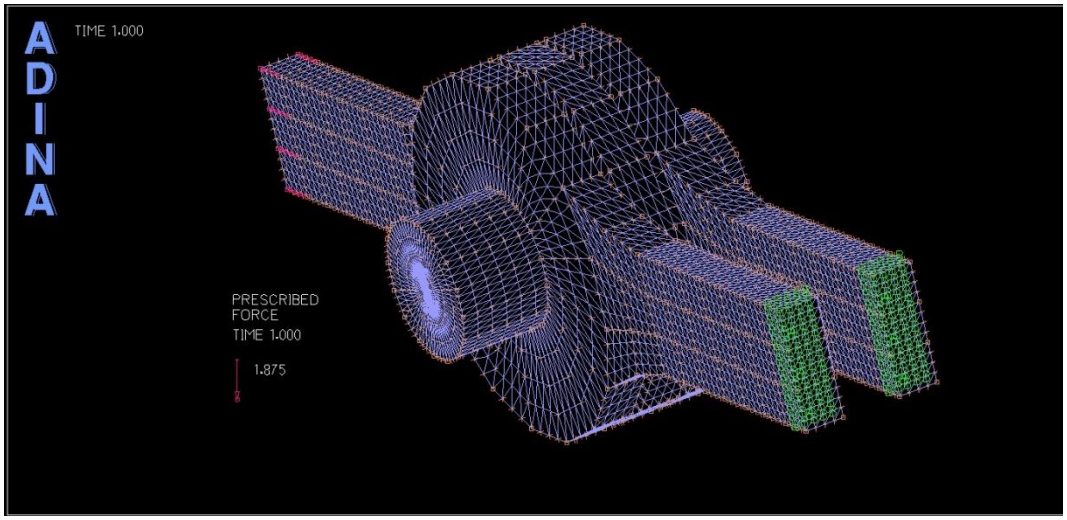

Figure 8.21 – Concentric connection model in which 1.875kip tensile force is applied to each of the eight nodes at the end of the left eye bar.

Figure 8.22 is a cross-section of the concentric model which shows the shear stress distribution on the outer face of the interior eye bar. Aside from the stress concentrations that occur at the load point, the maximum shear stresses from this vantage point are indicated by the darker green areas on the eye bars. This color appears in the eye bar in two locations. The first location is where the circular portion of the eye bar narrows into the smaller, rectangular portion eye bar. This is not surprising considering the reduction in geometry at this location. The shape of the stress distribution in this location indicates a bottlenecking effect.

The second location of maximum shear stress according to Figure 8.22 is where the circular portion of the eye bar is in tension and is formed to fit around the pin. This area of shear stress concentration is less intuitive. Unlike the first location of high shear stress, Figure 8.22 suggests the cross-sectional geometry of the bar to be large at this location. Under extreme tension, the eye bar would not even be in contact with the pin at this location as the circular opening would become elongated. In practice, this is a problematic region in terms of crack development and propagation. Figure 8.23 investigates this second location further.

Figure 8.23 shows the bottom half of the concentric connection. Here, it is clear to see the transfer of shear stresses among all of the elements. Again, high shear stresses are located within the rectangular portion of the eye bar where the geometry of the member is reduced. Because the scale has been altered, these same high stress concentrations are indicated in yellow and are approximately 2.1 ksi.

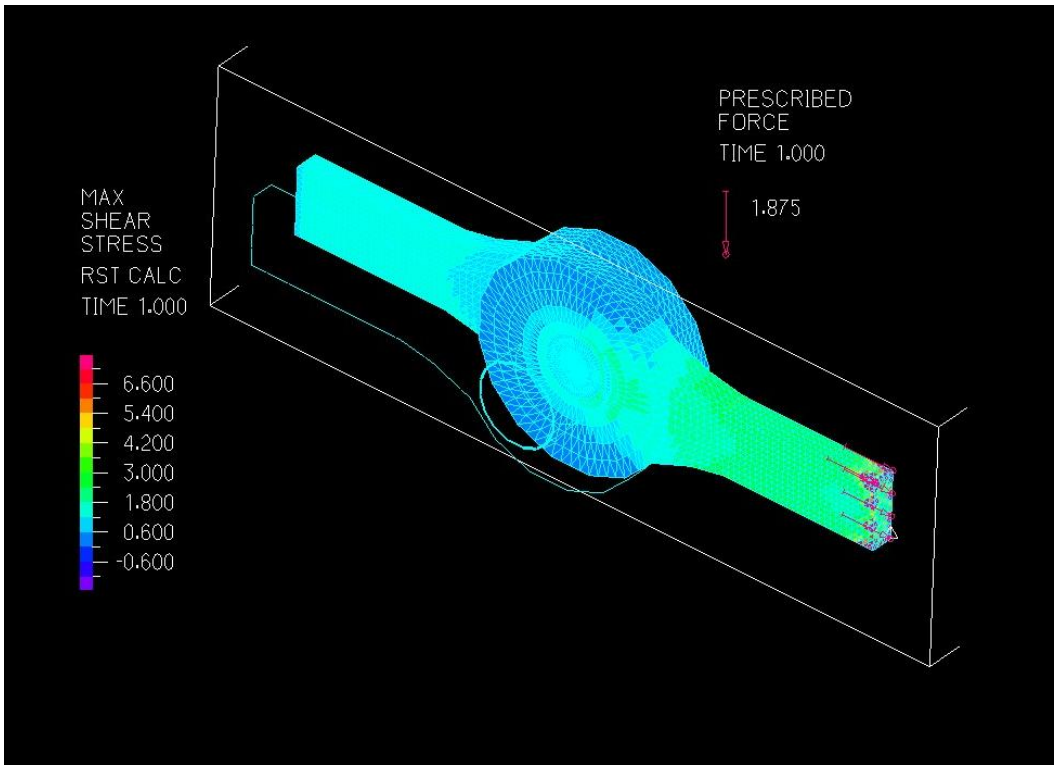

Figure 8.22 – Cross-section of concentric model showing shear stress distribution resulting from tensile load.

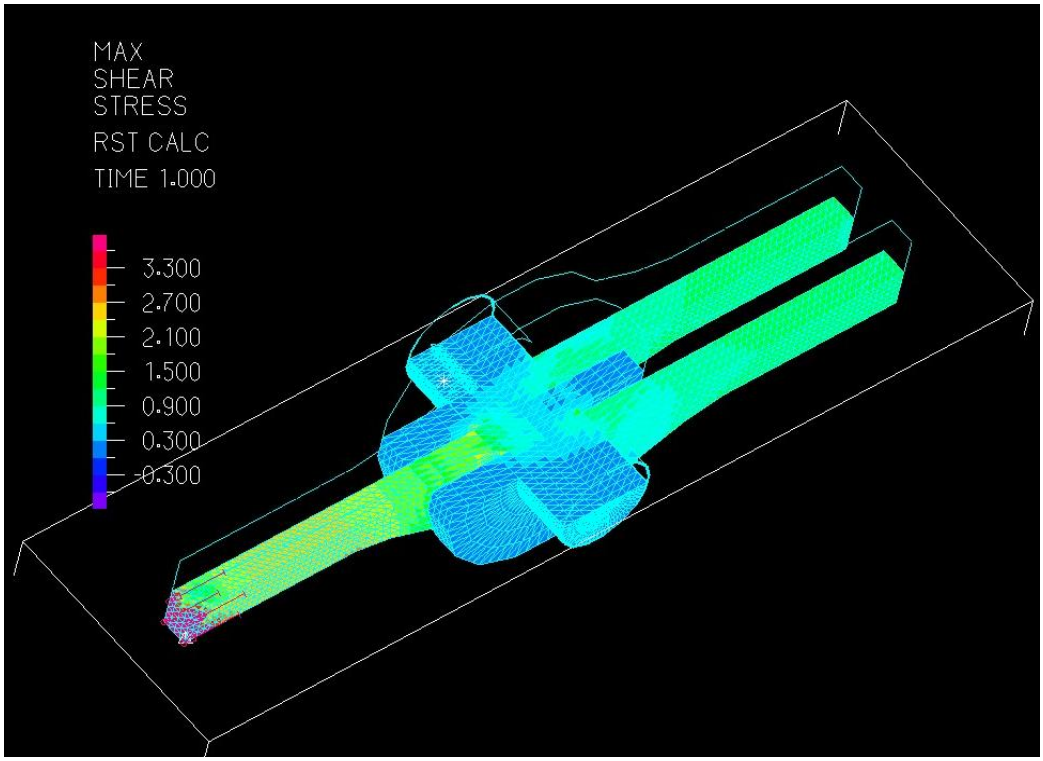

Figure 8.23– Cross-section of concentric model showing shear stress distribution resulting from tensile load.

The second location, near the interface between the eye bar and the pin, is also visible in Figure 8.23. In this figure, however, the reason for the elevated shear stress at this second location is clearer. Again, the stresses are forced to bottleneck. This is the result of the arrangement of the eye bars around the pin rather than the geometry of the eye bar. At this second location, the single eye bar must resist the force of the pin that is being pulled by the two outer eye bars in the opposite direction. This shear stress is not uniformly distributed along the eye bar to pin interface. It is concentrated at the outside face of the eye bar, which is reasonable considering that this is closer to the opposing forces of the outer eye bars and connected pin.

It is important to note that while Figures 8.22 and 8.23 provide valuable insight into the transfer of shear stresses through the truss connection as well as the location of shear stress concentrations within the eye bars, they do not entirely capture the maximum shear stresses withstood by the pin. For this reason, a third cross-section was investigated and is shown in Figure 8.24. This figure suggests that the maximum shear stresses within this cross section of the pin, shown in red and approximately 1.7ksi in value, are located at the outer surface where it is between the middle and outer eye bar. Figure 8.23 shows this same behavior, although it is more difficult to see due to the scale. This result is reasonable considering that between these two eye bars, the pin is resisting opposing forces that are trying to literally tear it apart.

The area inside the pin that is not adjacent to the surface is stressed considerably less. Note also from Figure 8.24 that the high shear stress in the rectangular portion of the eye bar is most critical at the bottom and top outer surfaces. Again, due to scaling, this was not clearly observed in the previous figures.

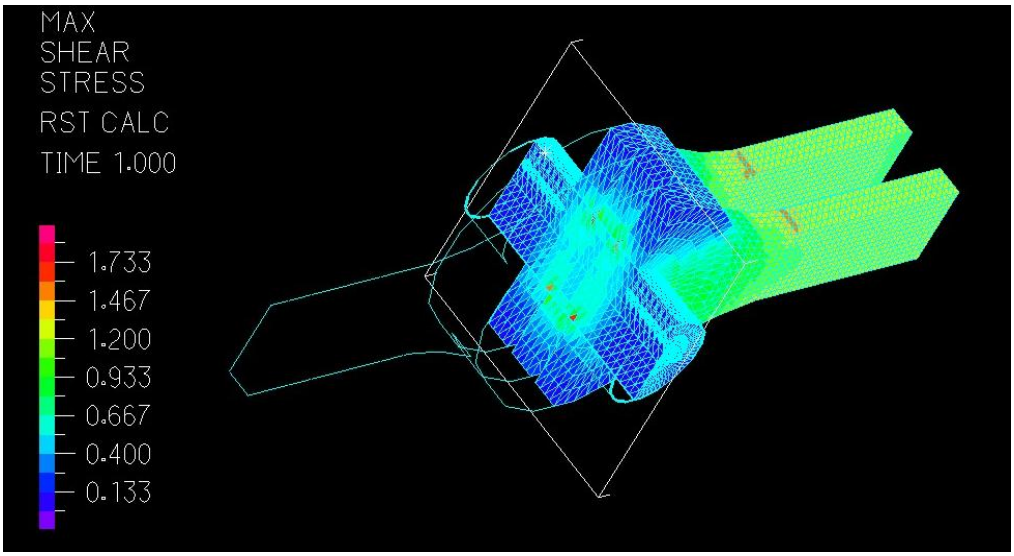

Figure 8.24– Cross-section of concentric model showing shear stress distribution resulting from tensile load.

Figure 8.25 shows three cross-sections of the shear stress distribution throughout the two bar eccentric model given the same loading used for the concentric model. From this figure, it is clear that half the model yields similar insights as those discussed above for the concentric model. The other half of the two bar model does not accurately represent the lenticular truss connection since the eye bar is in bending.

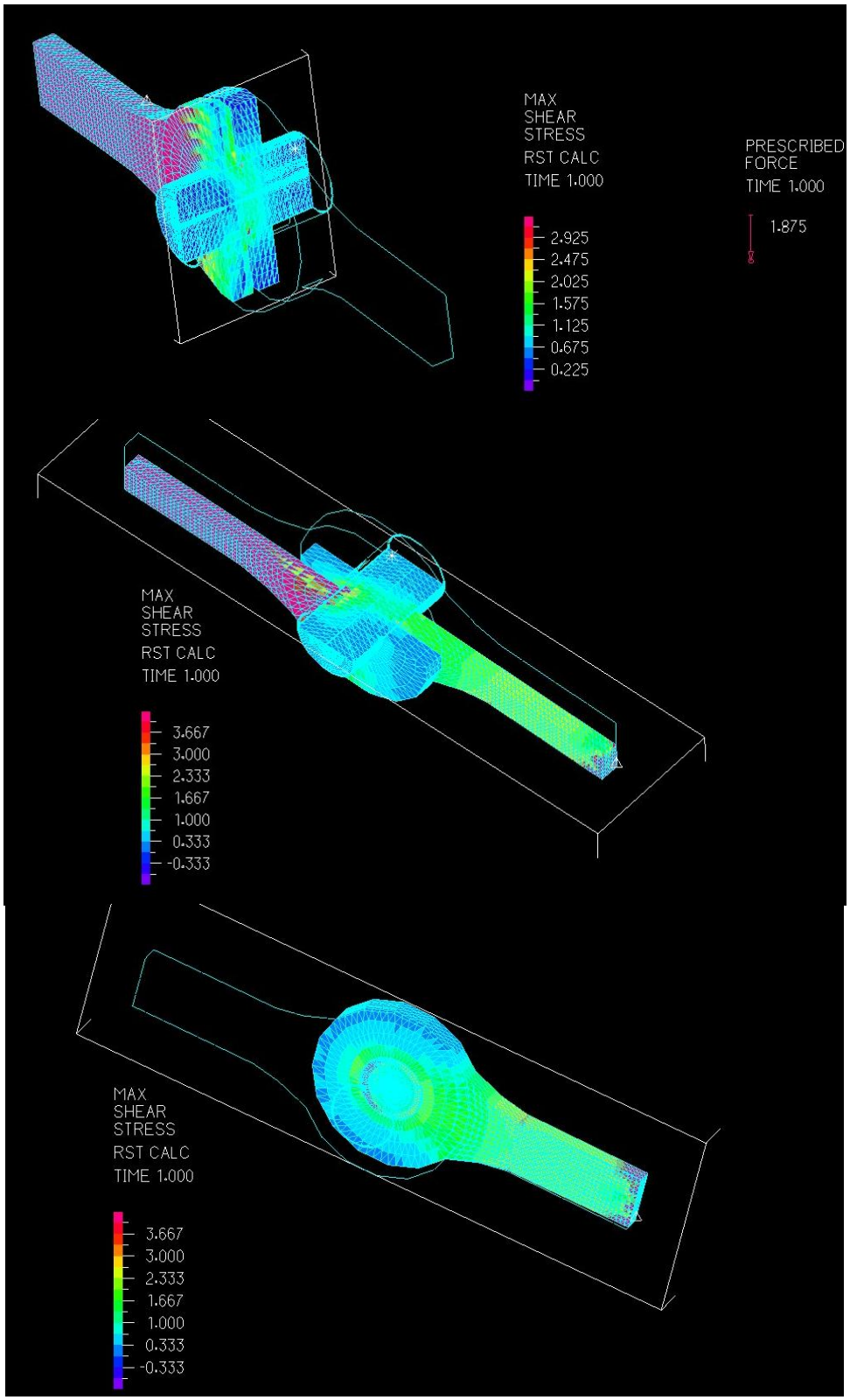

Figure 8.25 – Three cross-sections of shear distribution throughout eccentric truss connection model.

8.3 Preliminary Fatigue Analysis

By modeling the lower chord connection for the Bardwell's Ferry Bridge, not only have the critical locations within the connection been located but also the magnitudes of these maximum stresses have been determined. Knowing the magnitudes of stresses at these critical locations provide insight into the fatigue life expectancy of the connection. All that is required in addition to this information in order to evaluate the life expectancy of the connection is material data for wrought iron similar to that featured in the Bardwell's Ferry Bridge.

Literature about lenticular truss bridges and other truss types from the late 19th century, such as Boothby's paper "Engineering Investigations of Lenticular Truss Bridges", claim that tension members were commonly constructed with wrought iron while compression members were made from either cast or wrought iron. As a result, wrought iron is assumed to be the material used throughout Bardwell's Ferry Bridge. There are many sources that provide material data for modern ductile irons; however, it is difficult to find data specific to historic irons that were used during specific time periods. As a result, a modern S-N curve for ductile iron is used in this paper but it is recognized to be non-conservative. Figure 8.26 is provides S-N curves for both notched and unnotched annealed ferritic Ductile Iron with a tensile strength of 65.8ksi (454 MPa)[10]. This tensile strength is noticeably higher than the typical range for wrought iron; however, it serves as a rough indication of the connection's fatigue life expectancy in the absence of more specific data.

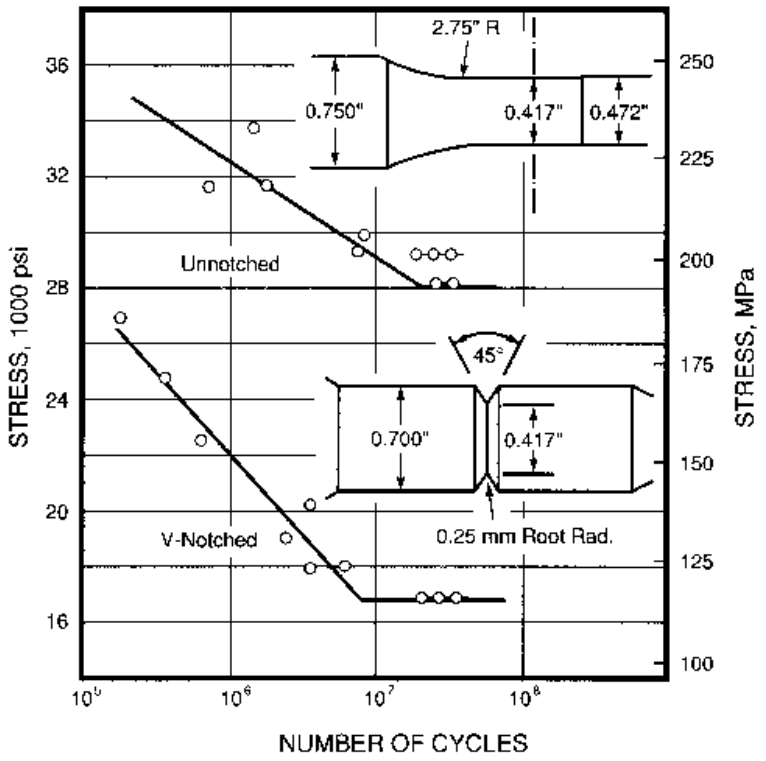

Figure 8.26 – S-N curve for notched and unnotched annealed ferritic ductile iron with a tensile strength of 65.8ksi (454 MPa)[10].

From the finite element model of a Bardwell's Ferry lower truss chord connection, the maximum tensile stress from a truck load equal to 200% the current posted capacity is 6.3ksi (see Table 8.3). Even if the V-notched curve from Figure 8.26 is used in order to determine the life expectancy of the connection, this stress is well below the endurance limit for ductile irons. Again, this data serves only as a rough an initial fatigue evaluation for this historic structure. However, the maximum tensile stress is so far below the endurance limit that it is likely that fatigue given the current weight posting is not a critical mode of failure. While it is not within the scope of this paper, material testing of Bardwell's Ferry Bridge would provide the required information to perform a more detailed fatigue analysis when considered in combination with the stresses determined from the finite element model developed.

CHAPTER 9

DISCUSSION OF RESULTS

Lenticular trusses are an intriguing part of early bridge engineering history in America. The Bardwell's Ferry Bridge in Conway, Ma is one of the few remaining examples of this bridge type in New England that is still open to vehicular traffic. In an attempt to aid preservation efforts by identifying elements within a critical connection that may require more frequent inspection or monitoring, a series of computer models were created to accurately describe the stresses in the connection given a known load. This was accomplished with the creation of both a global 2D model of the entire bridge and a series of local, more detailed 3D models of the connection.

A rolling load was first applied to the global model in order to quantify the axial forces that were needed to be transferred through a critical connection. Once the magnitude of axial forces at connection sites was obtained, they were placed on the ends of three local models. The local models varied in order to create a complete view of the maximum stresses that were possible in each of the connection members. Used in combination, a list of critical locations within the connection were determined for both shear and tensile stress conditions.

From the finite element stress analysis of the Bardwell's Ferry lower chord truss connection, several critical locations have been identified for use in future monitoring and preservation efforts. In terms of critical shear locations, the primary locations to monitor are the inside of the circular opening on the tension side of each eye bar, the surface of the pin where it is between two opposing eye bars, and the upper and lower surfaces of the rectangular portion of each eye bar. The latter critical location is

noteworthy because it is also the location of maximum axial stress due to tension. However, this location can be visually monitored and does not reach the same magnitude as those shear stresses found at the other two locations which are visually hard to inspect.

From Figure 8.24, these two locations reach stresses of approximately 2.1ksi. This value, when used in combination with a fatigue curve for wrought iron, is not enough to induce a fatigue fracture or failure regardless of the number of load cycles the connection is subjected to. However, experience has shown that small cracks tend to form at the inside opening of eye bars in historic truss bridges. This, together with a computer model of an existing historic connection that shows elevated shear stresses at this location, is cause to monitor extant historic truss bridges at this location. As mentioned previously, this location is difficult to visually inspect. Therefore, there is cause to install equipment (such as strain gauges) that can be routinely used to monitor the behavior of the bride over time.

In terms of critical axial stress locations, the critical point to monitor is the rectangular portion of the eye bar that is adjacent to the circular connection point. Due to the reduction in geometry, a bottlenecking effect takes place and results in elevated stresses throughout this portion of the bar. While the magnitude of axial stress at this location, 6.3ksi at 200% the posted frame capacity, is again below the fatigue threshold for failure, the upper and lower surfaces of this section are easily inspected visually.

It is important to note that a tensile axial stress of 6.3 ksi is higher than the axial stress one would calculate by dividing the force in the lower chord, provided by the global model, by the area of the lower truss chord. From the global model alone, one would assume the stress in the lower truss chord to be 60 kips divided by $12in^2$ (the area of four

rectangular bars with an area of $3in^2$ each). This simple formula would predict a tensile axial stress of 5ksi, which is an underestimate given the more detailed model that accounts for the changing geometry of the eye bar.

The computer models developed and used in this analysis of a critical lower chord truss connection featured in Bardwell's Ferry Bridge provide several significant insights for engineers invested in the preservation of historic bridges. First, this analysis specifically identifies critical locations of elevated stresses within the lower chord connections. The stress distributions provided by the model are in agreement with anticipated structural behavior of the connection. The majority of these critical locations where stresses are elevated is easily accessed and can be visually inspected for signs of fatigue. Only one of the critical locations discussed in this paper would require the use of mechanical equipment in order to monitor the stresses and strains at the location.

Second, this analysis shows that a rolling truck load that is 200% the current posted capacity causes stresses in the connection that are all below the fatigue threshold for wrought iron. One must remember, however, that the fatigue information used was for ductile iron. Fatigue data is not currently available for historic wrought iron from the time at which this bridge was constructed. The material testing of samples from historic bridges is an area of research that could be used in conjunction with the models presented in this paper in order to more accurately model and predict structural behavior. While this is not the exact same material as that used for the Bardwell's Ferry Bridge, the fact that maximum stresses are well below the endurance limit still speaks highly of the bridge's ability to withstand loads over time. Additionally, it is important to remember that while the lower chord connection appears to be below the limits that induce fatigue,

the nature of the other members and connections of the bridge are unaccounted for in this paper.

Third, a representative computer model of a specific connection has been made using commercially available finite element software. This was done using the measured geometry of the connection, creating frictional contact surfaces between each of the members, applying a scaled rolling vehicular load to a global bridge model and then taking the reactions from this global model and applying them to a more detailed, local model. This more detailed model predicts higher stresses than the global model would alone. Unfortunately, the use of global models is common practice in the professional engineering world. From the creation of specific bridge connections at this level of detail, more accurate factors of safety can be recommended for use in the professional engineering world that may not want to spend the time and money on the development of more detailed, local models.

Additionally, this same procedure can be applied to other historic structures in order to evaluate the structural behavior at as-inspected bridge conditions. The geometry used in the local model can be easily modified to account for section loss. This allows for as-inspected ratings of historic bridges to be performed and load capacities to be determined with more precision and certainty. With this procedure, not only can existing bridges be more efficiently monitored, inspected and rated, but also historic bridges that are currently in storage can be evaluated to determine whether or not they are suitable to return to service.

CHAPTER 10

CONCLUSION

America's bridge-building history is best expressed through the historical structures that are scattered throughout the country. Efforts towards preserving the ever-decreasing number of historic bridges that still stand can be aided with the application of modern technology and more specific historic bridge research. It is common practice to develop and use modern computer-based models to determine the capacity of bridges, both historic and contemporary. The intent of these computer models, however, seldom extends beyond load rating.

When bridges do not rate high enough to accommodate modern traffic loads, the bridge is posted with a reduced weight capacity. If the bridge rates low enough, it is closed entirely to traffic until a decision to either preserve or demolish it is made. Since the Woronoco Bridge is currently closed and the Bardwell's Ferry Bridge is posted at 10 tons, recent ratings of these bridges have presumably been performed. Therefore, load rating of historic bridges was not the purpose of this paper. Instead, the point of this paper was to explore two other applications of modern methods in the evaluation of historic structures that are not commonplace in today's professional engineering world.

Modern methods can be used to investigate the behavior of certain historic structures for a variety of purposes other than load rating. This paper highlights two such alternative applications. The first alternative is the development and use of representative computer-based models to investigate the design decisions made by early engineers who did not have these modern tools (Part I). The second alternative featured in this paper is the development and use of computer-based models to identify critical locations in order

to guide more informed inspections, monitoring and rehabilitation (Part II). Exploring these and other uses for modern analytical methods has the potential to benefit both professional and academic communities.

The historic structures that still stand today were designed and constructed prior to the age of computers. All of the decisions made during this time were based on experience, intuition and scaled physical models. With some historic structures surviving far beyond their life expectancy, there is much to be gained from their success. By using modern technology to investigate these early design and decision-making processes, we can expand our understanding of these methods and inform future design endeavors. The experience and skill of early engineers is a valuable tool for all individuals intending to pursue and practice engineering design, both at the professional and academic levels.

In addition to gaining understanding and insight from the development of representative historic computer-models, professionals would benefit from the standardization of these detailed, finite-element models. When evaluating an historic bridge currently, many computer models must be created for each example from scratch. There are a variety of software packages that exist that assist engineers in this task; however, they are limited in terms of the types of bridges that they specialize in modeling. Trusses with curved upper and lower chords, for example, would be problematic with the currently available truss-analysis software. Additionally, detailed finite element models are not commonly utilized to evaluate stress concentrations due to the time required to develop such models. Further research in the use of finite element methods for use in evaluation of critical bridge locations could lead to the standardization of such practices if the time required to effectively use this technology could be reduced.

Private engineering firms work within a budget, and if the majority of the budget is spent developing a representative model to serve as a base, less time is spent on the evaluation of rehabilitation and restoration options.

In addition to increasing the knowledge we have of early engineering practices and providing assistance for practicing engineers who are responsible for evaluating the rehabilitation options for historic structures, there is a third benefit from the application of modern methods in the evaluation of historic structures. The third benefit is the preservation of American history and culture. Historic structures can be documented and photographed, but this is nothing compared to the experience of the structure itself. Throughout the world, countries are identified by the remaining historic structures found there. While historic American bridges may not be as highly acclaimed as the Swiss bridges of Robert Maillart, they are a trademark of early American life. Having withstood the test of time, a greater sense of pride and importance should be placed on the appreciation and preservation of these structures.

REFERNECES

1. DeLony, E. and Klein, T. H. (2005, July). "Rehabilitation of Historic Bridges." *Journal of Professional Issues in Engineering Education and Practice*, vol. 131, issue 3, 178-186.
2. Library of Congress (Internet site at www.loc.gov/). Retrieved 2008.
3. "Concrete Arch Bridges." Retrieved September 8, 2008, from World Wide Web (www.marylandroads.com/).
4. Billington, D. (1979). "Robert Maillart's Bridges." New Jersey: Princeton University Press.
5. Guise, D. (2006, January/February). "Development of Lenticular Truss Bridge in America." *Journal of Bridge Engineering ASCE,* 120-129.
6. Lutenegger A. (2005, Spring/Summer). "Lenticular Iron Truss Bridges in Massachusetts." *Civil Engineering Practice*, 53-73.
7. Lamar, D. M. and Schafer, B. W. (2004, November/December). "Structural Analyses of Two Historic Covered Wooden Bridges." *Journal of Bridge Engineering ASCE*, 623-633.
8. Boothby, T. (2004). "Designing American Lenticular Truss Bridges 1878-1900." *IA, The Journal of the Society for Industrial Archeology*, vol. 30, 5-17.
9. American Institute of Steel Construction (2005). "Steel Construction Manual." 13th Edition, 16.1-349.
10. Ductile Iron Society (Internet site at http://www.ductile.org). Retrieved 2009.